NASA Technical Memorandum 101305

Optical Measurements of Soot in Premixed Flames

(NASA-TM-101305) OPTICAL MEASUREMENTS OF SOOT IN PREMIXED FLAMES Ph.D. Thesis - California Univ. (NASA) 180 p CSCL 20D

N88-30090

Unclas
G3/34 0165641

Valerie J. Lyons
Lewis Research Center
Cleveland, Ohio

August 1988

NASA

OPTICAL MEASUREMENTS OF SOOT IN PREMIXED FLAMES

Valerie J. Lyons

National Aeronautics and Space Administration
Lewis Research Center
Cleveland, Ohio 44135

ABSTRACT

Two laser diagnostic techniques were used to measure soot volume fractions, number densities and soot particle radii in premixed propane/oxygen flat flames. The two techniques used were two-wavelength extinction, using 514.5 nm-632.8 nm and 457.9 nm-632.8 nm wavelength combinations, and extinction/scattering using 514.5 nm light. The flames were fuel-rich (equivalence ratios from 1.8 to 2.8) and had cold gas velocities varying from 3.4 to 5.5 cm/s. Measurements were made at various heights above the sintered-bronze, water-cooled flat flame burner with the equivalence ratio and cold gas velocity fixed. Also, measurements were made at a fixed height above the burner and fixed cold gas velocity while varying the equivalence ratio. Both laser techniques are based on the same underlying assumptions of particle size distribution and soot optical properties. Full Mie theory was used to determine the extinction coefficients, K_{ext}, and the

scattering efficiencies, Q_{VV}. Temperature measurements in the flames were made using infra-red radiometry and fine-wire thermocouples.

Good agreement between the two techniques in terms of soot particle radii, number density and volume fraction was found for intensity ratios (I/I_o) between 0.1 and 0.8. For intensity ratios higher, or lower than this range, the differences in extinction coefficients at the wavelengths chosen for the two-wavelength method are too small to give accurate results for comparing particle radii and number densities. However, when comparing only soot volume fractions, the agreement between the two techniques continued to be good for intensity ratios up to 0.95.

ACKNOWLEDGEMENTS

I wish to thank Professor Patrick J. Pagni for suggesting this research project and for his help in completing and critiquing this work. I also appreciate the time spent by the other members of my thesis committee, Professors John W. Daily and R. Brady Williamson in reviewing this work.

NOMENCLATURE

a	Particle radius
C_o, C_1	Calibration Constants
C_1, C_2	Constants used in Planck's equation
C_{vv}	Size-dependent particle scattering cross-section
d	Distance through flame from probe volume towards scattering detector
d_o	Laser beam diameter leaving laser
dA	Differential area
dS	Differential pathlength
dV	Differential volume
di	Differential change in intensity
f_v	Particulate carbon volume/flame volume
I	Radiant intensity
i	Intensity
K	Extinction coefficient
K_s	Transfer function for radiometer system
L	Beam pathlength through flame
ℓ	Distance from edge of flame to probe volume along laser path
m	Complex index of refraction
n	Real index of refraction
nk	Imaginary index of refraction
N_o	Total particle concentration
N(R)dR	Particle concentration in size range dR about R
N_T	Effective radiance
N_r	Radiometer internal reference effective radiance

N_λ	Blackbody spectral radiance
Q_{ext}	Extinction efficiency
Q_{sca}	Efficiency factor
Q_{vv}	Scattering coefficient
R	Particle radius
R_λ	Normalized product of detector response and filter response
s	A pathlength
S	Radiometer electronic attenuation factor
S_p	Length of probe volume
T	Temperature
TAU	The integral in the expression for K_{ext}
V	Recorded output voltage
x	Characteristic size parameter = $2\pi R/\lambda$
XI	The integral in the expression for Q_{vv}

Greek

α_λ	Spectral absorptance
ξ	The integral in the expression for Q_{vv}
ε	Emissivity
Φ	Phase function
ϕ	Angular direction
λ	Wavelength
μ	Microns
σ	Stefan-Boltzmann constant, or standard deviation
σ_o	Scattering cross-section
τ'	Non-dimensional extinction coefficient
τ_λ	Spectral transmittance

θ	Angular direction
χ_{ij}	Normalized extinction coefficient for wavelengths i and j

Subscripts

app	apparent
bb	black body
d	direction
ext	extinction
fl	flame
i	first wavelength
j	second wavelength
m	mean
max	most probable, i.e., at maximum in N(R)
N_2	nitrogen
o	incident intensity
t	total

TABLE OF CONTENTS

Chapter 1: Introduction

The study of soot formation in both premixed and diffusion flames has occupied many researchers for many years. Soot particles are responsible for most of the emitted thermal radiation from a flame. This radiative heat transfer causes fires to spread when confined in flammable surroundings and reduces the life of combustors in gas turbine and reciprocating engines. Emission of soot from engines is also undesirable from an environmental impact point of view. In military situations, soot emission can increase visibility to the enemy. The new synthetic fuels, such as liquified coal and shale oil, which have a large proportion of hydrocarbons of high molecular weight, will produce large amounts of soot.[1] The complex polymers in modern building materials and furnishings are also copious soot producers.

Optical measurements of soot particle size and concentration in flames have been theorized and experimentally performed by many researchers. The earliest extinction measurements in flames were made by Stark[2] back in 1897, as well as Becker[3] (1909), Hottel and Broughton[4] (1932). These were followed in more recent years by Millikan[5] (1962), Bonne and Wagner[6] (1965) and Pagni and Bard[7] (1978). The scattering of light by soot

particles was first performed experimentally by Senftleben and Benedict[8] in 1919. Many recent studies have used this as a diagnostic tool: Dalzell, et.al.,[9] (1970), D'Allesio, et.al.,[10] (1972), Prado, et.al.,[11] (1981), Bockhorn, et.al.,[12] (1981), Santoro, et.al.,[13-14] (1983), and Dobbins, et.al.,[15] (1984). The electromagnetic theory of the scattering of light by an absorbing sphere was determined by Mie[16] in 1908. This theory was applied to soot particles by Pepperhoff[17] (1951), Roessler[18] (1953) and Stull and Plass[19] (1960), as well as by many others.

Much attention has been focused on the experimental techniques used for the measurement of soot particles in flames. Glassman and Yaccarino[20-21] measured sooting heights to determine the effects of oxygen concentration and temperature on sooting tendencies. Kadota, Hiroyasu, and Farazandehmehr[22] and Chakraborty and Long[23] collected soot from the combustion zone. Jagoda, Prado, and Lahaye[24] collected soot with probes and examined the samples under an electron microscope. This revealed soot clusters and chains, which lead to the controversy over whether the sampling process caused the particles to join together, or were there actually chains and clusters in the flame? Optical methods do not disturb the flow. D'Allesio, et. al.[26-27] combined light scattering and extinction measurements to yield particle size and

concentrations. Related experiments have been performed by Kent, Jander, and Wagner[28], Haynes, Jander and Wagner[29-30], Bockhorn, et.al.[12], and Santoro, Semerjian, and Dobbins[13]. Since transmission measurements are easier to perform than scattering techniques, Pagni and Bard[31-35] developed a multiwavelength laser transmission technique. This technique was subsequently used to make measurements in a combusting boundary layer by Beier and Pagni[36-38]. One advantage of this technique is that the effects of particle nonsphericity on the transmitted intensity are less than the effects on scattering measurements[39].

Both premixed and diffusion flames have been studied in terms of their soot production. Diffusion flames produce more soot than premixed flames, because pyrolysis of the fuel and soot formation reactions take place in a fuel-rich zone[36]. In premixed flames, pyrolysis and soot formation reactions occur simultaneously with oxidation reactions. Rapid oxidation of the fuel in premixed flames may prevent formation of soot precursors or promote oxidation of the precursors. Possible soot formation processes are reviewed by Palmer and Cullis[40], Wagner[41], and Bittner and Howard[42]. Excellent review articles on premixed flames are given by Haynes and Wagner[43] and Baumgärtner, Hesse, Jander, and Wagner[44].

In the present study, a premixed propane-oxygen flame is used to produce a steady, easily reproducible soot field. The volume fraction, particle size and number density of the soot is determined by two different laser diagnostic techniques. The laser light scattering/ extinction technique[10-15] and the multiwavelength (or, two-wavelength) technique[31-38] are used simultaneously. The equivalence ratio is varied for a given cold gas velocity while the soot concentration is measured at a particular height above the sintered flat flame burner surface. Also, for a given equivalence ratio and cold gas velocity, the height above the burner is varied and again soot concentration and size measurements are taken. Flame temperature measurements are taken using an infra-red radiometer and are compared with fine-wire thermocouples in non-sooting flames. Comparison of the agreement between the two laser techniques in various flow conditions gives operating ranges and shows the strengths and weaknesses for each of the techniques. The two techniques use the full Mie theory with a polydisperse size distribution in the analysis of the scattering and two-wavelength extinction experimental results.

Chapter 2: Flat Flame Burner

A laminar one-dimensional (flat) flame provides an easily-controlled environment in which to study soot formation, growth, agglomeration, and oxidation. The fuel, oxygen and nitrogen flowrates can all be independently varied to produce a wide variety of flames. The sintered-bronze burner was built by McKenna Products, Inc. to the design specifications determined by P.J. Pagni.[45] The burner also has the capability of surrounding the flame with a shroud of inert gas (eg. nitrogen) to reduce edge effects. A cross-section of the burner is shown in figure 2.1, where the water-cooling coils are seen embedded in the sintered material. Chromel-alumel thermocouples were placed in the water lines upstream and downstream of the burner, to monitor the increase in water temperature after passing through the burner.

The burner was mounted on a Velmex traverse system (model B4012Q1J with an 8300 Controller) which had two computer-controlled stepper motors (capable of 200 steps per revolution) to move the burner vertically and horizontally using precision lead screws with 1.0 mm LD, 10mm-1mm ISO threads. The burner and traverse system were surrounded by a very fine screen enclosure to protect the flame from drafts. The enclosure was vented to the roof through screens in the chimney to prevent down-drafts.

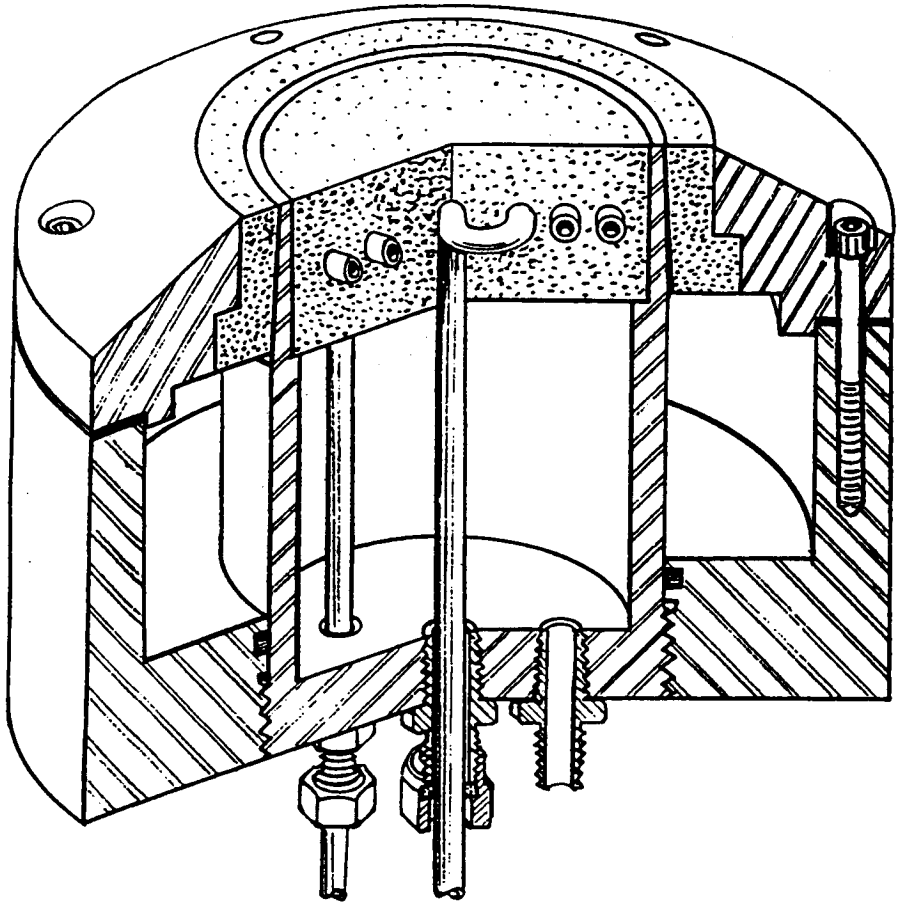

Figure 2.1 Cross-Section of Flat Flame Burner

A 15-centimeter square metal plate was suspended 3 centimeters from the burner's surface to act as a flame holder. This produced a steady flame zone up to 25 mm high. The fuel supply system for the burner is shown in figure 2.2. Nupro micrometer needle valves were used to control the gas flows and Flow Technologies turbine flowmeters were used to measure the flows after calibration with a volume flowmeter. Pressure and temperatures were measured and recorded for each gas downstream of the turbine flowmeter (15 cm. from the outlet, to avoid disturbing the flow through the flowmeter). The supply tubing was 0.64-cm diameter stainless steel, except for 25 cm upstream and 15 cm downstream of the turbine flowmeters where the tubing diameter was increased to 1.6 cm, which was the same as the inside diameter of the flowmeter. This produced a smooth transition from the tubing to the flowmeter, reducing the chance of flow disturbances and inaccurate flow measurements. Shut-off valves were used after each of the needle valves to provide positive shut-off capability and to allow the needle valves to be left in position when the burner was shut off. This allowed previous flow conditions to be accurately repeated.

The operating procedure was as follows. The water was sent to the burner from the filtered water supply from the laser. The oxygen and propane solenoid valves were opened. The propane was then allowed to flow to the

Figure 2.2 Flow System Schematic

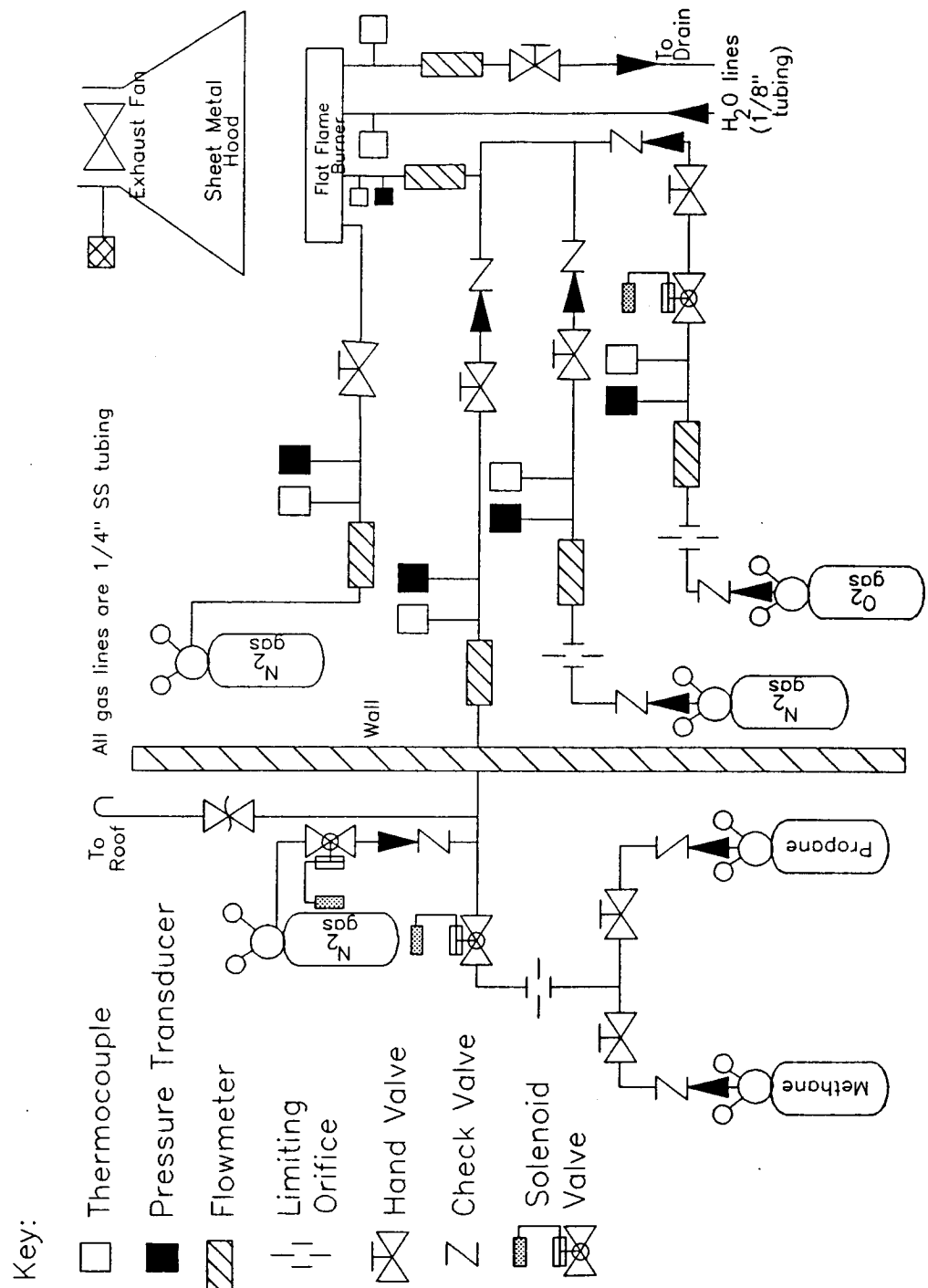

burner by opening the needle valve and the positive shut-off valve. The burner was lit using a butane fireplace-lighter. The oxygen was then turned on and the flow rates were adjusted to the desired equivalence ratio and cold gas velocity as calculated by the computer program "FLOWMETER" in Appendix B.

Chapter 3: Temperature Measurements

3.1 Introduction

The laws of radiation originated by Stefan-Boltzman, Wein, Planck and others establish definite and precise relationships between an object's temperature and composition and the radiation it emits. Conversely, by making accurate spectral measurements of the radiation received from a remote object, much can be learned about its thermal history and composition.[46]

These spectral measurements are made using radiometry. The conventional process of radiometric data interpretation involves the use of the basic laws of radiation together with a detailed consideration of the characteristics of the optical, electronic and detector elements of the instrument. One approach treats the radiometer as a system which has a transfer function, or coefficient, K_s, which converts the radiometer output voltage and scale settings to an absolute radiation measurement.

3.2 Theory

The radiometer system response factor is defined as[47]:

$$K_s = \frac{S \quad V}{N_T - N_r} \qquad (3.1)$$

where:

N_T = effective radiance (watts/cm^2·steradian)

N_r = effective radiance of radiometer internal reference, from calibration (watts/cm^2·steradian)

S = instrument electronic attenuation factor

V = recorded output voltage

First, N_T must be determined using a graphical technique along with the calibration data of the radiometer. We define N_T as:

$$N_T = \int_{\lambda_1}^{\lambda_2} R_\lambda N_\lambda \, d\lambda \qquad (3.2)$$

where:

R_λ = normalized product of detector response and optical filter transmission characteristics.

N_λ = blackbody spectral radiance at selected temperature given by Planck's equation:

$$N_\lambda = \frac{C_1}{\lambda^5} \left[\frac{1}{e^{C_2/\lambda T} - 1} \right] \qquad (3.3)$$

where:

C_1 = 1.19 x 10^4 watts^4·micron/steradian·cm^2

C_2 = 1.438 x 10^4 micron·degrees

T = blackbody temperature in degrees Kelvin

λ = all wavelengths in range of detector and filter (from λ_1 to λ_2)

In order to determine R_λ, the radiometer detector must be calibrated over a range of wavelengths and the detector response must be normalized and plotted versus wavelength (see figure 3.1). Then the optical filter must be calibrated in a similar fashion and produce a normalized calibration curve shown in figure 3.2. The value of the detector response and the filter response at a given wavelength are multiplied together and the resulting curve is again normalized. This new curve is R_λ, which is used in equation (3.2) along with equation (3.3) to determine N_T.

Evaluating the integral in equation (3.2) for a selected temperature will give its corresponding value of N_T. These results can be presented in a table so that in the future, when an experimental value of N_T is found, the table will provide the corresponding temperature. For instance, the table is immediately useful to determine N_r for equation (3.1). The internal reference temperature was measured at the time of calibration. We now use the radiance versus temperature (N_T versus T) table to look up this reference temperature, and find N_r.

After using a blackbody source to supply a known temperature to calibrate our system and determine K_s, we can proceed to determine unknown temperatures using equation (3.1) rearranged as:

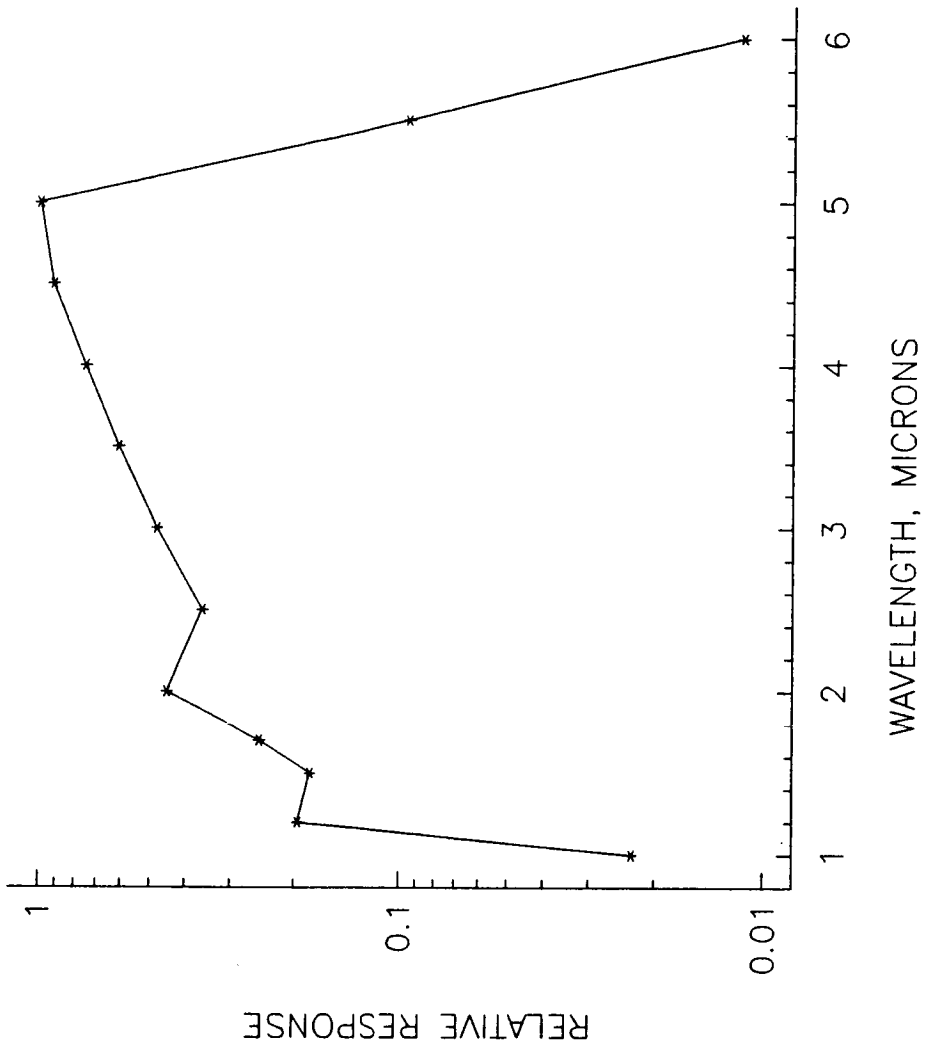

Figure 3.1 Normalized Radiometer Detector Calibration

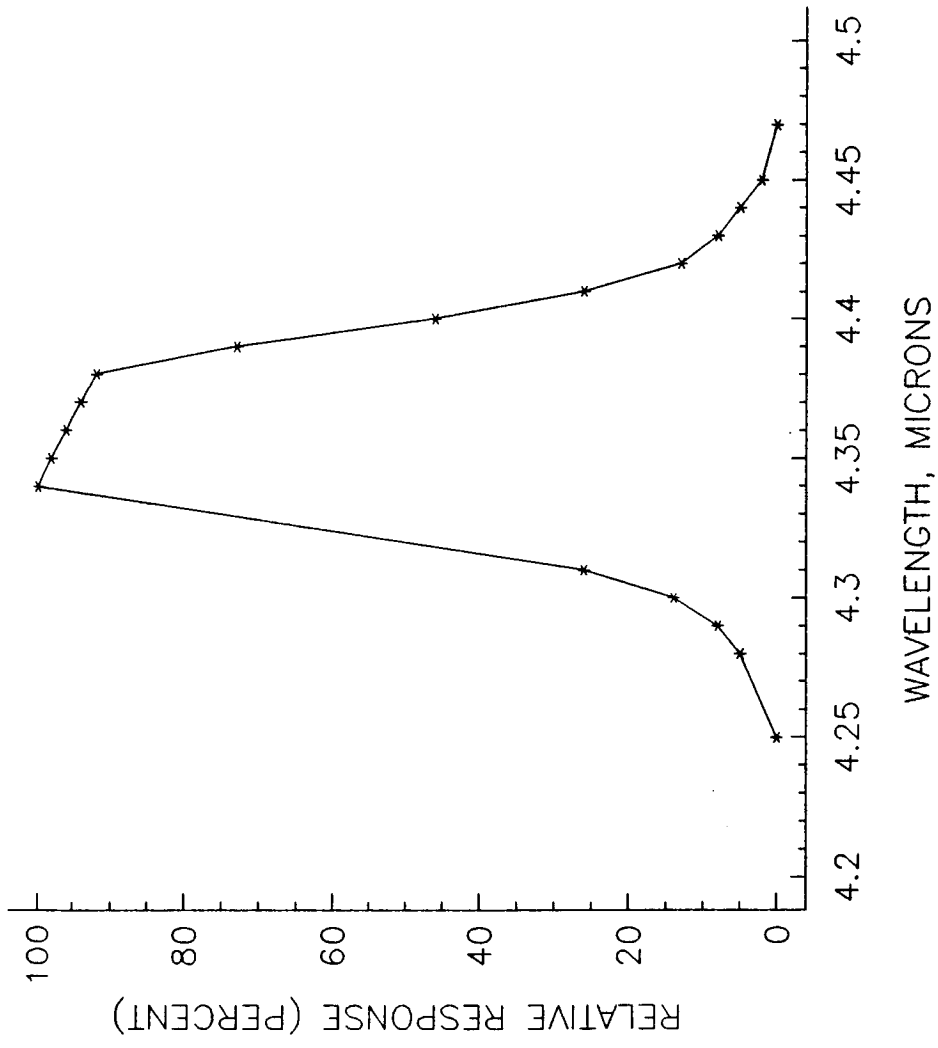

Figure 3.2 Normalized Radiometer Filter Calibration

$$N_T = N_r + \frac{S \quad V}{K_s} \qquad (3.4)$$

3.3 Experimental Method

When attempting to measure a flame temperature, it cannot be assumed that the flame is a blackbody (emissivity = 1). The flame emissivity must be determined experimentally. Neglecting the effects of the surrounding atmosphere and assuming the flame is at a uniform temperature, we seek the flame spectral emittance, $\varepsilon_{\lambda_1 f}$, at λ_1, chosen to be 4.4 μ for our study in order to collect CO_2 radiation, since CO_2 is plentiful in combustion products. The following definitions will be used :

$\alpha_{\lambda_1 f}$ (spectral absorptance of the flame) = $\varepsilon_{\lambda_1 f}$ (spectral emittance of the flame)

$\tau_{\lambda_1 f}$ (spectral transmittance) such that $1 = \alpha + \tau$

Since the voltage measured by the radiometer is a measure of the radiation intensity, voltages and radiation intensity will be thought of as interchangeable in the following analysis. This method[48] requires four voltages to be obtained (see figure 3.3):

V_o = blackbody covered with shutter

V_{bb} = blackbody radiation only

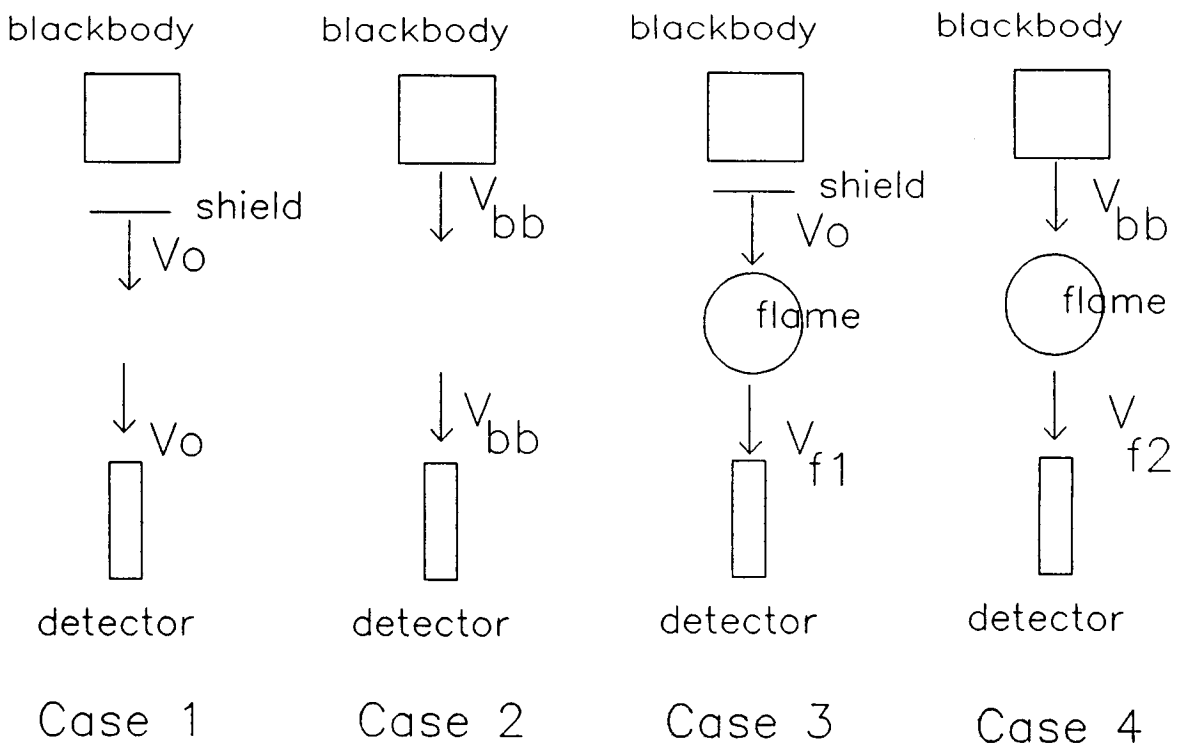

Figure 3.3 Required Voltage Readings for Radiometer Flame Temperature Measurements

V_{f1} = flame radiation only

V_{f2} = flame plus transmitted blackbody radiation

Two equations can be written for cases 3 and 4 seen in figure 3.3:

$$V_{f1} = V_o \tau_{\lambda_1 f} + \alpha_{\lambda_1 f} V_{\lambda_1 bf} \qquad (3.5)$$

$$V_{f2} = V_{bb} \tau_{\lambda_1 f} + \alpha_{\lambda_1 f} V_{\lambda_1 bf} \qquad (3.6)$$

where $V_{\lambda_1 bf}$ is the voltage that would be recorded if the flame were a blackbody. Since the flame is not a blackbody, this voltage (radiation intensity) must be multiplied by the flame absorptance in these equations.

Subtraction of equations (3.5) and (3.6) yields:

$$V_{f2} - V_{f1} = \tau_{\lambda_1 f} \left(V_{bb} - V_o \right)$$

which can be solved for the flame transmittance:

$$\tau_{\lambda_1 f} = \frac{V_{f2} - V_{f1}}{V_{bb} - V_o} \qquad (3.7)$$

Now, either equation (3.5) or (3.6) can be used to find $V_{\lambda_1 bf}$, the voltage that would be measured if the flame were a blackbody source radiating at the flame temperature. For example, using equation (3.5):

$$V_{\lambda_1 bf} = \frac{V_{f1} - V_o \tau_{\lambda_1 f}}{\alpha_{\lambda_1 f}}$$

which, upon using $\alpha = 1 - \tau$, becomes:

$$V_{\lambda_1 bf} = \frac{V_{f1} - V_o \tau_{\lambda_1 f}}{1 - \tau_{\lambda_1 f}} \qquad (3.8)$$

Returning to the radiometer equation (3.4), using the voltage $V_{\lambda_1 bf}$ which corrects the flame to a "black" flame, an N_T is determined which is the effective flame radiance corrected for flame emittance.

$$N_T = N_r + \frac{S V_{\lambda_1 bf}}{K_s} \qquad (3.9)$$

Using this N_T, the corresponding flame temperature is found from our table (or curvefit to this table).

With this method, if there is soot in the flame, the soot will also radiate in the 4.4 μ wavelength along with the CO_2. It is unnecessary to differentiate between the radiation from the soot and the radiation from the CO_2, however. This is because the CO_2 and soot are approximately at the same (flame) temperature and will both produce radiation which will be interpreted by the radiometer and converted to the flame temperature. Of course, the flame emissivity will be different when there is soot, but the emissivity is measured and taken into account by the calculations when determining the flame temperature.

3.4 Thermocouple Temperature Measurements

An energy balance between convection to and net radiation away from the spherical thermocouple bead is required to extract the true gas temperature from the bead temperature reading. By aligning the leads along an isotherm, it is assumed that there is no conduction down the leads. The convective heat transfer coefficient is approximated using Nusselt number (Nu) correlations, where for a sphere in the creeping flow regime:

$$Nu = \frac{hD}{k} = 2 + 0.37\ Re^{0.6}\ Pr^{0.33} \qquad (3.10)$$

for all Reynolds (Re) and Prandtl (Pr) numbers of interest in the flat flame flow field. Here h is the average heat transfer coefficient (watt/m^2-^{0}K), D is the bead diameter (m), and k is the gas thermal conductivity (w/m-^{0}K). For the propane/oxygen flame, assuming only water and carbon dioxide products, for each mole of propane, 4 moles of CO_2 and 3 moles of H_2O are formed. The thermal conductivities of CO_2 and H_2O are found as a function of temperature[49] and then $k = 4/7\ k_{CO_2} + 3/7\ k_{H_2O}$.

An energy balance is then made around the thermocouple bead using an optically thin approximation, where the gas and soot particles emit but do not attenuate radiation. Radiation is exchanged between the bead, the burner surface, the

upper stabilizing plate, the gases, the soot, and the ambient atmosphere. Surfaces are assumed to be in local thermal equilibrium, diffuse and gray, except for the ambience, which is assumed to be black. The net radiation flux out of the bead is then:

$$q''_r = \varepsilon_b\sigma T_b^4 - \alpha_b F_{bp}\varepsilon_p\sigma T_p^4 - \alpha_b F_{bB}\varepsilon_B\sigma T_B^4 - \alpha_b F_{bs}\varepsilon_s\sigma T_s^4 - \alpha_b F_{bg}\varepsilon_g\sigma T_g^4 - \alpha_b F_{b\infty}\sigma T_\infty^4 \qquad (3.11)$$

where the subscripts indicate b, bead, p, upper plate, B, burner surface, s, soot, g, gas, and ∞, ambient. ε is the emissivity; α is the absorptivity; and F_{ij} are view factors.

Kirchoff's law and the gray assumption are used to substitute the emissivity for the absorptivity of the bead. This emissivity is found as a function of temperature from[50]:

$$\varepsilon_b = 1.507\text{x}10^{-4}T_b - 1.596\text{x}10^{-8}\,T_b^2 \qquad (3.12)$$
$$0 < T_b < 2230\ \text{K}$$

The emissivities of the steel plate and bronze burner surface are approximately[51] $\varepsilon_p \approx 0.3$ and $\varepsilon_B \approx 0.1$. The emissivity of the gases are found from:

$$\varepsilon_g = \varepsilon_{CO_2} + \varepsilon_{H_2O} - \Delta\varepsilon \qquad (3.13)$$

Where the ε of each of the gases is dependent on the partial pressure and the pathlength through the gas

from the bead. Figures showing the emissivities for carbon dioxide and for water vapor are found in Siegel and Howell[51]. The $\Delta\varepsilon$ corrects for the spectral overlap of the absorption bands of CO_2 and H_2O and was found to be negligible for this small flame (pathlength = 15 mm). Then $\varepsilon_g \approx 0.025 + 0.0095 - 0 = 0.0345$.

The shape factors were determined using a model[51] of a sphere over a circular plate (radius = 3 cm), giving $F_{bp}=F_{bB}= 0.276$, then $F_{b\infty}= 1-F_{bp}-F_{bB} = 0.448$, while the gas surrounding the bead gives $F_{bg}=1$. There was no soot present in the flame for the thermocouple measurements. This reduces equation 3.11 to:

$$q_r'' = \varepsilon_b\sigma\left[T_b^4 - 0.0828\ T_p^4 - 0.0276\ T_B^4 - 0.0345\ T_g^4 - 0.448 T_\infty^4\right]$$

This radiative heat transfer is balanced by the convective heat transfer $q_c'' = h\Delta T = q_r''$, where $\Delta T = T_g - T_b$, so the gas temperature is found from:

$$T_g = T_b + \frac{\varepsilon_b\sigma}{h}\left[\ T_b^4 - 0.0828\ T_p^4 - 0.0276\ T_B^4 - 0.0345\ T_g^4 - 0.448\ T_\infty^4\ \right] \qquad (3.14)$$

Iteration is required since the gas conductivity is a function of temperature and this equation includes a fourth power term in T_g. For example, for a thermocouple reading of 1780 K, the burner surface was nearly 800 K, the plate was approximately 1000 K, and the gas temperature was:

$T_g = 1780 + 58 - 0.47 - 0.07 - 2.42 - 0.02 = 1835$ K

This shows that the major contributions to the thermocouple correction comes from the radiation loss from the bead itself and from the additional radiation from the hot flame gases. The contributions from the burner surface, the plate and the ambient atmosphere were negligible. An error analysis on this method[52,53] showed the ΔT ($= T_g - T_b$) to be accurate to ±15% in a non-sooting flame, with an error in T_b of ±3% and the error in T_g to be approximately the same as that of T_b.

3.5 Results

The flame temperature as determined by the radiometer is seen as a function of equivalence ratio in figure 3.4a, for three cold gas velocities: 6, 9 and 12 cm/s at a height above the burner of 15 mm. These flames were non-sooting in order to allow comparison with fine wire (.08 mm diameter) platinum-platinum/rhodium thermocouples. For the higher flow rates (9 and 12 cm/s), there is an increase in temperature with an increase in equivalence ratio until nearing stoichiometric. The temperature dips near stoichiometric, then continues to climb until near an equivalence ratio of 1.3, the temperature begins to drop again. This is characteristic of the flat flame burner. The flame speed increases with increasing equivalence ratio and begins to nestle closer to the water-cooled

burner surface, losing heat to the burner. Since the flame speed is maximum at stoichiometric, the greatest heat loss to the burner is seen here, even though the flame temperature should be the highest. Above stoichiometric, the flame speed begins to decrease, allowing the flame to lift farther from the burner surface and become more adiabatic. This lessening of the heat transfer to the burner overcomes the lowering of the flame temperature due to equivalence ratio. This is seen as an overall increase in the flame temperature until the equivalence ratio effect wins out when the flame has reached a position far enough away from the burner to be essentially adiabatic. At this point (near an equivalence ratio of 1.3), the temperature begins to drop with an increase in equivalence ratio. The low flow rate case (6 cm/s) has a low enough flow velocity that the flame is nearly at the same position for all equivalence ratios. The temperature increases with increasing equivalence ratio to near stoichiometric and decreasing thereafter, not showing the effect of changing flame speeds.

The comparison of fine wire thermocouple readings with the radiometer temperature measurements of figure 3.4a is seen in figure 3.4b. The 45-degree line shows where perfect agreement would occur. The two techniques are very good for temperatures below 1700 degrees K. Above this temperature, radiation losses from the thermocouple begin to have greater effect and the thermocouple reads

low. The thermocouple readings for the 12 cm/s case were corrected for this radiation loss and are seen as solid symbols in figure 3.4b. This correction does not fully account for the difference in temperature measurement between the radiometer and thermocouple. To further improve the correction, it would be worthwhile taking electron micrographs of the thermocouple bead to verify its sphericity. Also, the flame radiation contribution was not easily determined and could have increased the thermocouple readings, resulting in better agreement with the radiometer measurements.

The radiometer was then used to measure a sooting flame temperature as a function of equivalence ratio for a cold gas velocity of 3.4 cm/s, at a height above the burner of 15 mm. This temperature is shown in figure 3.5 along with the soot volume fraction as measured by scattering/extinction for the same flame. As expected, the flame temperature decreases with increasing (rich) equivalence ratio, as the soot volume fraction increases and radiates heat to the environment.

Figure 3.4a Flame Temperature Determined by Radiometry

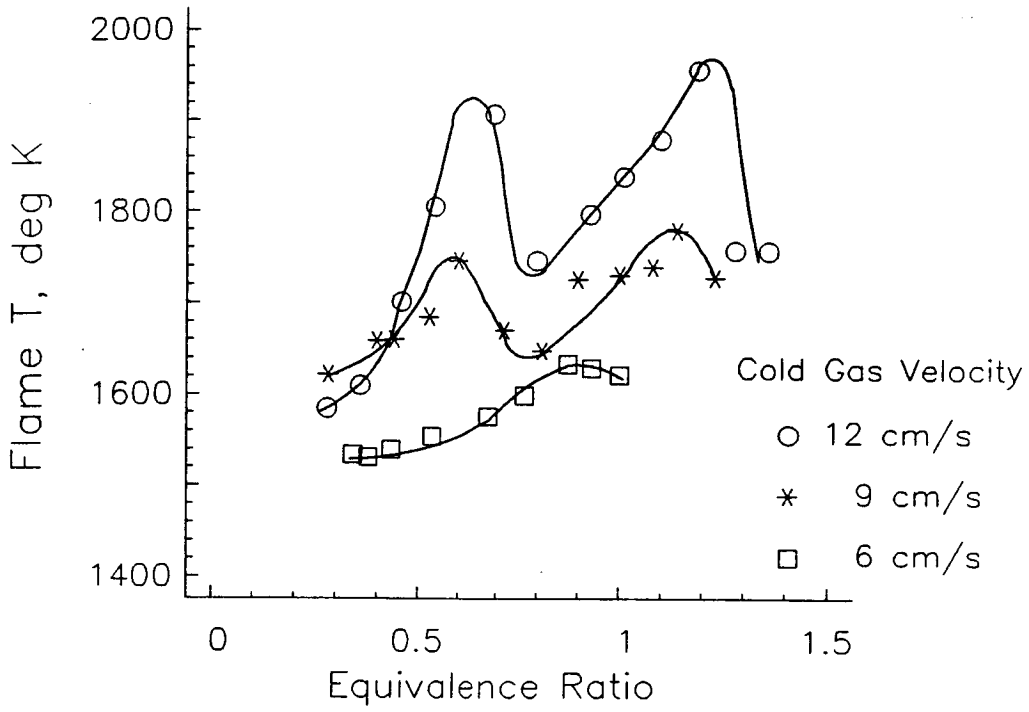

Figure 3.4b Comparison of Radiometer and Thermocouple Temperature Measurements

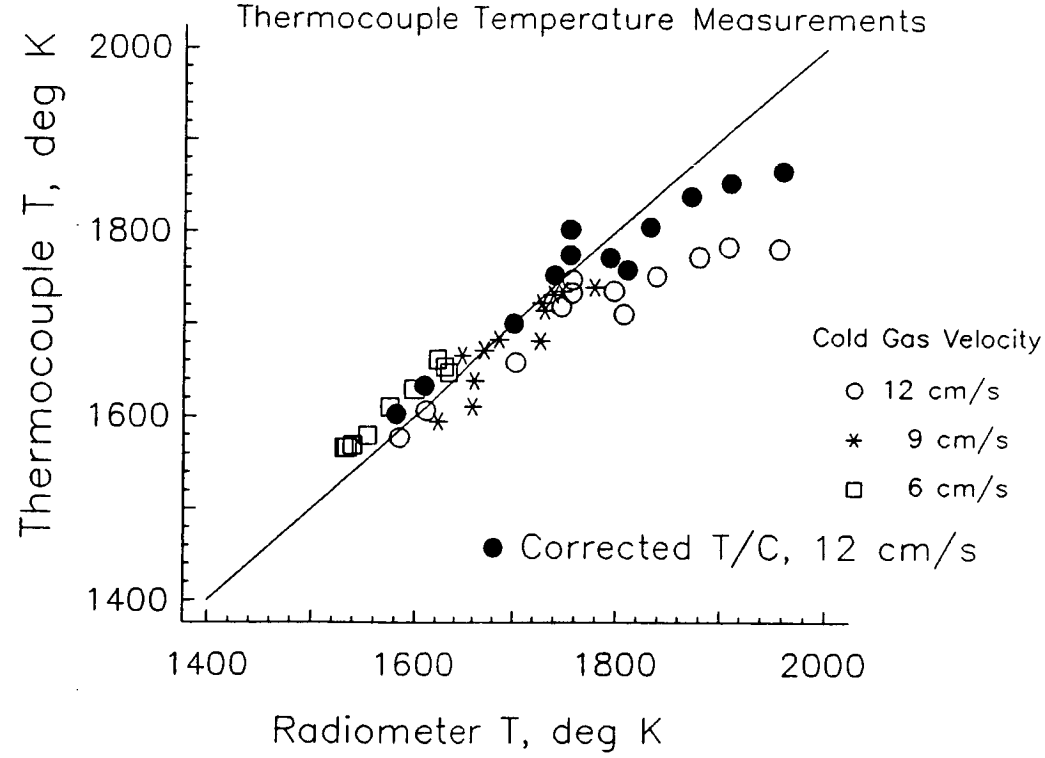

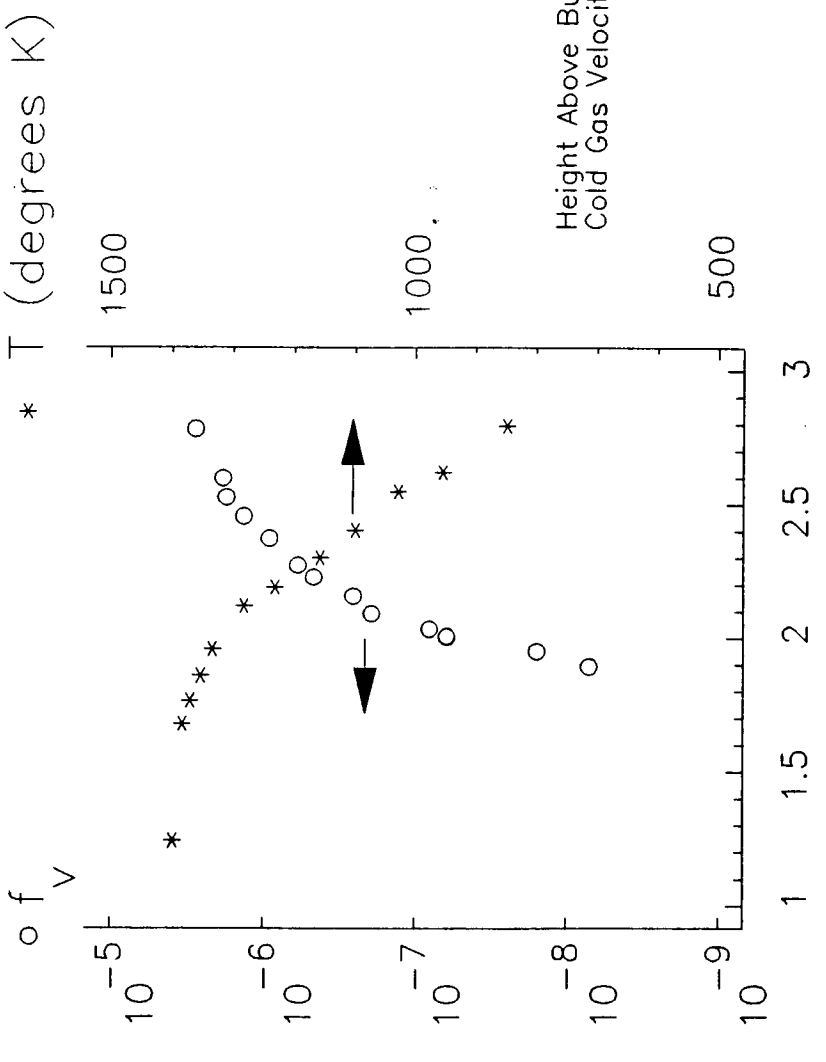

Figure 3.5 Soot Volume Fractions and Flame Temperatures as a Function of Equivalence Ratio.

Chapter 4: Scattering/Extinction Technique Apparatus and Procedure

4.1 Apparatus

A four-watt argon ion laser (Lexel Model 95-4), operating in multi-line mode, was used as the light source for the scattering and absorption measurements. The laser and all optical components were mounted on a Newport honeycomb table (Model RS-410-12) with four vibration isolation support legs. The overall optical system is seen in figure 4.1. A polarization rotator (Lexel Model 506) was used to vertically polarize the light which was then focused into the test section using a 400-mm focal length, uncoated achromatic lens. In order to distinguish the laser light from the background radiation, a light chopper (Ithaco Model 220) operating at 400 hz. was used just before the 400-mm lens. The $1/e^2$ diameter of the beam at the focus, d, with an unfocused beam diameter, d_o, of 1.3 mm for a wavelength, λ, of 514.5 nm, was[1]:

$$d = \frac{4 \lambda f}{\pi d_o} = 0.21 \text{ mm}$$

Two 2.5-mm diameter beam stops were placed after the 400-mm lens, 10-cm and 20-cm away, in order to prevent stray laser light produced by reflection from the lens surfaces from reaching the test section. After passing

Figure 4.1 Sketch of Scattering/Extinction Apparatus

1) Argon Laser
3) Mirrors
7) Cathetometer
8) Apertures
9) Lenses
10) Polarizer
11) 1 mm Pin Hole
12) Line Filters
13) Photomultiplier Tube
14) Burner
16) Prisms
17) Neutral Density Filter
19) Lock-In Amplifiers
20) A/D Card
21) PC
22) Light Shield
23) Polarizer Rotator
24) Light Chopper

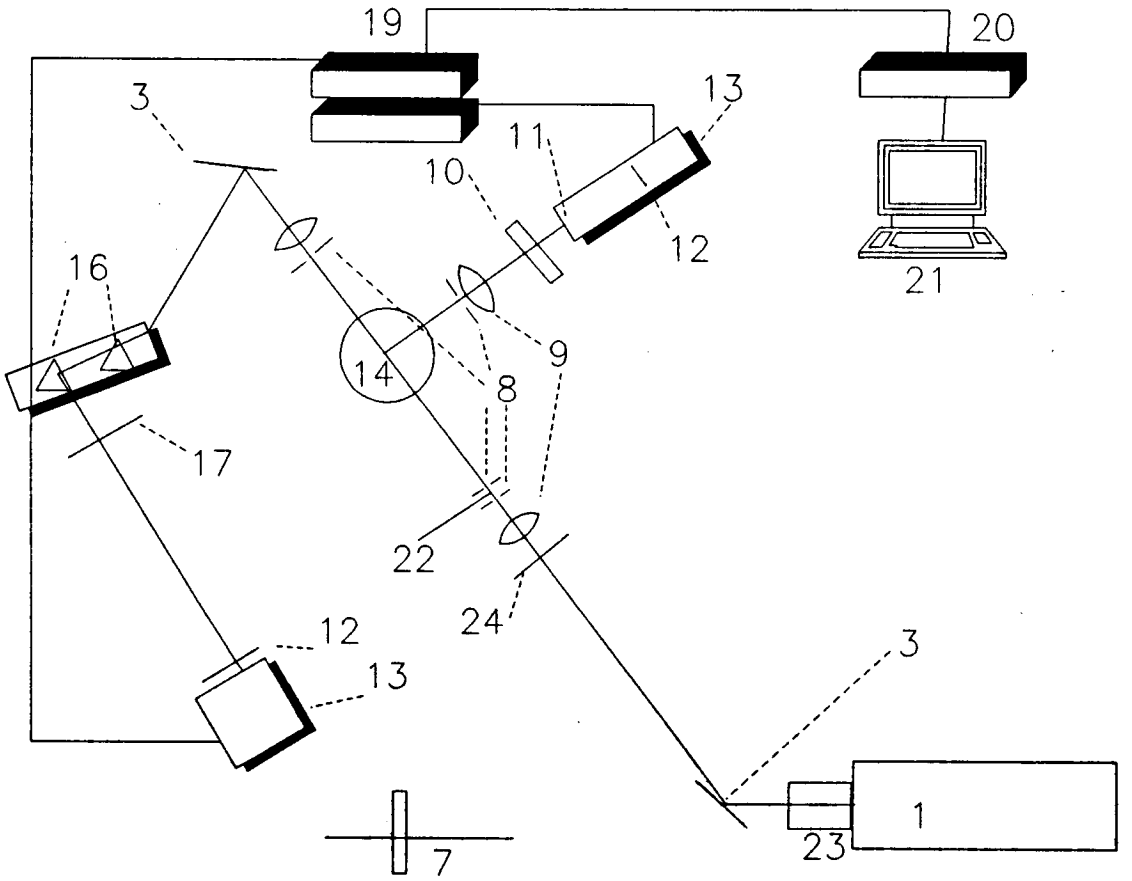

through the flame the light was then collected by a 160-mm focal length lens which was preceded by a 5-mm beam stop to reduce flame radiation to the collection optics and focused onto a photomultiplier (TSI Model 9162) after passing through a neutral density filter (ND=3) to lower the light intensity to a level compatible with the highly sensitive detector. A 514.5 ±10nm laser line filter (Melles Griot Model 03 FIL 004) was also placed in front of the detector to reduce the flame radiation to the photomultiplier. The transmitted intensity was very sensitive to small changes in beam direction due to the Schlieren effects in the flame. This was overcome by using a lens to focus the test section onto the photomultiplier. The photomultiplier signal was sent to a lock-in amplifier which only amplified the laser light which was in constant phase with the chopper (400 hz.). This method eliminated any constant radiation from the flame from being included in the signal.

The scattered light at 90 degrees to the beam path was measured by a separate photomultiplier/lock-in amplifier system. The scattered light detecting system consisted of a 10-mm diameter light stop (Oriel Model 7136) just before a 160-mm focal length focusing lens, a polarization analyzer (Oriel Model 2730), a pin-hole (1 mm) aperture and a very narrow bandwidth (514.5 ±1 nm) line filter (Oriel Model 52660) placed on the end of a 15-cm long

black cylinder which was placed on the front of an end-window photomultiplier (Thorn EMI Model 9789-B). The light stop (10-mm diameter) cut down on the amount of flame radiation to the scattering system. The lens focused the test section center on the 1-mm pin-hole aperture which determined the solid angle over which the scattered light was collected. The scattering system was set up to have unity magnification by placing the 160-mm focal length lens 320 mm from the laser beam and 320 mm from the pin-hole aperture. After the polarization rotator on the laser output was adjusted to produce maximum signal (vertically polarized), the polarization analyzer was adjusted to measure vertically-polarized scattered light only. The narrow band line filter was used to reduce the background radiation from the flame. The photomultiplier output was processed through a lock-in amplifier (EG&G Model 5207) and sent to an analog-digital converter (Metrabyte Model DASH-16) installed in an IBM-PC/AT computer.

The alignment procedure for this optical system required first assuring that the laser beam was parallel to the table top by using two alignment blocks (metal plates with 1-mm pin-holes in the same place on each block). The laser beam was adjusted using a beam steering device consisting of two mirrors on a vertical support (Newport Research Model 675) placed in front of the argon ion laser output. After adding the lenses and focusing

the beam on the test section (in the center of the flat flame burner), other optical components were added to the optical path one at a time, checking each time to be sure the beam path was not deflected. A cube beam-splitter was used to align the scattering detector. The cube beam-splitter was placed at the test section and small pins were placed at ninety-degree intervals perpendicular to the center of each cube face to allow the laser light to be split into three beams (see figure 4.2). The beam-splitter was positioned so the beam 90 degrees to the main optical path was also parallel to the table surface. This beam was then used to align the optical components for the scattering system. The polarization analyzer position was determined by rotating the analyzer until a minimum scattering signal was read by the photomultiplier while the laser light was scattered from nitrogen gas molecules. The analyzer was then rotated 90 degrees to maximize the laser power. This technique allowed a more exact positioning of the analyzer since at low power a small change in position produced a more noticeable change in signal than at high power.

The calibration of the electronic instruments was carried out in accordance with the instrument manuals. Neutral density filters of known optical densities were introduced singly and in combinations into the optical path to verify the linearity of the optics and electronics.

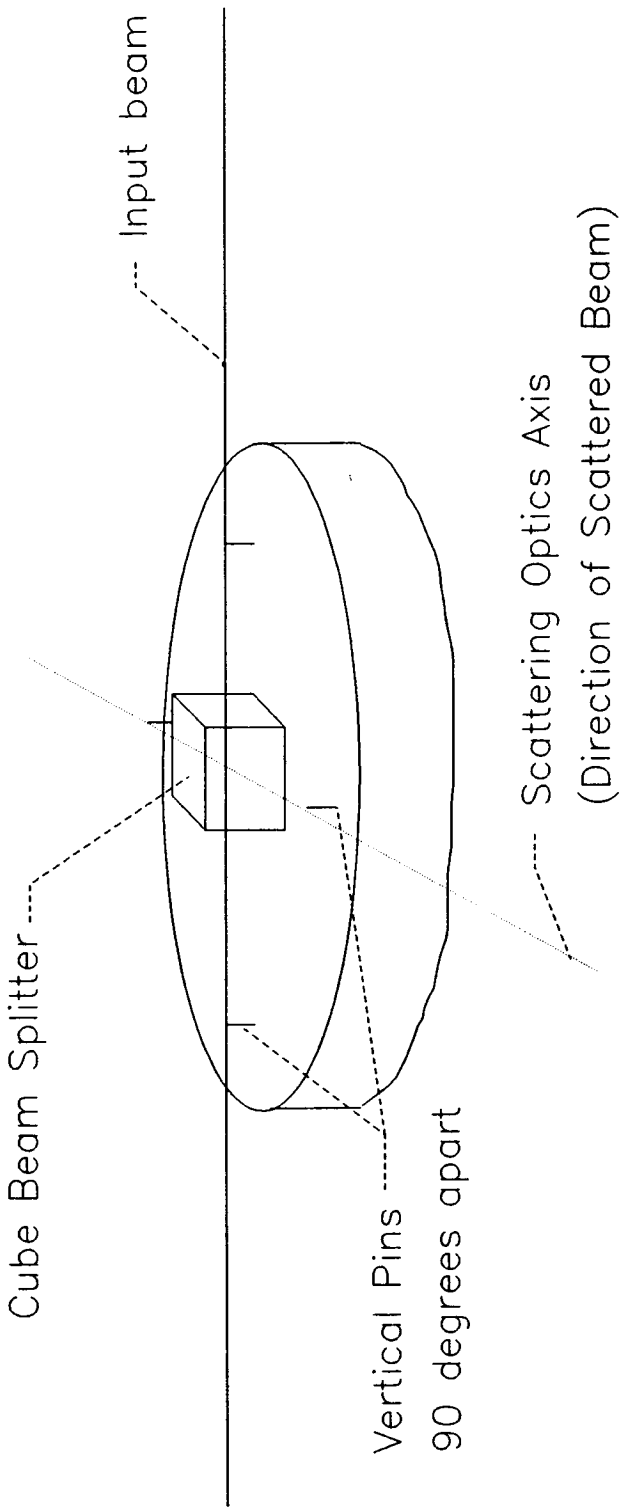

Figure 4.2 Method of Defining Axis for Scattering Optics

4.2 Calibration Theory

By using a gas with a known scattering cross section, σ_o, the optical system can be calibrated and then used to determine the soot volume fraction. This scattering cross section is the apparent area that an object presents to an incident beam that represents its ability to deflect radiation from that beam. This apparent cross section depends not only on the physical size of the particle, but also on its shape, optical properties, and the wavelength, polarization and coherence of the incident radiation. The ratio of σ_o to the actual geometric cross section is called the efficiency factor, Q_{sca}.

The scattering cross section for nitrogen and other gases was determined experimentally by Rudder and Bach.[54] Using the nomenclature seen in figure 4.3 and following the derivation of Siegel and Howell[51], the ratio of the portion of the incident intensity scattered to all 4π steradians, di_t (shown as $di_{\text{total scattered}}$) to the intensity i of the incident beam is equal to the ratio of the apparent projected scattering area dA_{app} occupied by all scattering particles, to the cross-sectional area of the incident beam dA. So, for a beam of a particular

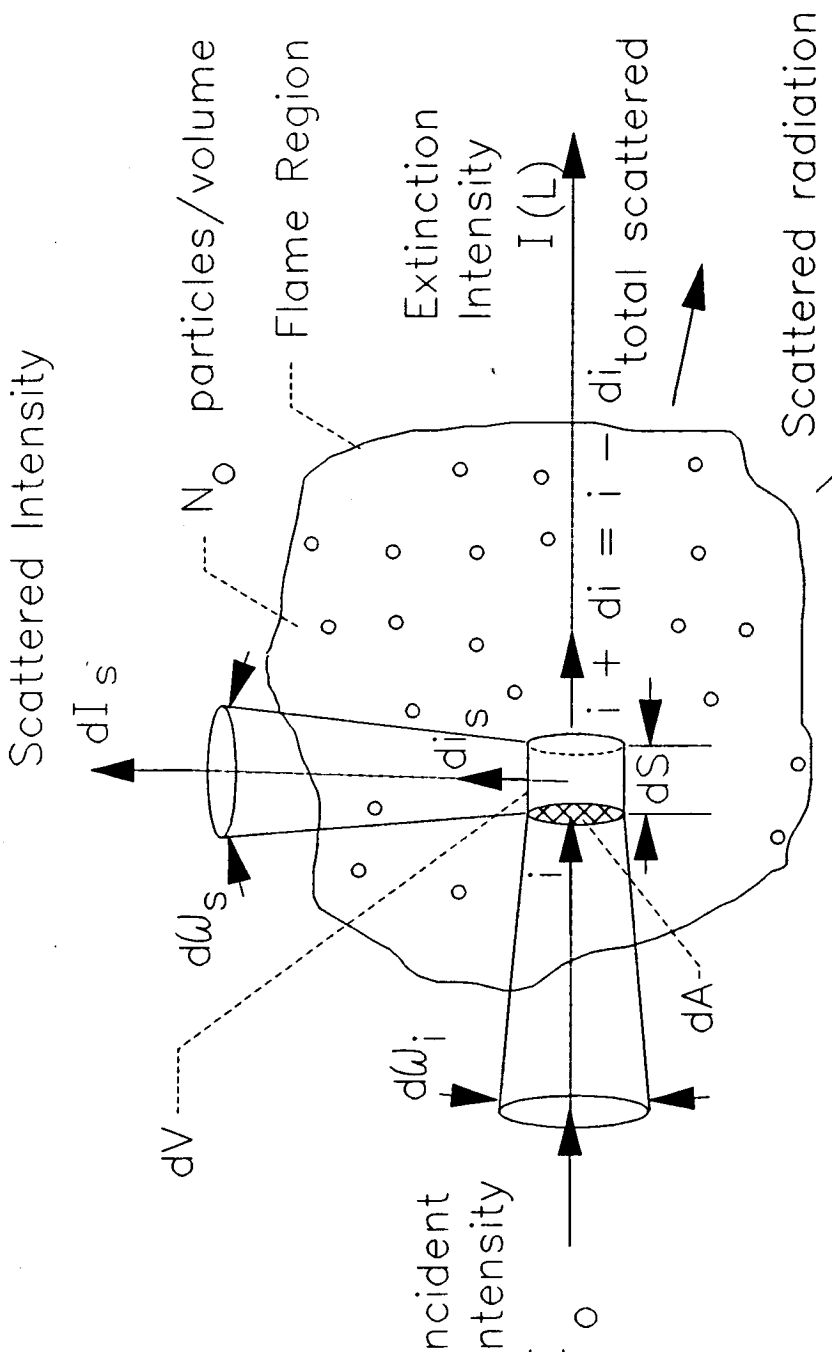

Figure 4.3 Light Scattering from particles as measured perpendicular to the incoming beam path and perpendicular to its plane of polarization

wavelength, λ, traveling a differential distance, dS, within a medium in which it encounters a scattering area dA_{app}:

$$\frac{d\ i_t}{i} = \frac{d\ A_{app}}{d\ A} \tag{4.1}$$

The apparent scattering area presented by a group of particles of number density N_o, having a uniform scattering cross section σ_o in a differential volume dV would be:

$$dA_{app} = \sigma_o\ N_o\ dV = \sigma_o\ N_o\ dA\ dS \tag{4.2}$$

The change, di, of the incident intensity due to scattering from the differential volume can be found from using (4.2) in (4.1):

$$-\frac{d\ i}{i} = \frac{d\ i_t}{i} = \frac{\sigma_o\ N_o dA\ dS}{dA} = \sigma_o\ N_o\ dS \tag{4.3}$$

For a finite, cylindrical probe volume of length S_p (see figure 4.3), integrating (4.3) over a path from 0 to S_p, the resulting intensity at S_p due <u>only</u> to scattering from a beam with original intensity i is:

$$i(S_p) = i\ \exp\left(-\int_0^{S_p} \sigma_o\ N_o dS^*\right) \tag{4.4}$$

This means that the portion of the incident intensity

scattered away along the path S_p is:

$$i - i(S_p) = i \left[1 - \exp\left(- \int_0^{S_p} \sigma_o N_o dS^* \right) \right] \qquad (4.5)$$

This represents the amount of light scattered in all directions.

The magnitude of the intensity scattered in a given (ϕ,θ) direction, $i_d(\phi,\theta)$ depends on the phase function[51,55] $\Phi(\phi,\theta)$, which describes the angular distribution of the scattered energy:

$$i_d(\phi,\theta) = \frac{\Phi(\phi,\theta)}{4\pi} \left[i - i(S_p) \right] \qquad (4.5a)$$

The physical interpretation of the phase function is the scattered intensity in a direction divided by the intensity that would be scattered in that direction if the scattering were isotropic.[51] For the special case of Rayleigh scatterers with an incident beam perpendicularly polarized with respect to the scattering plane, the scattered intensity in the scattering (yz) plane is independent of angle and is given by Kerker[56] as:

$$i_d = \frac{16\pi^4 a^6}{\lambda^4} \left| \frac{m^2 - 1}{m^2 + 2} \right|^2 \qquad (4.5b)$$

Here, a is the particle radius. For this same case, the

total intensity scattered in all directions (also known as the scattering cross section) is given by:

$$i - i\,(S_p) = \frac{128\,\pi^5\,a^6}{3\,\lambda^4}\left|\frac{m^2-1}{m^2+2}\right|^2 \qquad (4.5c)$$

Using equations (4.5b) and (4.5c) in (4.5a), the phase function can be solved for:

$$\frac{16\,\pi^4 a^6}{\lambda^4}\left|\frac{m^2-1}{m^2+2}\right|^2 = \frac{128\,\pi^5\,a^6}{3\,\lambda^4}\left|\frac{m^2-1}{m^2+2}\right|^2 \frac{\Phi}{4\pi}$$

$$\therefore\ \Phi = \frac{(16)(3)(4)}{128} = \frac{3}{2} \qquad (4.5d)$$

So, for the position of the photodetector in the present study, the intensity seen by the detector is:

$$i_s = i_d(90^o, 90^o) = \frac{3}{8\,\pi}\left[\,i - i(S_p)\right] \qquad (4.5e)$$

In terms of the scattering coefficient, Q_{vv} :

$$Q_{vv} \equiv \sigma_o\, N_o \qquad (4.6)$$

equation (4.4) then becomes:

$$i(S_p) = i\ \exp\left(-\int_0^{S_p} Q_{vv}(S^*)\,dS^*\right) \qquad (4.7)$$

Equation 4.7 is the pure scattering form of Bouguer's law.[51] This can be generalized to particles having a

distribution of sizes in a radius range from R to R+dR where $\sigma(R)$ is the scattering cross section for a particle of radius R, and N(R)dR is the number of particles per unit volume. Then by integrating over all the particle sizes, the scattering coefficient becomes:

$$Q_{vv} = \int_0^\infty \sigma(R)\ N(R)\ dR \qquad (4.8)$$

There are also losses due to absorption as well as scattering as the beam travels along a pathlength s. This is described by Beer's law in which the extinction coefficient K is defined:

$$\frac{I(s)}{I_o} = \exp\ (-K\ s) \qquad (4.9)$$

Using the notation shown in figure 4.4, and equation (4.9), the following relations can be made between the intensities:

$$\frac{I_s}{i_s} = e^{-Kd} \quad \text{represents attenuation along d} \qquad (4.10)$$

$$\frac{i}{I_o} = e^{-K\ell} \quad \text{represents attenuation along } \ell \qquad (4.11)$$

Using equation (4.7), taking into account the phase function factor (see equation (4.5e)), and assuming a uniform flow field in which Q_{vv} is not a function of

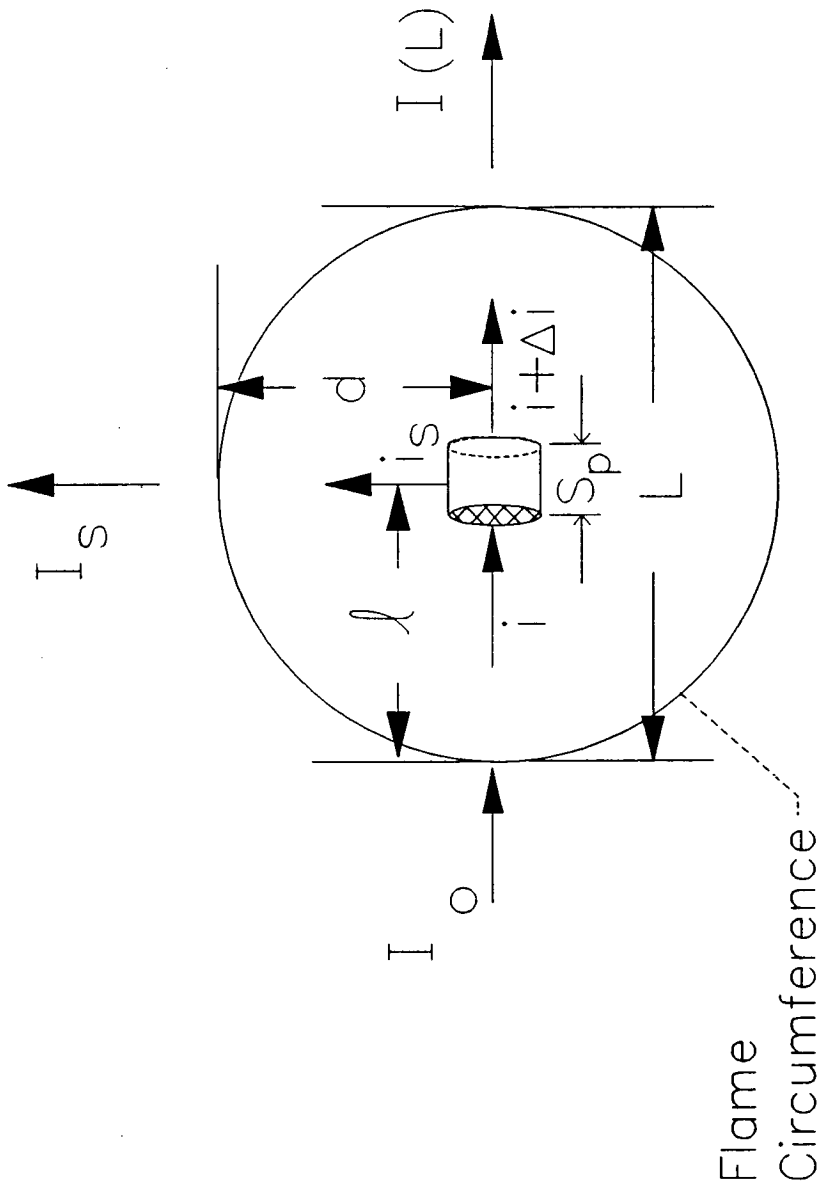

Figure 4.4 Location of probe volume within flame

position, the scattered intensity in the direction of the scattering detector become:

$$\frac{i_s}{i} = \left[1 - \exp\left(-Q_{vv} S_p \right) \right] \frac{3}{8\pi} \qquad (4.12)$$

4.3 Application of Equations

Equations (4.10) through (4.12) can be used to determine the ratio of the measured scattered light to the measured incoming beam intensity if we include a calibration constant C_0 to account for optical and electronic efficiencies in the experimental set-up:

$$\frac{I_s}{I_o} = C_0 \frac{I_s}{i_s} \frac{i}{I_o} \frac{i_s}{i} \qquad (4.13)$$

Substituting for the ratios in (4.13) gives:

$$\frac{I_s}{I_o} = C_1 e^{-Kd} e^{-K\ell} \left[1 - \exp\left(-Q_{vv} S_p \right) \right] \qquad (4.14)$$

Note that the factor from the phase function ($3/8\pi$) has been absorbed into the calibration constant C_0, making C_1. The calibration constant can be determined by measuring the scattered light from a gas with a known scattering cross section. For example, the scattering cross section of nitrogen has been found experimentally by

Rudder and Bach[54] to be $\sigma_{o,N_2} = 2.12 \times 10^{-28}$ cm^2 for scattering 694.3-nm wavelength light. For 514.5 nm light:

$$\sigma_{o,N_2} = 2.12 \times 10^{-28} \left(\frac{694.3}{514.5}\right)^4 = 7.03 \times 10^{-28} \text{cm}^2$$

Then, if nitrogen is chosen as a calibration gas, assuming negligible extinction through the nitrogen, equation (4.14) along with (4.6) becomes for nitrogen:

$$I_{s,N_2} = C_1 I_o \left[1 - \exp\left(-(\sigma_o N_o)_{N_2} S_p\right)\right] \qquad (4.15)$$

If the scattered light from soot particles is now measured using the same optical system, so that the calibration constant, C_1 is the same, equation (4.14) becomes for soot:

$$I_{s,soot} = C_1 I_o \left[1 - \exp\left(-Q_{vv,soot} S_p \right)\right] e^{-K(\ell+d)} \qquad (4.16)$$

Dividing equation (4.16) by equation (4.15) gives:

$$\frac{I_{s,soot}}{I_{s,N_2}} = \frac{1 - \exp\left(-Q_{vv,soot} S_p \right)}{1 - \exp\left(-(\sigma_o N_o)_{N_2} S_p \right)} e^{-K(\ell+d)} \qquad (4.17)$$

For this experimental set-up, S_p was approximately 1 mm, as determined by the 1-mm pin-hole aperture in front of the scattering detector and the unity magnification of the scattering optics. Using the expression:

$$e^x = \sum_{n=0}^{\infty} x^n = 1 + x + \text{higher order terms}$$

for small values of x, $e^x \approx 1 + x$. Since at T = 298 degrees K and P = 1 atm., N_o for nitrogen is approximately 2.46×10^{19} molecules/cm^3:

$$\left(\sigma_o N_o \right)_{N_2} S_p \approx 7.03\text{x}10^{-28} cm^2 \text{x } 2.46\text{x}10^{19} cm^{-3} \text{x } 0.1 \text{ cm}$$
$$\approx 1.73\text{x}10^{-9}$$

and the expansion is quite accurate. $Q_{vv,soot}$ will be larger than the corresponding nitrogen scattering (some experimental results had Q_{vv} as high as $1\text{x}10^{-2}$), but will still be small enough to allow use of the expansion so that equation (4.17) will become:

$$\frac{I_{s,soot}}{I_{s,N_2}} = \frac{\left(1 - \left(1 - Q_{vv,soot} S_p \right) \right)}{\left(1 - \left(1 - \left(\sigma_o N_o \right)_{N_2} S_p \right) \right)} \; e^{-K(\ell+d)} \qquad (4.18)$$

Solving equation (4.18) for Q_{vv} gives:

$$Q_{vv,soot} = \left(\sigma_o N_o \right)_{N_2} \frac{I_{s,soot}}{I_{s,N_2}} \; e^{K(\ell+d)} \qquad (4.19)$$

where $(\sigma_o N_o)_{N_2}$ for the experimental conditions (P= 1 atm., T=298 deg. K) = $1.73\text{x}10^{-8}$ cm^{-1}.

If emission from the flame is eliminated from both the measured scattered and extinction signals by chopping the

incoming laser light and only detecting the signals produced by this light using a lock-in amplifier, the extinction coefficient for a total flame pathlength L is:

$$K = -\frac{1}{L} \ln\left(\frac{I(L)}{I_o} \right) \tag{4.20}$$

which, when substituted for K in equation (4.19) gives the expression for the volumetric scattering cross section, Q_{vv}, for soot as determined from experimental measurements of light scattering and extinction:

$$Q_{vv,\ soot} = \left(\sigma_o N_o \right)_{N_2} \frac{I_{s,soot}}{I_{s,N_2}} \left(\frac{I(L)}{I_o} \right)^{-(\ell+d)/L} \tag{4.21}$$

where d, ℓ, and L are shown in figure 4.4. Note that in the ratio $I(L)/I_o$, the numerator and the denominator are voltages corresponding to light intensities read by the same (extinction) photomultiplier tube, through the same optics, electronics, etc. Also, the ratio $I_{s,soot}/I_{s,N_2}$ was formed from voltages corresponding to light scattering intensities measured by the same (scattering) detector so that any undefined optical or electronic efficiencies (as represented by the constant C_1) divided out. Also, when the probe volume is in the center of the cylindrical flame, ℓ=d=L/2, simplifying the exponent to -1.

4.4 Calibration Procedure

The system was calibrated and the required value of $I_{s,N2}$ was found by using gases of known scattering cross-

sections: nitrogen and methane. The calibration measurements were carried out with nitrogen or methane flowing through the flat flame burner near enough to the burner surface to avoid contamination by air or dust (5 mm above the burner). The ratio of scattered intensity for methane to scattered intensity for nitrogen is theoretically[54] 2.15. If a different ratio was measured, the optical alignment, photomultiplier, or electronic equipment had to be corrected. The nitrogen Rayleigh scattering differential cross-section was chosen as the standard for all measurements. The nitrogen calibration was carried out after each data point (approximately every 30 seconds) to check the optical system.

4.5 Experimental Procedure

Prior to each test, the laser and photomultipliers and electronic instrumentation were allowed to warm up for an hour. The scattering system was checked and calibrated using the nitrogen and methane calibration procedure previously described. The extinction system was checked by flowing nitrogen through the burner and examining the photodetector signal to be sure the detector was not saturated and the lock-in amplifier range was set to an appropriate scale. A reference height above the burner was determined by raising the burner until the laser beam just touched its surface. This was considered the "zero" height above the burner. A reading of the scattered light

from nitrogen was taken with all room lights out and black panels blocking all stray laser light. This reading was taken at a height above the burner of 5 mm since at this low height there is enough nitrogen to prevent mixing of air and dust into the test section.

For each set of data, the following information was recorded and stored in the computer with the raw data:

1. Propane flow rate, temperature and pressure.
2. Laser pathlength through the sooting flame.
3. Oxygen flow rate, temperature and pressure.
4. Burner nitrogen flow rate, temperature and pressure.
5. Shroud nitrogen flow rate, temperature and pressure.
6. Height above the burner.
7. Burner cooling water flow rate, temperature in and out.
8. Scattering detector lock-in amplifier range (this can be extended using neutral density filters of known transmissivity to reduce the scattered intensity when the maximum amplifier range is exceeded).
9. Run number, date and time stored in the computer.

In twenty seconds, a total of 400 data points are taken for each A/D converter channel (each photodetector). These were then averaged and the mean values were used in the data reduction. The data reduction consisted of

determining the experimental values of Q_{VV} (the volumetric scattering coefficient for vertically polarized incident and scattered light) for soot and K, the extinction coefficient.

First, the burner was lit and adjusted to the desired flow conditions, which was determined by use of a computer program to calculate the equivalence ratio and cold gas flow velocity at the burner surface. The flow velocity is an important parameter in a flat flame burner since it affects the flame temperature. It was necessary to keep the flow velocity constant when trying to understand the effect of equivalence ratio or height above the burner on the soot formation process. This required a reduction (/increase) in the oxygen flow when the propane flow was increased (/decreased) when studying the effect of equivalence ratio change at a given height above the burner. Profiles of soot size, number density, and volume fraction at various heights (from 5 to 25 mm) above the burner were also measured at several fixed equivalence ratios. At each height (or at each equivalence ratio), the beam pathlength was measured using a cathetometer. This device is basically a telescope mounted on a vernier scale with cross-hairs in the view-finder to allow a measurement of the distance from one edge of the sooting region of the flame to the other along the laser beam's path. A permanent record of the flame was also made with

a video camera. After the data point was taken with the flame on, the flame was immediately shut off and nitrogen passed through the burner. This allowed a calibration point to be recorded within 30 seconds after the flame data point. This minimized any drift in laser power or electronics with time.

The flame stabilization plate, mentioned in the description of the burner, had to be cleaned after as little as two hours of use, for very sooty flames, to prevent large chunks of soot from falling onto the burner surface. A cover was placed over the sintered metal to prevent soot particles from being dropped onto the burner during this cleaning process. The burner itself required cleaning with a mild acid solution and water rinsing through the sintered metal after several months of use. This was less frequent than expected due to the use of high purity gases (99.995 percent pure methane, 99.95 percent pure propane, and 99.5 percent pure oxygen) to produce the flame.

Chapter 5: Analysis of Scattering/Extinction Technique

5.1 Extinction

For a polydisperse aerosol, the extinction coefficient K in equation (4.9) is defined as:

$$K = \int_0^\infty N(R)\ Q_{ext}(\lambda,m,R)\ \pi R^2\ dR \qquad (5.1)$$

where N(R) is the particle concentration in the size range dR about R, Q_{ext} is the particle extinction efficiency, m is the complex index of refraction, and R is the particle radius. For soot, the real index of refraction, n, and the imaginary index of refraction, nk, together make up the complex index, m = n(1-ik). Table 1 shows the soot index of refraction as a function of wavelength of light. These values are those found by Lee and Tien.[60-61] Assuming homogeneous, spherical soot particles, the extinction efficiency $Q_{ext}(\lambda,m,R)$ is given by the Mie scattering theory[16,56] as:

$$Q_{ext} = \frac{2}{x^2} \sum_{n=1}^{\infty} (2n+1)\left[Re(a_n) + Re(b_n)\right] \qquad (5.2)$$

where

$x = \frac{2\ \pi\ R}{\lambda}$ is the particle size parameter

Table 1

Soot Refractive Indices as a Function of Wavelength of Light

Wavelength (nm)	Refractive Index
457.9	1.94−i0.58
488.0	1.94−i0.54
514.5	1.93−i0.52
632.8	1.89−i0.48
1060.0	1.90−i0.60

$$a_n = \frac{\Psi_n(x)\,\Psi_n'(\beta) - m\,\Psi_n(\beta)\,\Psi_n'(x)}{\mathcal{C}_n(x)\,\Psi_n'(\beta) - m\,\Psi_n(\beta)\,\mathcal{C}_n'(x)}$$

$$b_n = \frac{m\,\Psi_n(x)\,\Psi_n'(\beta) - \Psi_n(\beta)\,\Psi_n'(x)}{m\,\mathcal{C}_n(x)\,\Psi_n'(\beta) - \Psi_n(\beta)\,\mathcal{C}_n'(x)}$$

$$\beta = mx$$

$$\Psi_n(z) = \left(\frac{\pi z}{2}\right)^{1/2} J_{n+1/2}(z)$$

$$\mathcal{C}_n(z) = \left(\frac{\pi z}{2}\right)^{1/2} H^{(2)}_{n+1/2}(z)$$

$J_{n+1/2}(z)$ = half-integral order Bessel functions of the first kind

$H^{(2)}_{n+1/2}(z)$ = half-integral order Hankel functions of the second kind

Re(z) represents the real part of a complex number, z, and primes denote derivatives with respect to the argument.

The size distribution N(R) is given by a three-

parameter Gamma distribution with the constraint of a specified ratio of standard deviation to mean particle radius[57]: $\sigma/R_m = 1/2$. In terms of the most probable radius, R_{max}, and the total particle concentration, N_o, the form of the distribution is:

$$N(R) = N_o \left(\frac{27\ R^3}{2\ R_{max}^4} \right) \exp \left(\frac{-3\ R}{R_{max}} \right) \qquad (5.3)$$

Substituting equations (5.3) and (5.2) into equation (5.1) yields an equation for K in terms of the two unknowns N_o and R_{max}. The other equation needed to determine these two parameters is provided either by extinction measurements at another wavelength (two-wavelength technique) or scattering measurements at the same wavelength (scattering/extinction technique).

5.2 Scattering

Two optical quantities are of interest when considering plane polarized light scattering from a sample volume of a polydisperse aerosol. The first is the size-dependent particle scattering cross section $C_{vv}(\theta,\lambda,R,m)$ (cm^2), which was termed σ_o for gases in chapter 4. This is the intensity of light scattered by particles of radius R within the sample volume at the angle θ measured from the direction of propagation, per unit of incident intensity, per particle. The first subscript denotes

scattered light polarized perpendicularly to the plane of observation, while the second subscript denotes the same polarization state for the incident light[13]. Figure 5.1 indicates the relevant geometry for scattering from a single particle. In the laboratory, incident light propagates along the +z axis in a horizontal (yz) plane (parallel to the table), with its electric vector aligned with the local vertical (x) axis. Scattered light, also vertically polarized, is measured along the y-axis, with $\theta = \phi = 90$ degrees. Where, as seen in figure 5.1, θ is the angle measured from the laser beam path and ϕ is the angle measured from the vertical (x) axis to the scattering detector position.

The second quantity of interest is $Q_{VV}(\theta,\lambda,m)$, the volumetric scattering cross section (cm^{-1}). It is the intensity of light scattered by particles within the sample volume with a size distribution and concentration given by N(R) at the angle θ, per unit of incident intensity. Q_{VV} is given by:

$$Q_{VV}(\theta,\lambda,m) = \int_0^\infty N(R)\ C_{VV}(\theta,\lambda,R,m)\ dR \qquad (5.4)$$

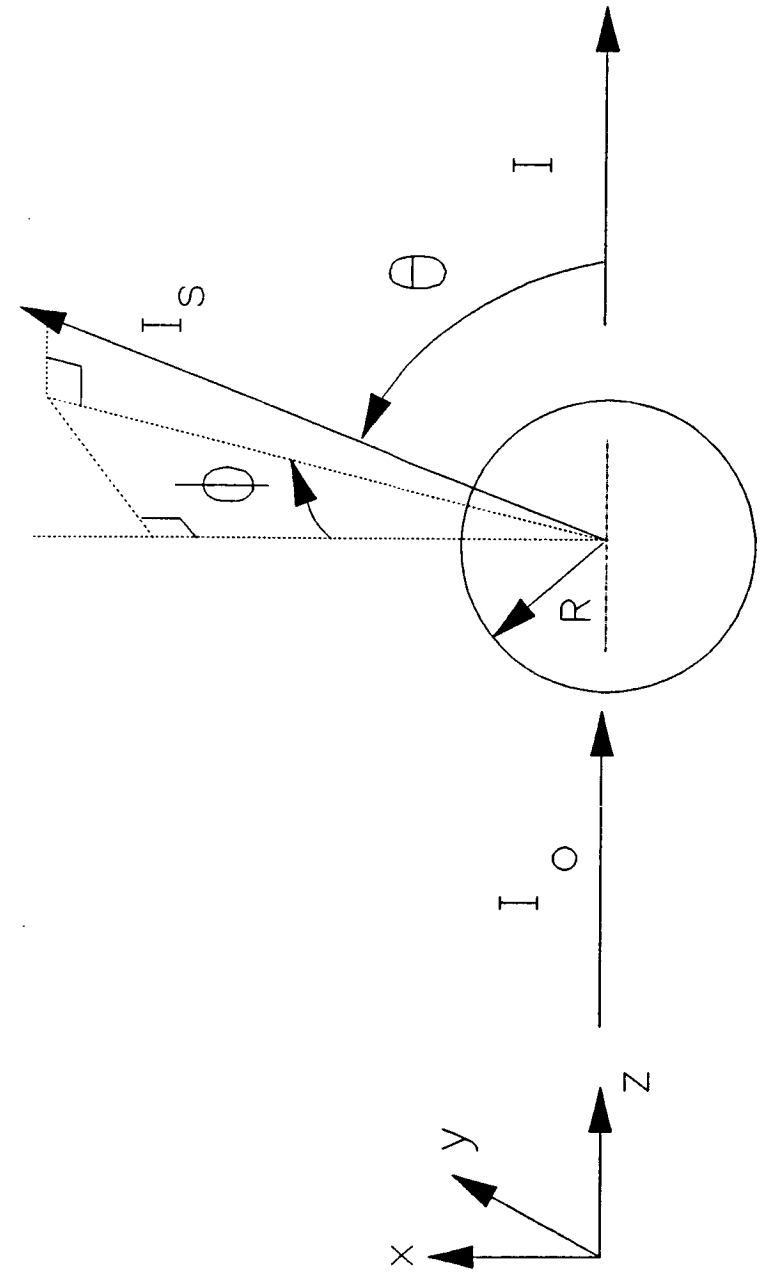

Figure 5.1 Coordinate system for scattering from a soot particle of radius R

Note the distinction between Q_{vv} and the Mie scattering efficiency $Q_{sca}(\lambda,m,R)$, which is defined as the fraction of energy geometrically incident upon a particle of radius R which is scattered in all directions[56].

From Mie scattering theory, C_{vv} is given by:

$$C_{vv}(\theta) = \left(\frac{\lambda}{2\pi}\right)^2 |S_1(\theta)|^2 \sin^2\phi \qquad (5.5)$$

where

$$S_1(\theta) = \sum_{n=1}^{\infty} \frac{2n+1}{n(n+1)} \left[a_n \Pi_n(\cos\theta) + b_n \mathcal{J}_n(\cos\theta) \right]$$

$$\Pi_n(\cos\theta) = \frac{P_n^{(1)}(\cos\theta)}{\sin\theta}$$

$$\mathcal{J}_n(\cos\theta) = \frac{d}{d\theta}\left[P_n^{(1)}(\cos\theta) \right]$$

where $P_n^{(1)}$ are first degree Legendre polynomials of order n. For the geometry of figure 5.1, $\theta = \phi = 90$ degrees. The coefficients a_n and b_n are the same as those in equation (5.2).

Substituting equations (5.5) and (5.3) into equation (5.2) gives a second equation involving N_o and R_{max}. This allows the total particle concentration N_o to be eliminated by dividing equation (5.4) by equation (5.1):

$$\frac{Q_{vv}(\theta,\lambda,m)}{K(\lambda,m)} = \frac{\int_0^\infty \frac{R^3}{R_{max}^4} \exp\left(\frac{-3R}{R_{max}}\right) C_{vv}(\theta,\lambda,R,m)\, dR}{\int_0^\infty \frac{R^3}{R_{max}^4} \exp\left(\frac{-3R}{R_{max}}\right) Q_{ext}(\lambda,R,m)\, \pi R^2 dR} \quad (5.6)$$

Equation (5.6) is then solved numerically for the ratio Q_{vv}/K as a function of R_{max} using the Mie theory computer code from Bohren and Huffman.[58] The integration was performed using a Fortran subroutine from the public domain software at NASA Lewis Research Center (author unknown) based on Simpson's Rule and Newton's 3/8 Rule following Hildebrand.[59] The results of the calculations are shown in figure 5.2. Here the numerator of equation (5.6) is called XI and the denominator is called TAU. Both XI and TAU are plotted as functions of R_{max} and the ratio Q_{vv}/K_{ext} is also shown as a function of R_{max} in figure 5.2. A table of the values of R_{max}, Q_{vv}/K_{ext}, XI, and TAU is shown in Table 2. When the experimental values of Q_{vv} and K_{ext} are determined using equations (4.20) and (4.21), R_{max} can be found from linear interpolation of this table using the ratio Q_{vv}/K_{ext}. Using equation (5.4), the particle number density, N_o, can be determined upon substitution of equation (5.3):

Figure 5.2 Results of Mie Theory Calculations for Scattering/Extinction Technique

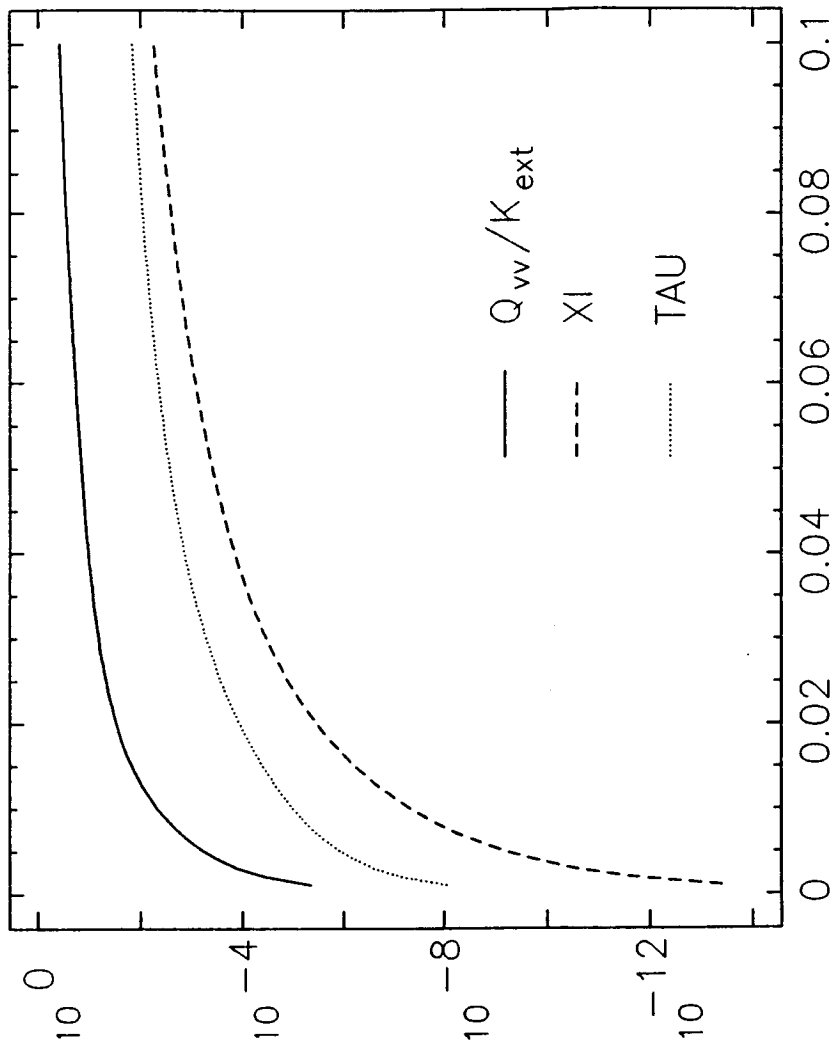

TABLE 2: Mie Theory Calculations for Scattering-Extinction Technique

Rmax (uM)	Qvv/Kext	XI	TAU
1.000E-03	4.519E-06	4.075E-14	9.018E-09
2.000E-03	3.623E-05	2.621E-12	7.236E-08
3.000E-03	1.226E-04	3.011E-11	2.456E-07
4.000E-03	2.916E-04	1.711E-10	5.868E-07
5.000E-03	5.716E-04	6.621E-10	1.158E-06
6.000E-03	9.909E-04	2.010E-09	2.029E-06
7.000E-03	1.577E-03	5.166E-09	3.275E-06
8.000E-03	2.358E-03	1.175E-08	4.983E-06
9.000E-03	3.356E-03	2.434E-08	7.252E-06
1.000E-02	4.593E-03	4.684E-08	1.020E-05
1.100E-02	6.083E-03	8.486E-08	1.395E-05
1.200E-02	7.834E-03	1.462E-07	1.866E-05
1.300E-02	9.847E-03	2.412E-07	2.450E-05
1.400E-02	1.212E-02	3.834E-07	3.164E-05
1.500E-02	1.463E-02	5.897E-07	4.031E-05
1.600E-02	1.736E-02	8.807E-07	5.072E-05
1.700E-02	2.030E-02	1.281E-06	6.311E-05
1.800E-02	2.341E-02	1.819E-06	7.772E-05
1.900E-02	2.666E-02	2.528E-06	9.482E-05
2.000E-02	3.003E-02	3.443E-06	1.146E-04
2.100E-02	3.350E-02	4.605E-06	1.375E-04
2.200E-02	3.704E-02	6.056E-06	1.635E-04
2.300E-02	4.063E-02	7.843E-06	1.930E-04
2.400E-02	4.427E-02	1.001E-05	2.262E-04
2.500E-02	4.792E-02	1.262E-05	2.634E-04
2.600E-02	5.160E-02	1.572E-05	3.046E-04
2.700E-02	5.528E-02	1.935E-05	3.501E-04
2.800E-02	5.897E-02	2.359E-05	4.000E-04
2.900E-02	6.266E-02	2.848E-05	4.545E-04
3.000E-02	6.636E-02	3.408E-05	5.136E-04
3.100E-02	7.005E-02	4.045E-05	5.775E-04
3.200E-02	7.375E-02	4.766E-05	6.462E-04
3.300E-02	7.745E-02	5.576E-05	7.199E-04
3.400E-02	8.116E-02	6.481E-05	7.984E-04
3.500E-02	8.488E-02	7.487E-05	8.820E-04
3.600E-02	8.861E-02	8.600E-05	9.705E-04
3.700E-02	9.235E-02	9.827E-05	1.064E-03
3.800E-02	9.611E-02	1.117E-04	1.162E-03
3.900E-02	9.989E-02	1.264E-04	1.266E-03
4.000E-02	1.037E-01	1.425E-04	1.374E-03
4.100E-02	1.075E-01	1.599E-04	1.487E-03
4.200E-02	1.113E-01	1.788E-04	1.606E-03
4.300E-02	1.152E-01	1.991E-04	1.728E-03
4.400E-02	1.191E-01	2.210E-04	1.856E-03
4.500E-02	1.230E-01	2.446E-04	1.988E-03

TABLE 2 (continued)

Rmax (uM)	Qvv/Kext	XI	TAU
4.600E-02	1.270E-01	2.698E-04	2.125E-03
4.700E-02	1.309E-01	2.968E-04	2.266E-03
4.800E-02	1.350E-01	3.255E-04	2.412E-03
4.900E-02	1.390E-01	3.561E-04	2.562E-03
5.000E-02	1.431E-01	3.887E-04	2.717E-03
5.100E-02	1.472E-01	4.232E-04	2.876E-03
5.200E-02	1.513E-01	4.598E-04	3.038E-03
5.300E-02	1.555E-01	4.984E-04	3.206E-03
5.400E-02	1.597E-01	5.392E-04	3.377E-03
5.500E-02	1.639E-01	5.822E-04	3.551E-03
5.600E-02	1.682E-01	6.275E-04	3.730E-03
5.700E-02	1.725E-01	6.751E-04	3.913E-03
5.800E-02	1.769E-01	7.251E-04	4.099E-03
5.900E-02	1.813E-01	7.775E-04	4.289E-03
6.000E-02	1.857E-01	8.324E-04	4.483E-03
6.100E-02	1.901E-01	8.898E-04	4.680E-03
6.200E-02	1.946E-01	9.499E-04	4.880E-03
6.300E-02	1.992E-01	1.013E-03	5.084E-03
6.400E-02	2.037E-01	1.078E-03	5.291E-03
6.500E-02	2.083E-01	1.146E-03	5.501E-03
6.600E-02	2.130E-01	1.217E-03	5.715E-03
6.700E-02	2.176E-01	1.291E-03	5.931E-03
6.800E-02	2.223E-01	1.367E-03	6.151E-03
6.900E-02	2.271E-01	1.447E-03	6.373E-03
7.000E-02	2.318E-01	1.530E-03	6.598E-03
7.100E-02	2.366E-01	1.615E-03	6.827E-03
7.200E-02	2.414E-01	1.704E-03	7.057E-03
7.300E-02	2.463E-01	1.796E-03	7.291E-03
7.400E-02	2.512E-01	1.891E-03	7.527E-03
7.500E-02	2.561E-01	1.989E-03	7.766E-03
7.600E-02	2.610E-01	2.090E-03	8.007E-03
7.700E-02	2.660E-01	2.194E-03	8.251E-03
7.800E-02	2.709E-01	2.302E-03	8.496E-03
7.900E-02	2.759E-01	2.413E-03	8.745E-03
8.000E-02	2.809E-01	2.527E-03	8.995E-03
8.500E-02	3.062E-01	3.147E-03	1.028E-02
9.000E-02	3.317E-01	3.849E-03	1.160E-02
9.500E-02	3.571E-01	4.629E-03	1.296E-02
1.000E-01	3.822E-01	5.484E-03	1.435E-02

$$Q_{vv} = \frac{27}{2} N_o \int_0^{\infty} \frac{R^3}{R_{max}^4} \exp\left(\frac{-3R}{R_{max}} \right) C_{vv} \, dR = \frac{27}{2} N_o \quad \xi$$

$$\therefore \quad N_o = \frac{2 Q_{vv}}{27 \quad \xi} \tag{5.7}$$

where ξ represents the integral. The soot volume fraction f_v is then given by:

$$f_v = \frac{4 \pi}{3} \int_0^{\infty} R^3 N(R) \, dR \tag{5.8}$$

Substituting equation (5.3) into equation (5.8) and performing the integration gives:

$$f_v = \frac{2 \pi \Gamma(7)}{3^5} N_o R_{max}^3 = 18.62 N_o R_{max}^3 \tag{5.9}$$

5.3 Scattering/Extinction Results

Some results obtained by using the scattering-extinction technique are seen in figures 5.3 and 5.4. In figure 5.3, the soot volume fraction, most probable radius, and number density are shown as functions of the height above burner for an equivalence ratio of 2.5 and three cold gas velocities: 3.92, 4.71, and 5.50 cm/s. Soot first appears near a height above the burner of 2 mm. A very large number (near 10^{12} particles/cm^3) of small

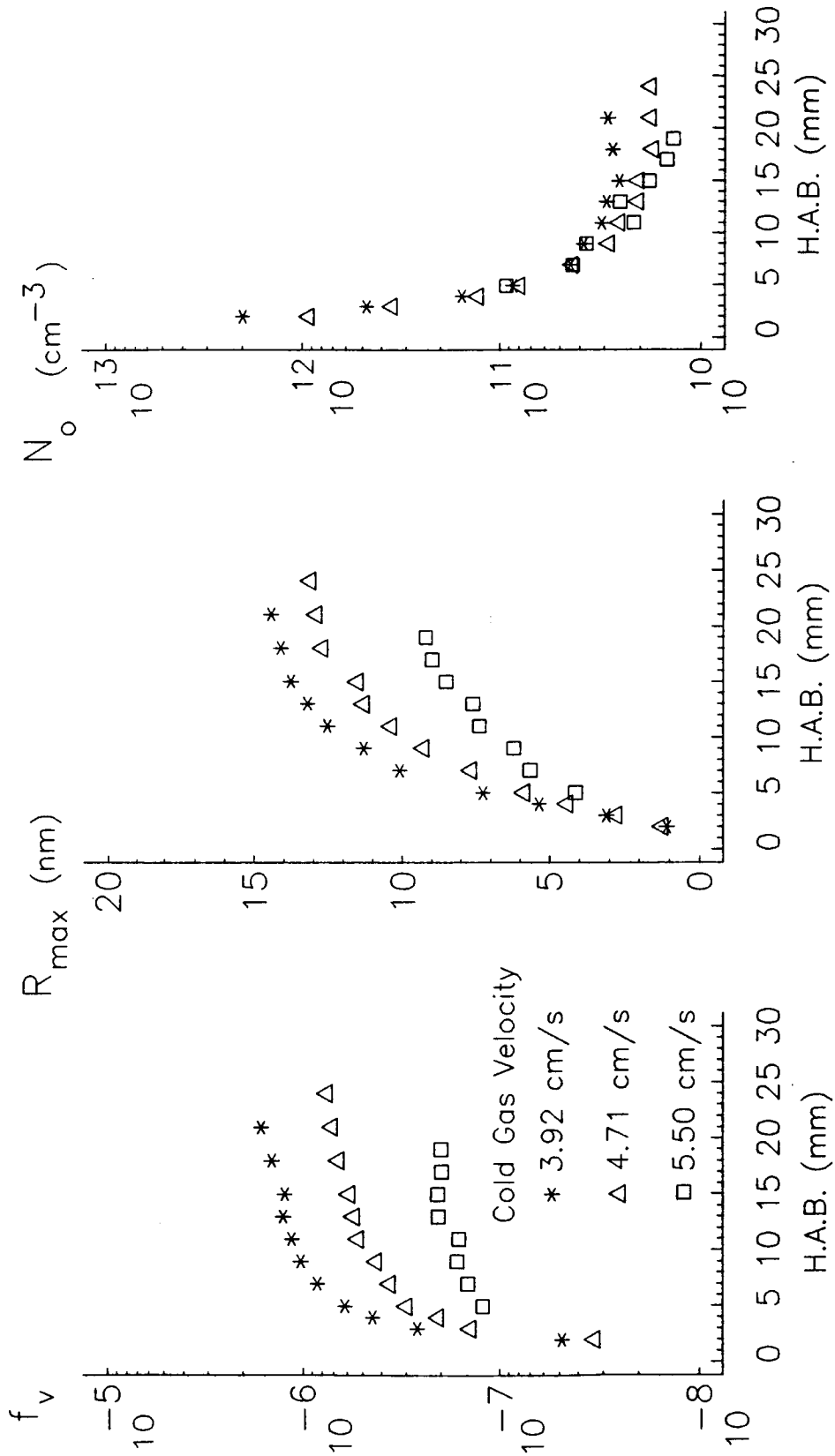

Figure 5.3 Soot Volume Fractions, Radii and Number Densities as a Function of Height Above Burner as Determined by Scattering/Extinction for an Equivalence Ratio of 2.5

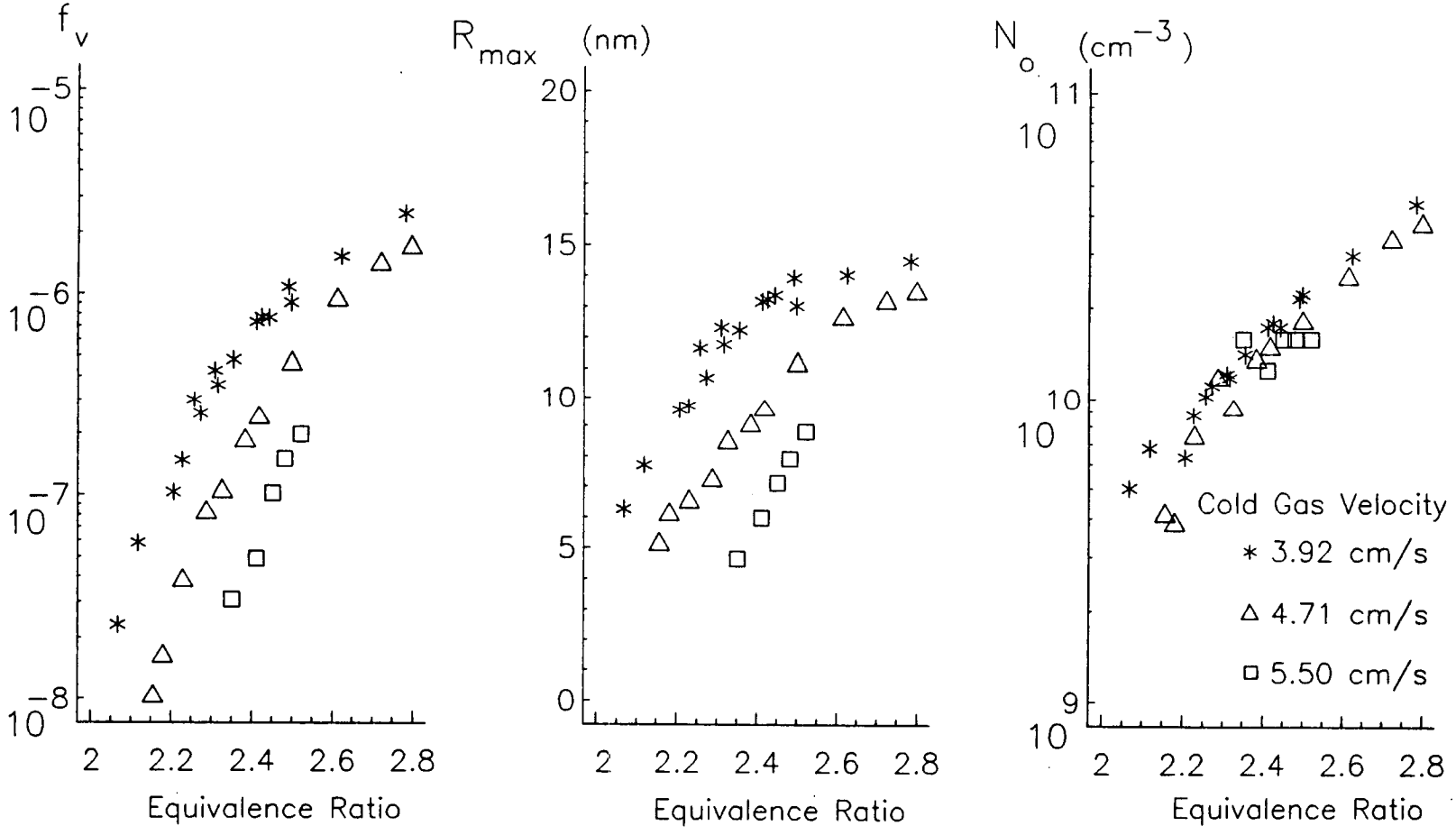

Figure 5.4 Soot Volume Fractions, Radii and Number Densities as a Function of Equivalence Ratio as Determined by Scattering/Extinction at a Height Above Burner of 15 mm

(nearly 1-nm radius) soot particles first appear and quickly agglomerate, forming fewer, larger particles. Near a height above the burner of 10 mm, the number density reaches a value near $10^{10}/cm^3$. Further increases in height show less, if any change in number density. However, the particle size continues to increase, but at a diminishing rate at heights above 10 mm. The soot volume fraction, f_v, is a function of N_o and R_{max}^3. Even though the number density, N_o, decreases, the particle radius, Rmax, increases, resulting in an increase in f_v. For larger cold gas velocities, smaller soot particles are formed at a particular height above the burner. The number density is only a weak function of cold gas velocity. This suggests that the residence time in the flame has little effect on the agglomeration process. The soot volume fraction is less for higher cold gas flow rates. This reflects that the shorter residence time in the flame reduces the amount of particle surface build-up (making smaller particles).

The effect of equivalence ratio on the soot formation process is seen in figure 5.4 for the same three cold gas velocities at a height above the burner of 15 mm. As expected, the soot volume fraction increases with increasing equivalence ratio. Both the size of the particles and the number of particles increases with increasing equivalence ratio, producing a sharply

increasing volume fraction. The same trends are seen for each of the cold gas velocities. Again the increase in cold gas velocity produces smaller particles, but has little effect on the number of particles formed. This is again reflected in the net decrease in soot volume fraction with increasing cold gas velocity. For all three velocities, the first measurable soot particles were approximately 5 nm in radius (at this H.A.B. of 15 mm). This occurred near an equivalence ratio of 2.07 for the 3.92 cm/s case, near 2.15 for 4.71 cm/s, and near 2.35 for the 5.50 cm/s cold gas flow velocity. This occurred at nearly the same number density ($5x10^{9}/cm^{3}$) for the 3.92 and 4.71 cm/s velocities, but for a higher (over $1x10^{10}/cm^{3}$) number of particles for the 5.50 cm/s case. The largest soot particles were seen to be approximately 14 nm in radius. The 3.92 cm/s case reached this value near an equivalence ratio of 2.5 and further increase in equivalence ratio had little effect on the particle size, although the number of particles continued to increase.

Chapter 6: Two-Wavelength Technique Experimental Apparatus and Procedure

The experimental setup, shown in figure 6.1, was based on the one described by Bard[33]. A two-watt (Lexel model 95) argon-ion laser operating near 500 milliwatts was used in multi-line mode to supply 457.9 nm and 514.5 nm wavelengths of light. A fifteen-milliwatt (Spectra-Physics model 120) helium-neon laser supplies the 632.8 nm wavelength. A cube beam splitter and a beam steering device (Newport Research model 675) are used to superimpose the two laser beams. A 400-mm focal length lens was used to focus the beam in the middle of the flame. Two 2.5-mm diameter beam stops positioned 10 cm. and 20 cm. from the lens are used to rid the beam of stray light after passing through the lens. A 160-mm lens collects the transmitted light. This collecting lens was placed such that it bisects the distance from the center of the burner to the prism, which was set at four times the lens' focal length. This projects an image of the beams at the flame center onto the prism. Since the linear displacement of the beams was small at the flame center, the movement of the beams was small at the prism. This reduces the fluctuation of the beams on the photodetectors. Another beam stop (5 mm diameter) was used just before the collecting optics to reduce the amount of light from the flame radiation reaching the photodetectors. The

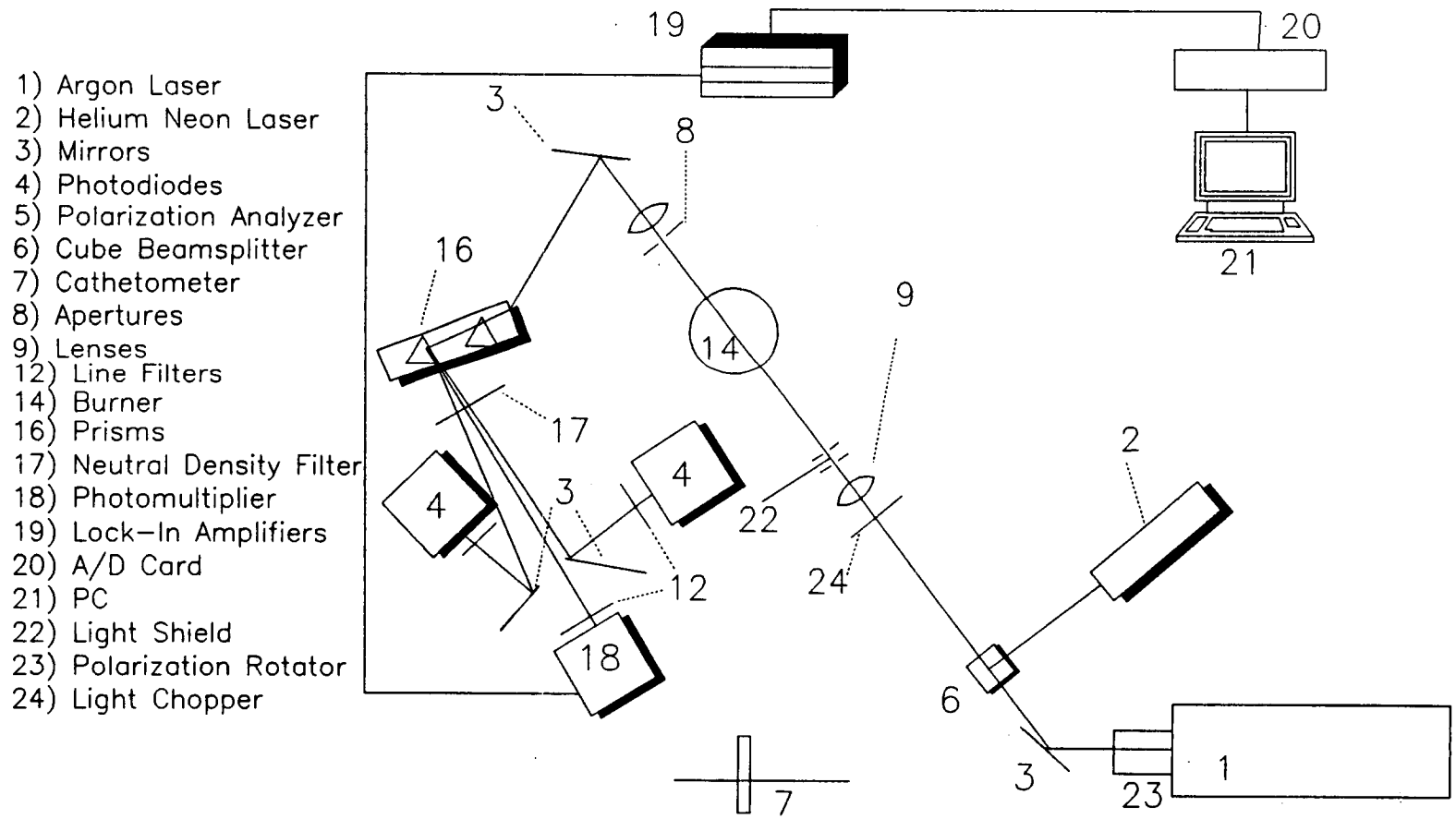

Figure 6.1 Sketch of Two-Wavelength Technique Apparatus

beams are then separated using two equilateral prisms and a mirror which allows the green laser light to pass by its edge and onto one TSI model 9162 photomultiplier tube while the red and purple beams are reflected by two mirrors onto two other TSI model 9162 photomultiplier tubes. Before each photomultiplier tube there are neutral density filters (ND=3) to reduce the light intensity to a level compatible with the photo-multiplier tubes and 10-nm bandwidth interference filters for each corresponding laser wavelength. The cube beam-splitter also supplies a second beam from each laser which was split by another prism and monitored as reference intensities for each of the three wavelengths by three Oriel model 7072 photodiodes which also have laser line filters before them. The signals from the photodiodes were sent to their corresponding read-out devices, then were amplified using Preston model 8300 amplifiers and sent to a Metrabyte model DASH-16 analog to digital converter board in an IBM PC/AT for data storage and analysis. The signals from the photomultiplier tubes were sent to (Princeton Applied Research model 126) lock-in amplifiers. An HMS model 220 Light Beam Chopper was used to impart a 400-hertz frequency to the laser beams just before passing through the flame. This frequency was the target frequency for the lock-in amplifiers so that only the signal from the laser light was amplified and sent to the computer. The lasers and electronic equipment were allowed to warm

up for at least an hour before taking data. All signals from the various detectors had to be amplified to between 0 and 10 volts full scale for the analog-digital converter. This required an initial check to be sure there was good resolution (high enough signal) with no flame present, and to be sure no signal was over-range. The burner was lit and allowed to thermally stabilize for a half hour before final adjustment of the equivalence ratio and cold gas flow rate (which was kept constant for each set of data).

The laser pathlength through the flame was measured using a cathetometer (PTI model 2210), which is a telescope mounted on a vernier horizontal scale with cross-hairs in the view-finder. The zero position for the burner was found by raising the burner until the surface just contacted the laser beams. A vertical scan was made by lowering the burner from this point. At each position the output of each of the photodetectors was read 400 times within a 20-second interval. Any reading that was outside of two standard deviations from the mean was rejected. It was difficult to obtain steady readings above 25 mm from the burner surface due to flame fluctuations, so this was the maximum burner height recorded. The flame pathlength, L, was measured and recorded for each height above the burner as well as fuel, oxygen and nitrogen flowrates, burner cooling water inlet

and outlet temperatures and flowrate, and burner shroud nitrogen flowrate.

The optical system was calibrated by taking a measurement at 5-mm above the burner while flowing nitrogen gas through the burner. This was the reference condition (no flame). A reference measurement was taken immediately (within 30 seconds) following each data point taken in the flame. This minimized the effect of electronic drift of the system with time.

The measured values of intensity ratios $I(L)/I_o$ for each set of two different wavelengths are used in the extinction analysis to calculate R_{max}, N_o, and f_v. It was sometimes necessary to use another wavelength pair to isolate the correct value of R_{max}. The most effective sets of wavelength pairs are 457.9 nm with 632.8 nm and 514.5 nm with 632.8 nm, as seen by Bard[33] and Beier[36]. This provides data from sets of wavelengths relatively far apart which are used to produce one unambiguous set of data.

Chapter 7: Two-Wavelength Extinction Analysis

As previously described in Chapter 5, for a polydisperse aerosol having a given refractive index, m=n(1-ik) and size distribution, N(R), the transmitted intensity I, of a monochromatic beam passing through the aerosol is related to the initial intensity I_o by:

$$\frac{I(\lambda)}{I_o(\lambda)} = \exp\left[-K_{ext}(\lambda) \quad L \right] \tag{7.1}$$

where the beam pathlength is L. The extinction coefficient K_{ext} is given by:

$$K_{ext}(\lambda,m,R) = \int_0^\infty N(R)\ Q_{ext}(\lambda,m,R)\ \pi R^2 dR \tag{7.2}$$

where Q_{ext}, the particle extinction efficiency for spherical particles, has been given in chapter 5 on Mie scattering/extinction theory. The optical properties of soot used were those of Lee and Tien[60-61], which also depend on the wavelength of light, as seen in the previous Table 1. The size distibution chosen[57] is a Gauss size distribution with $\sigma/R_m = 1/2$:

$$\frac{N(R)}{N_o} = \left[\frac{27\ R^3}{2\ R^4_{max}} \right] \exp\left[\frac{-3\ R}{R_{max}} \right] \tag{7.3}$$

where R_{max} is the most probable radius and N_o is the total particle concentration. Equation (7.2) is then integrated numerically at fixed wavelengths 457.9 nm, 514.5 nm and 632.8 nm for various values of R_{max}. These extinction coefficients are then presented as non-dimensional extinction coefficients defined as:

$$\tau'(x_{max},\lambda,m) \equiv \frac{K_{ext}\ (x_{max},\lambda,m)}{N_o\ R_{max}^2} \tag{7.4}$$

where x_{max} is the characteristic size parameter, $x = 2\pi R/\lambda$ at $R = R_{max}$. If $x<<1$, the absorption limit applies where K_{ext} is independent of the size distribution and only depends on the optical properties of the particles. Then the ratio of K_{ext}'s at two different wavelengths is:

$$\frac{K_{ext}(\lambda_i)}{K_{ext}(\lambda_j)} \equiv \frac{K_i}{K_j} = \frac{\lambda_j\ F_a(\lambda_i)}{\lambda_i\ F_a(\lambda_j)} \tag{7.5}$$

where

$$F_a(\lambda) = \frac{n^2\ k}{\left(\ n^2 - (nk)^2 + 2\ \right)^2 + 4n^4k^2} \tag{7.6}$$

In the large particle limit, $x>>1$, $Q_{ext} \to 2$ for all λ, so $K_i/K_j \to 1$. Pagni and Bard[31-35] suggested a normalized extinction coefficient defined as:

$$X_{ij} \equiv \frac{\left[K_i/K_j - 1 \right]}{\left[K_i/K_j - 1 \right]_{abs}} \tag{7.7}$$

Using equation (7.1), and the fact that the two laser beams are superimposed ($L_i = L_j$) :

$$\frac{K_i}{K_j} = \frac{\ln \left(I/I_o \right)_i}{\ln \left(I/I_o \right)_j} \tag{7.8}$$

The experimental values for the light intensity ratios at each wavelength are used in equation (7.8) and substituted into equation (7.7) to find the experimental value for X_{ij}. Values of X_{ij} are listed as a function of R_{max} in Tables 3 and 4 for the wavelength pairs used. The experimental X_{ij} is found in the tables and after interpolation (if necessary), R_{max} and τ' are read from the tables. If $X_{ij} > 1$, two possible values of R_{max} are found in the tables. More than one wavelength pair is then used to determine the correct R_{max}. Using τ' and the experimental K_{ext} in equation (7.4) determines the value of N_o.

The soot volume fraction is then found from:

$$f_v = \frac{4}{3} \pi \int_0^\infty N(R) \; R^3 dR \tag{7.9}$$

Performing the integration in equation (7.9), after

substituting for N(R) from equation (7.3), the volume fraction is found from:

$$f_v = \frac{54\ \pi}{3^8}\ \Gamma(7)\ N_o R_{max}^3 = 18.62\ N_o R_{max}^3 \qquad (7.10)$$

TABLE 3: Calculated Values for the Two-Wavelength Technique for Wavelengths 0.4579 and 0.6328 uM

Rmax (uM)	TAU'(0.4579)	TAU'(0.6328)	Xij
0.0010	0.1501	0.0949	1.0026
0.0020	0.3014	0.1902	1.0078
0.0030	0.4554	0.2863	1.0181
0.0040	0.6136	0.3836	1.0332
0.0050	0.7777	0.4827	1.0534
0.0060	0.9497	0.5840	1.0789
0.0070	1.1314	0.6882	1.1098
0.0080	1.3251	0.7958	1.1461
0.0090	1.5329	0.9075	1.1875
0.0100	1.7569	1.0239	1.2335
0.0110	1.9992	1.1459	1.2832
0.0120	2.2613	1.2739	1.3355
0.0130	2.5446	1.4089	1.3891
0.0140	2.8500	1.5514	1.4423
0.0150	3.1776	1.7022	1.4937
0.0160	3.5273	1.8617	1.5416
0.0170	3.8982	2.0307	1.5848
0.0180	4.2890	2.2094	1.6219
0.0190	4.6979	2.3983	1.6522
0.0200	5.1228	2.5976	1.6751
0.0210	5.5613	2.8075	1.6903
0.0220	6.0110	3.0279	1.6977
0.0230	6.4692	3.2587	1.6977
0.0240	6.9334	3.4996	1.6908
0.0250	7.4011	3.7504	1.6773
0.0260	7.8699	4.0107	1.6581
0.0270	8.3376	4.2797	1.6339
0.0280	8.8022	4.5570	1.6053
0.0290	9.2619	4.8418	1.5731
0.0300	9.7150	5.1335	1.5379
0.0310	10.1602	5.4312	1.5004
0.0320	10.5963	5.7342	1.4611
0.0330	11.0222	6.0416	1.4206
0.0340	11.4372	6.3526	1.3792
0.0350	11.8405	6.6666	1.3374
0.0360	12.2317	6.9826	1.2954
0.0370	12.6103	7.2999	1.2535
0.0380	12.9762	7.6178	1.2121
0.0390	13.3290	7.9357	1.1711
0.0400	13.6689	8.2528	1.1309
0.0410	13.9957	8.5686	1.0914
0.0420	14.3096	8.8825	1.0529
0.0430	14.6107	9.1939	1.0152
0.0440	14.8992	9.5025	0.9786
0.0450	15.1752	9.8077	0.9430

TABLE 3 (continued)

Rmax (uM)	TAU'(0.4579)	TAU'(0.6328)	Xij
0.0460	15.4391	10.1092	0.9085
0.0470	15.6911	10.4066	0.8750
0.0480	15.9316	10.6996	0.8426
0.0490	16.1608	10.9879	0.8112
0.0500	16.3791	11.2713	0.7809
0.0510	16.5868	11.5495	0.7516
0.0520	16.7843	11.8224	0.7232
0.0530	16.9719	12.0899	0.6958
0.0540	17.1500	12.3517	0.6694
0.0550	17.3189	12.6079	0.6439
0.0560	17.4790	12.8582	0.6192
0.0570	17.6306	13.1027	0.5955
0.0580	17.7740	13.3414	0.5725
0.0590	17.9095	13.5741	0.5504
0.0600	18.0376	13.8010	0.5290
0.0610	18.1584	14.0219	0.5083
0.0620	18.2724	14.2369	0.4884
0.0630	18.3797	14.4462	0.4692
0.0640	18.4808	14.6496	0.4507
0.0650	18.5758	14.8472	0.4327
0.0700	18.9694	15.7517	0.3520
0.0750	19.2486	16.5240	0.2841
0.0800	19.4382	17.1763	0.2269
0.0900	19.6250	18.1724	0.1377
0.1000	19.6456	18.8390	0.0738

TABLE 4: Calculated Values for the Two-Wavelength Technique for Wavelengths 0.5145 and 0.6328 uM

Rmax (uM)	TAU'(0.5145)	TAU'(0.6328)	Xij
0.0010	0.1217	0.0949	1.0033
0.0020	0.2442	0.1902	1.0072
0.0030	0.3683	0.2863	1.0170
0.0040	0.4951	0.3836	1.0311
0.0050	0.6255	0.4827	1.0501
0.0060	0.7608	0.5840	1.0741
0.0070	0.9022	0.6882	1.1034
0.0080	1.0511	0.7958	1.1379
0.0090	1.2088	0.9075	1.1777
0.0100	1.3768	1.0239	1.2223
0.0110	1.5565	1.1459	1.2714
0.0120	1.7494	1.2739	1.3240
0.0130	1.9567	1.4089	1.3794
0.0140	2.1795	1.5514	1.4362
0.0150	2.4187	1.7022	1.4932
0.0160	2.6747	1.8617	1.5491
0.0170	2.9480	2.0307	1.6026
0.0180	3.2385	2.2094	1.6523
0.0190	3.5458	2.3983	1.6973
0.0200	3.8692	2.5976	1.7366
0.0210	4.2079	2.8075	1.7696
0.0220	4.5607	3.0279	1.7958
0.0230	4.9261	3.2587	1.8152
0.0240	5.3027	3.4996	1.8276
0.0250	5.6888	3.7504	1.8334
0.0260	6.0828	4.0107	1.8328
0.0270	6.4829	4.2797	1.8262
0.0280	6.8876	4.5570	1.8143
0.0290	7.2951	4.8418	1.7974
0.0300	7.7039	5.1335	1.7762
0.0310	8.1125	5.4312	1.7513
0.0320	8.5197	5.7342	1.7232
0.0330	8.9240	6.0416	1.6925
0.0340	9.3244	6.3526	1.6595
0.0350	9.7199	6.6666	1.6247
0.0360	10.1095	6.9826	1.5886
0.0370	10.4925	7.2999	1.5514
0.0380	10.8681	7.6178	1.5136
0.0390	11.2359	7.9357	1.4752
0.0400	11.5952	8.2528	1.4367
0.0410	11.9457	8.5686	1.3981
0.0420	12.2871	8.8825	1.3597
0.0430	12.6190	9.1939	1.3215
0.0440	12.9414	9.5025	1.2838
0.0450	13.2541	9.8077	1.2465

TABLE 4 (continued)

Rmax (uM)	TAU'(0.5145)	TAU'(0.6328)	Xij
0.0460	13.5570	10.1092	1.2099
0.0470	13.8501	10.4066	1.1738
0.0480	14.1334	10.6996	1.1385
0.0490	14.4070	10.9879	1.1038
0.0500	14.6709	11.2713	1.0700
0.0510	14.9252	11.5495	1.0368
0.0520	15.1701	11.8224	1.0045
0.0530	15.4057	12.0899	0.9729
0.0540	15.6322	12.3517	0.9422
0.0550	15.8498	12.6079	0.9122
0.0560	16.0587	12.8582	0.8830
0.0570	16.2590	13.1027	0.8545
0.0580	16.4511	13.3414	0.8269
0.0590	16.6350	13.5741	0.7999
0.0600	16.8111	13.8010	0.7737
0.0610	16.9795	14.0219	0.7482
0.0620	17.1404	14.2369	0.7235
0.0630	17.2942	14.4462	0.6994
0.0640	17.4410	14.6496	0.6759
0.0650	17.5810	14.8472	0.6532
0.0700	18.1876	15.7517	0.5486
0.0750	18.6570	16.5240	0.4579
0.0800	19.0131	17.1763	0.3794
0.0900	19.4648	18.1724	0.2523
0.1000	19.6727	18.8390	0.1570

Chapter 8: Results of Two-Wavelength Technique with Comparison to Scattering/Extinction Method

8.1 Varying Height Above Burner

The soot volume fractions as measured by the two-wavelength technique is shown as a function of height above the burner in figure 8.1 for an equivalence ratio of 2.5 and a cold gas velocity of 3.92 cm/s. Also shown is the soot volume fractions as determined by the scattering/extinction method. There is excellent agreement between the two methods down to a height above the burner of 4 mm. In figure 8.2, the soot particle size is plotted as a function of height above burner for the two techniques. The two-wavelength technique predicts a nearly constant particle size of approximately 15 nm radius for all heights above the burner, while the scattering technique shows an increasing particle size up to a height of approximately 10 mm, with a very slowly increasing size thereafter. The two methods predict nearly the same particle size for heights above the burner over 7 mm. The soot particle number density is shown in figure 8.3. The two-wavelength technique predicts a nearly constant number density for heights above the burner slightly over 5 mm, with decreasing numbers of particles at lower heights. The scattering/extinction results agree well with the two-wavelength method above

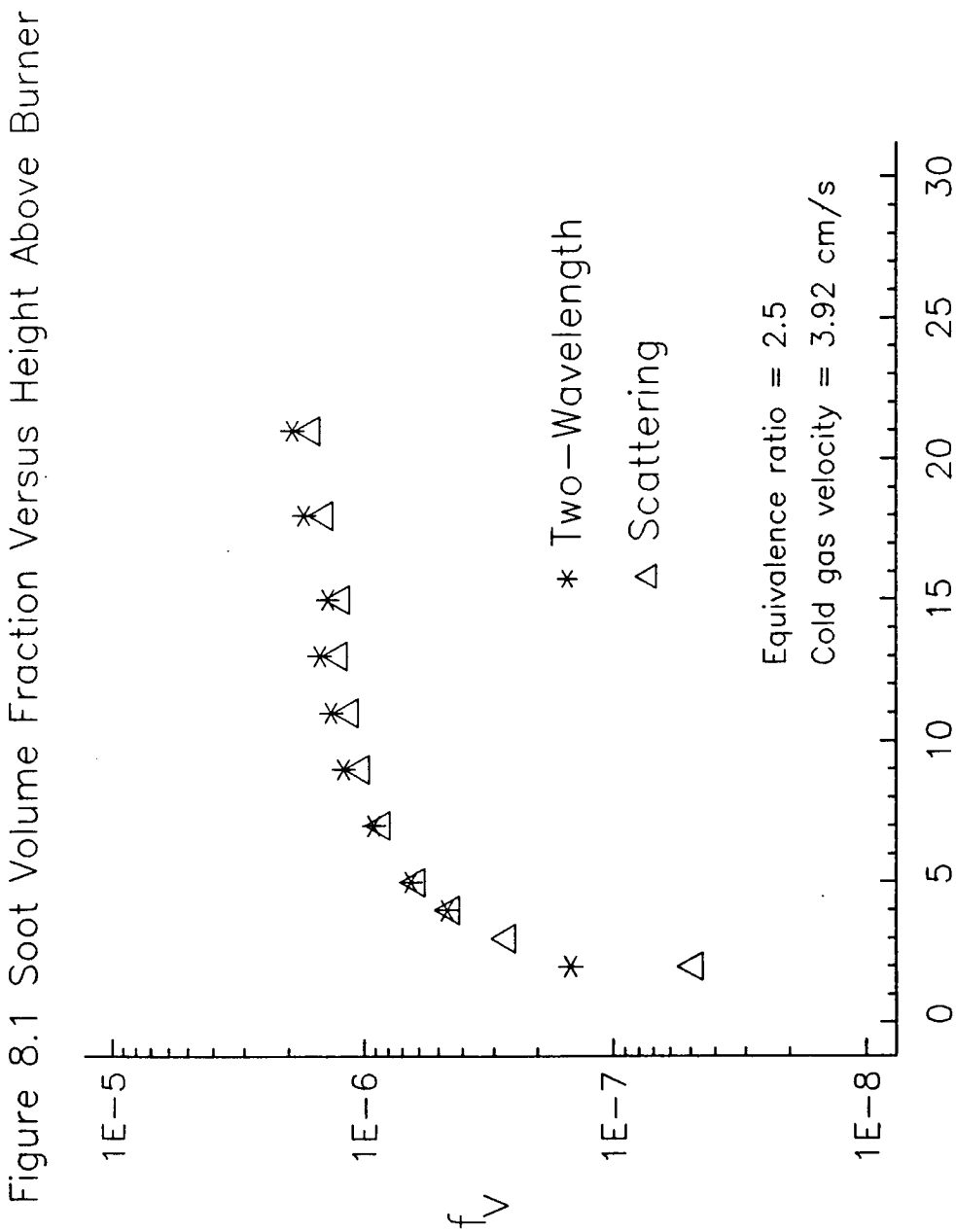

Figure 8.1 Soot Volume Fraction Versus Height Above Burner

Figure 8.2 Soot Radius Versus Height Above Burner

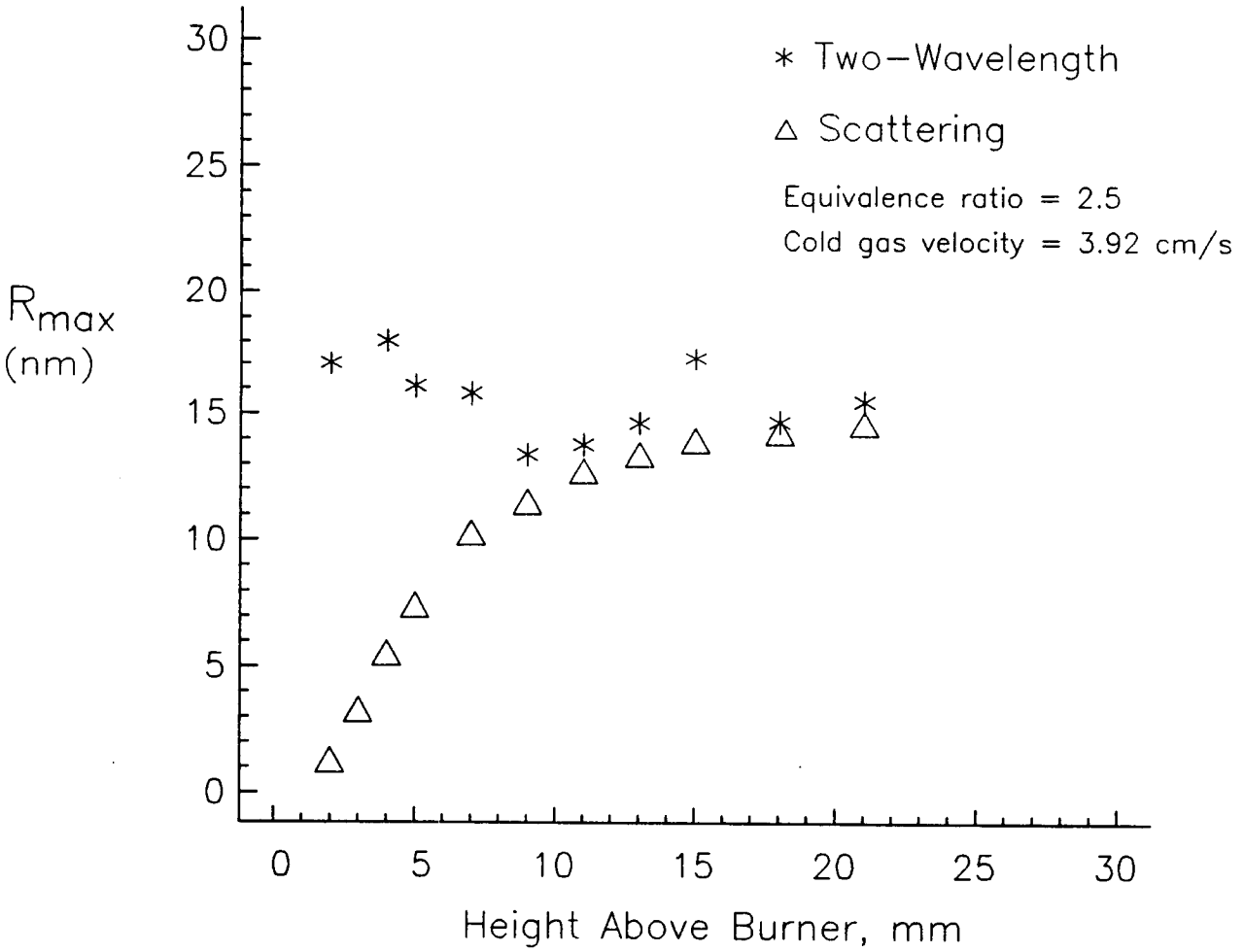

Figure 8.3 Soot Number Density Versus Height Above Burner

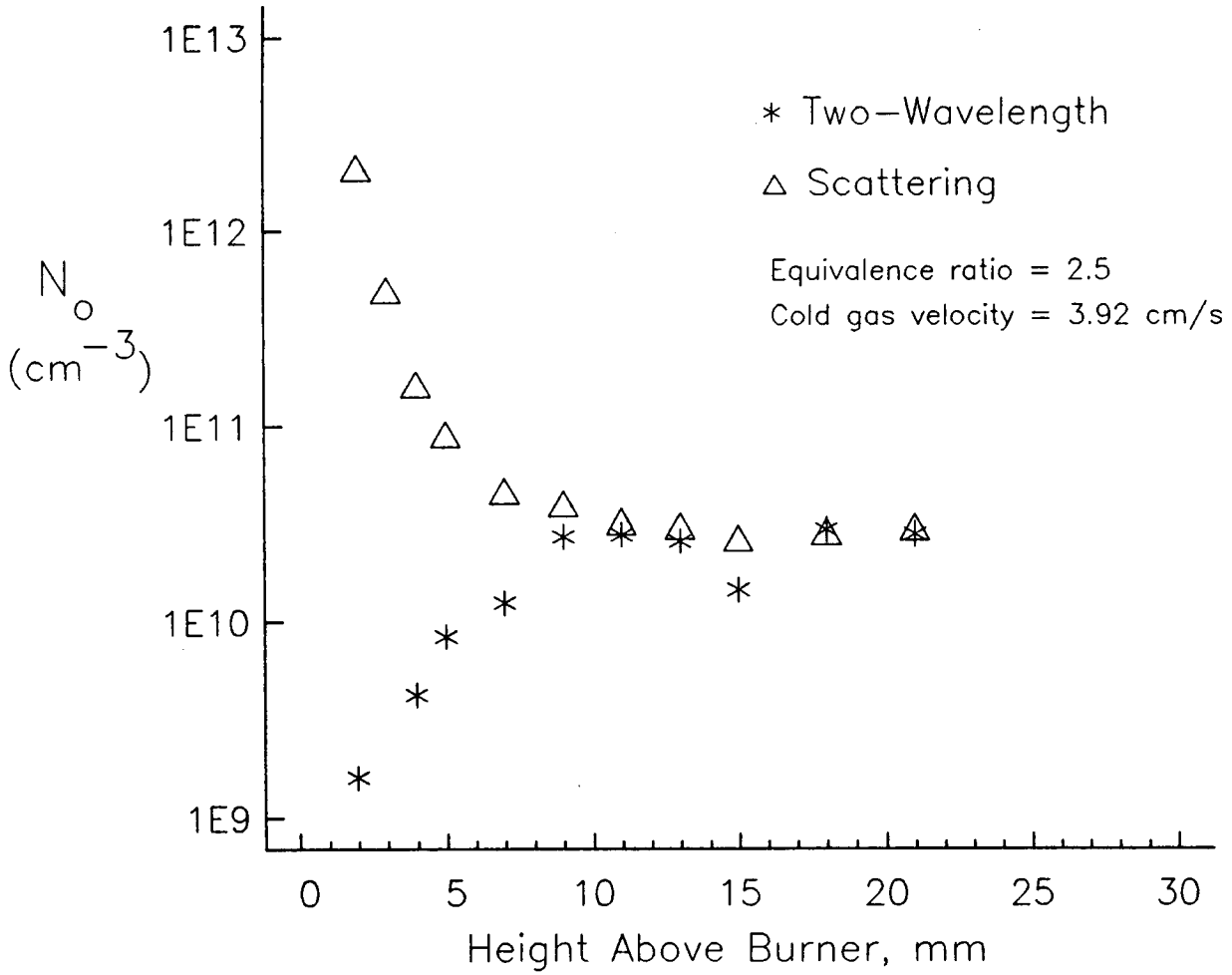

7-mm burner heights, but an opposite trend is seen below 7 mm. The scattering technique predicts a larger number of particles with decreasing height above burner instead of a smaller number predicted by the two-wavelength technique.

The results for a cold gas velocity of 4.71 cm/s are seen in figures 8.4, 8.5 and 8.6. Figure 8.4 shows continued good agreement between the two diagnostic methods in measuring the soot volume fraction at various heights above the burner at an equivalence ratio of 2.5. Figure 8.5 shows the predicted particle sizes. The two-wavelength technique again shows nearly no change in particle size with increasing height above the burner and little change in sizes compared to the 3.92 cm/s cold gas velocity case. The scattering results show smaller particles than the 3.92 cm/s case and smaller particles than the two-wavelength method for all heights above the burner, although there is not a great difference in the sizes predicted by the two methods. The number density is shown in figure 8.6. There is a nearly constant number density predicted by the two-wavelength method, where the scattering/extinction results show a decrease in number density with increase in height up to about 9 mm, when the number density decreases only slightly with an increase in height. There is still reasonable agreement between the two techniques in predicted the number densities for heights above 9 mm.

Figure 8.4 Soot Volume Fraction Versus Height Above Burner

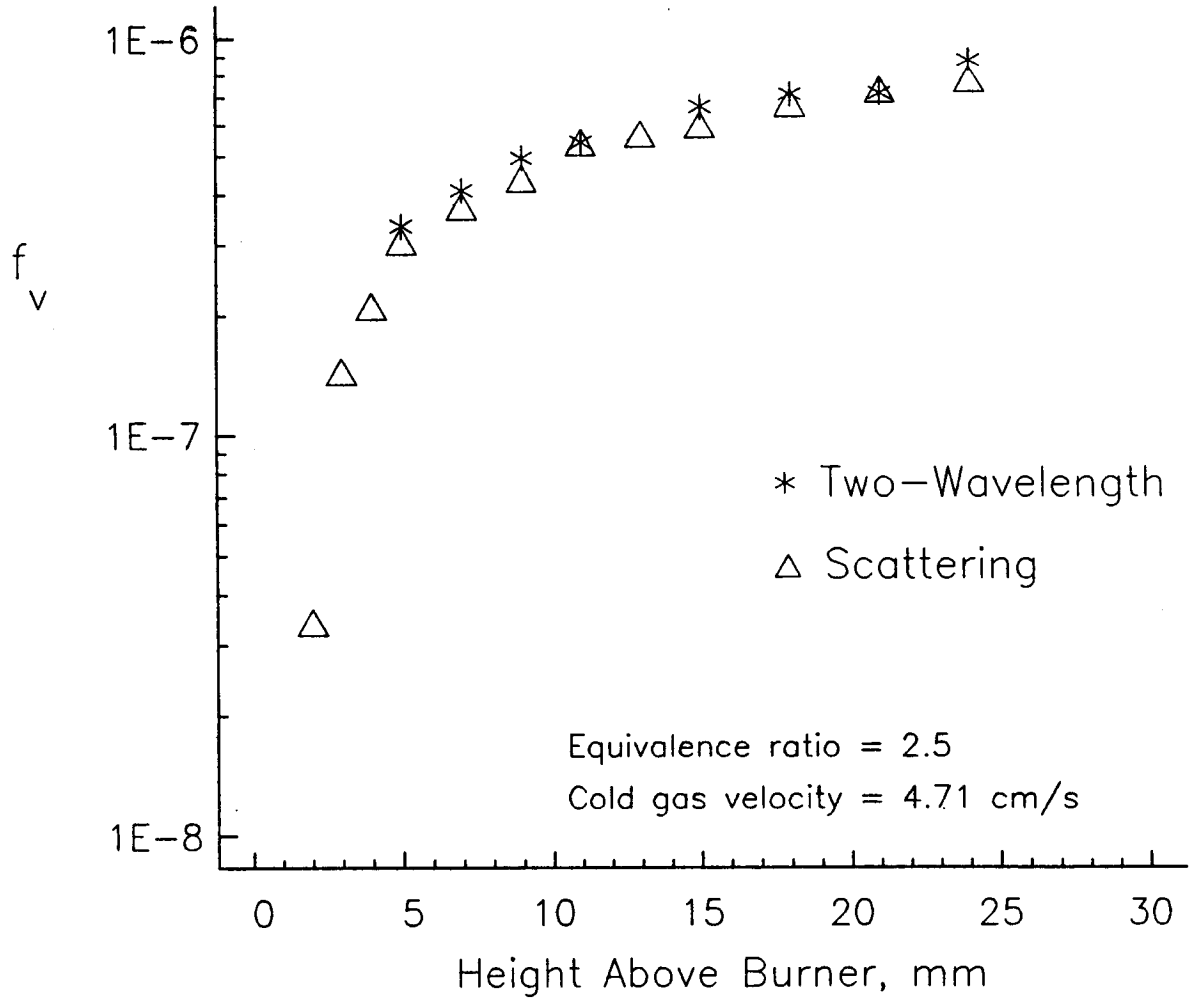

Figure 8.5 Soot Radius Versus Height Above Burner

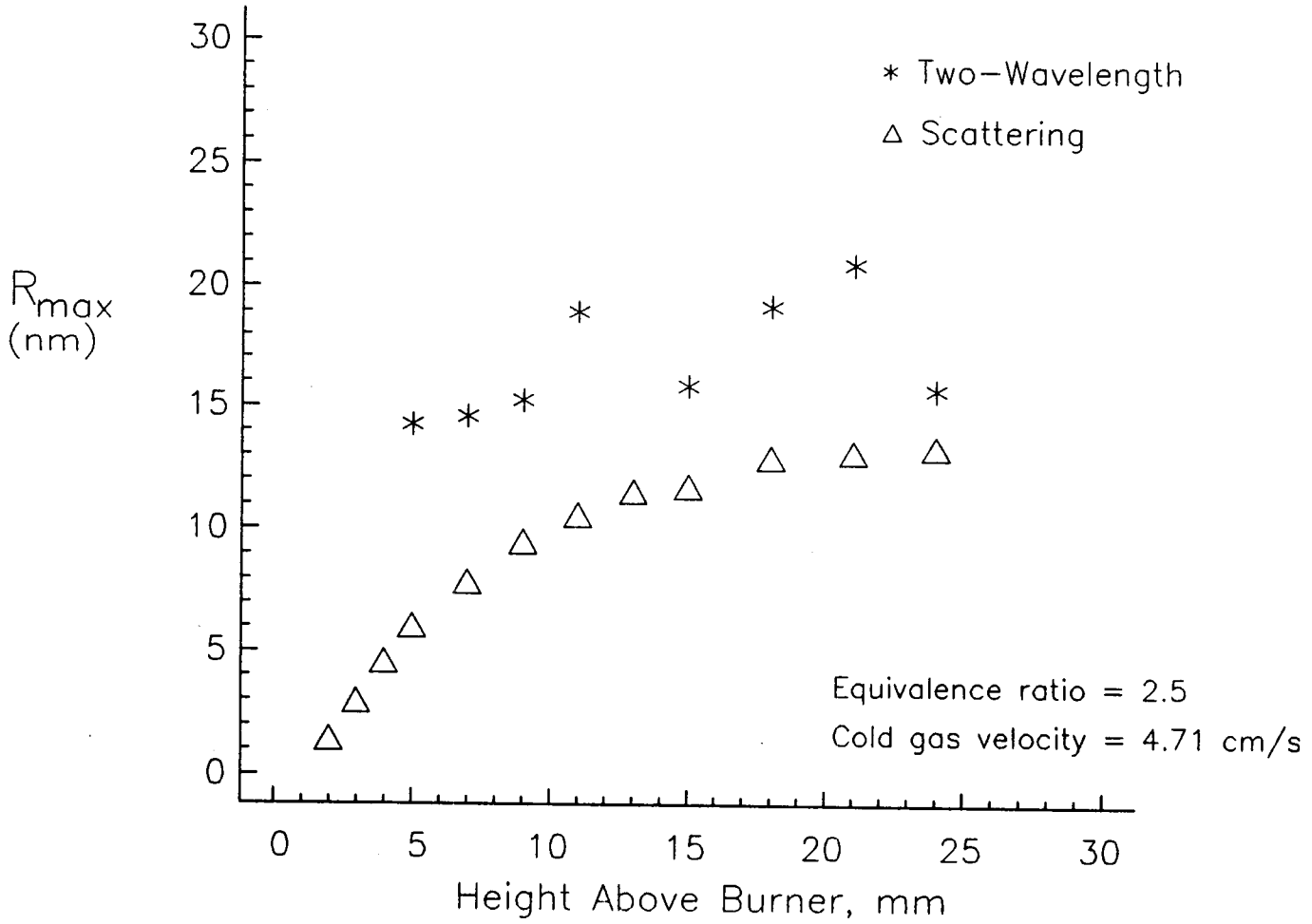

Figure 8.6 Soot Number Density Versus Height Above Burner

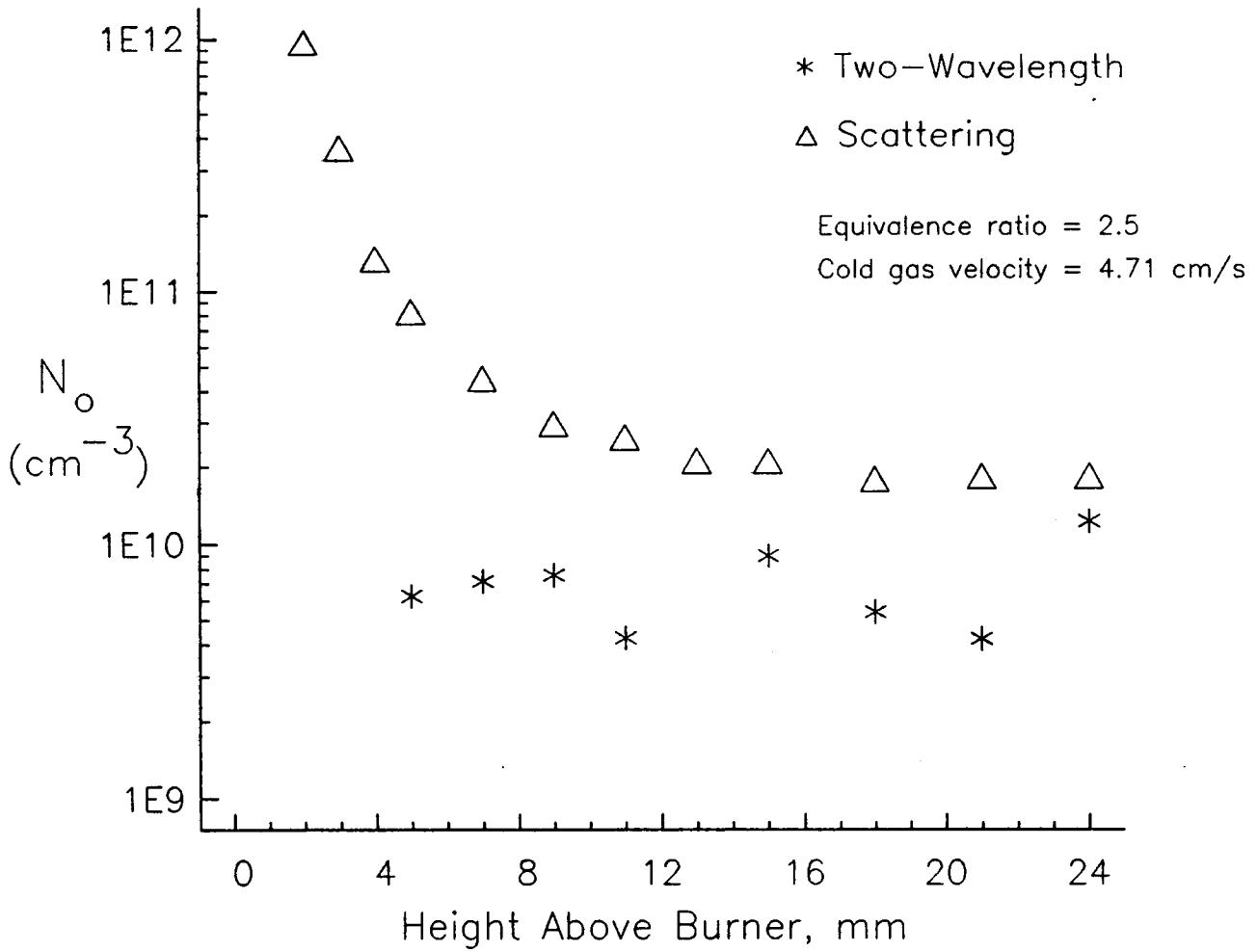

The results for measurements made at a cold gas velocity of 5.50 cm/s are shown in figures 8.7, 8.8, and 8.9, again for an equivalence ratio of 2.5. The agreement between the techniques in predicting the soot volume fraction is fair, although the two-wavelength method is lower than the scattering/extinction results for all heights above the burner, seen in figure 8.7. The prediction of soot particle sizes is very different for the two techniques. For the increased cold gas velocity, the scattering technique predicts smaller particles at a given height above the burner, but the two-wavelength method predicts a very large increase in particle radius compared to the 3.92 and 4.71 cm/s velocities. A very large difference in number densities between the two techniques is seen in figure 8.8. The two-wavelength method predicts a very low particle number density ($10^7/cm^3$), while the scattering/extinction result is near $10^{10}/cm^3$.

8.2 Varying Equivalence Ratio

Due to the poor agreement between the two techniques at the 2.5 equivalence ratio (which was the maximum attainable by the fuel turbine flowmeter at the 5.50 cm/s cold gas velocity), it was not possible to produce a comparison of the two techniques by varying the equivalence ratios at this velocity. However, figures 8.10 through 8.18 show the effect of varying the

Figure 8.7 Soot Volume Fraction Versus Height Above Burner

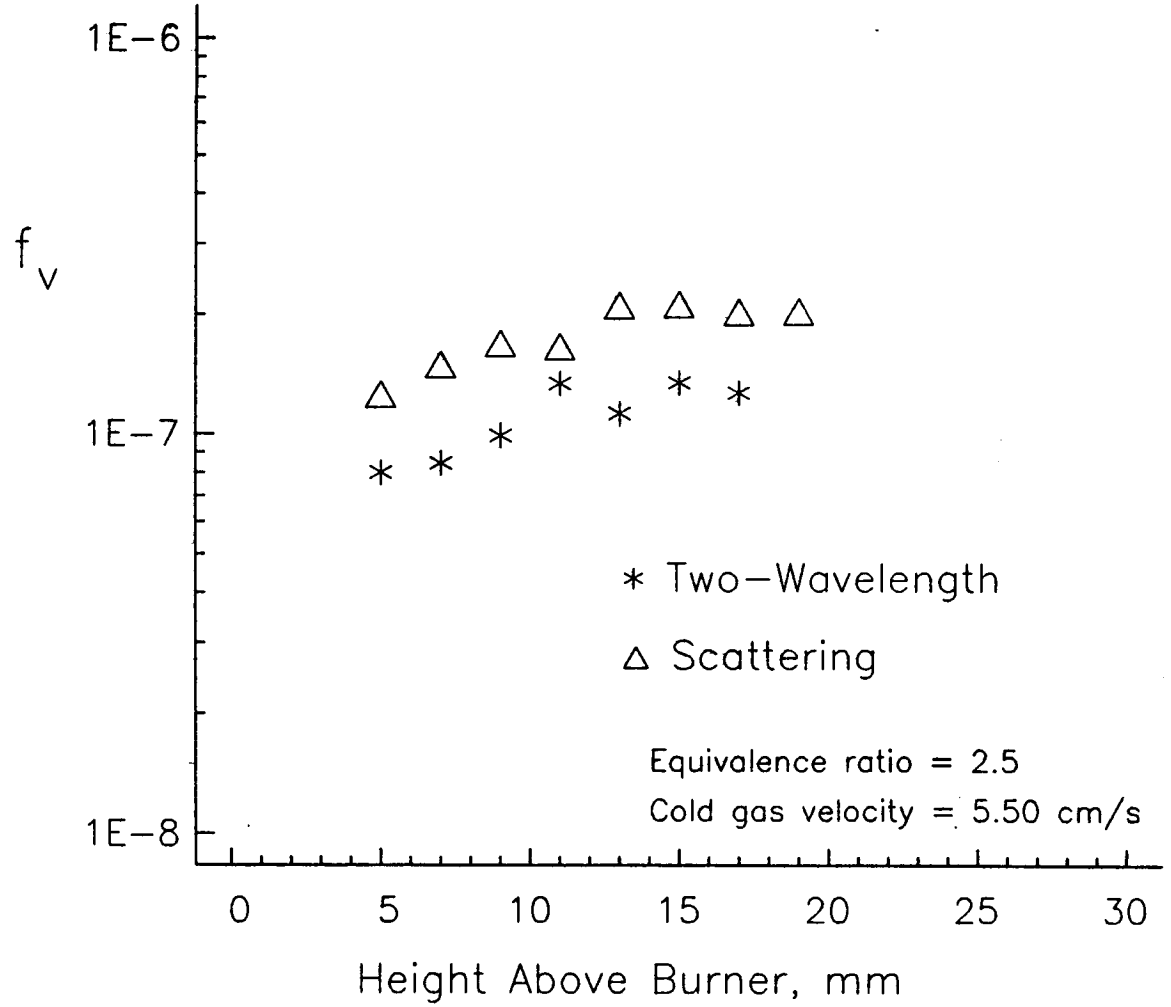

Figure 8.8 Soot Radius Versus Height Above Burner

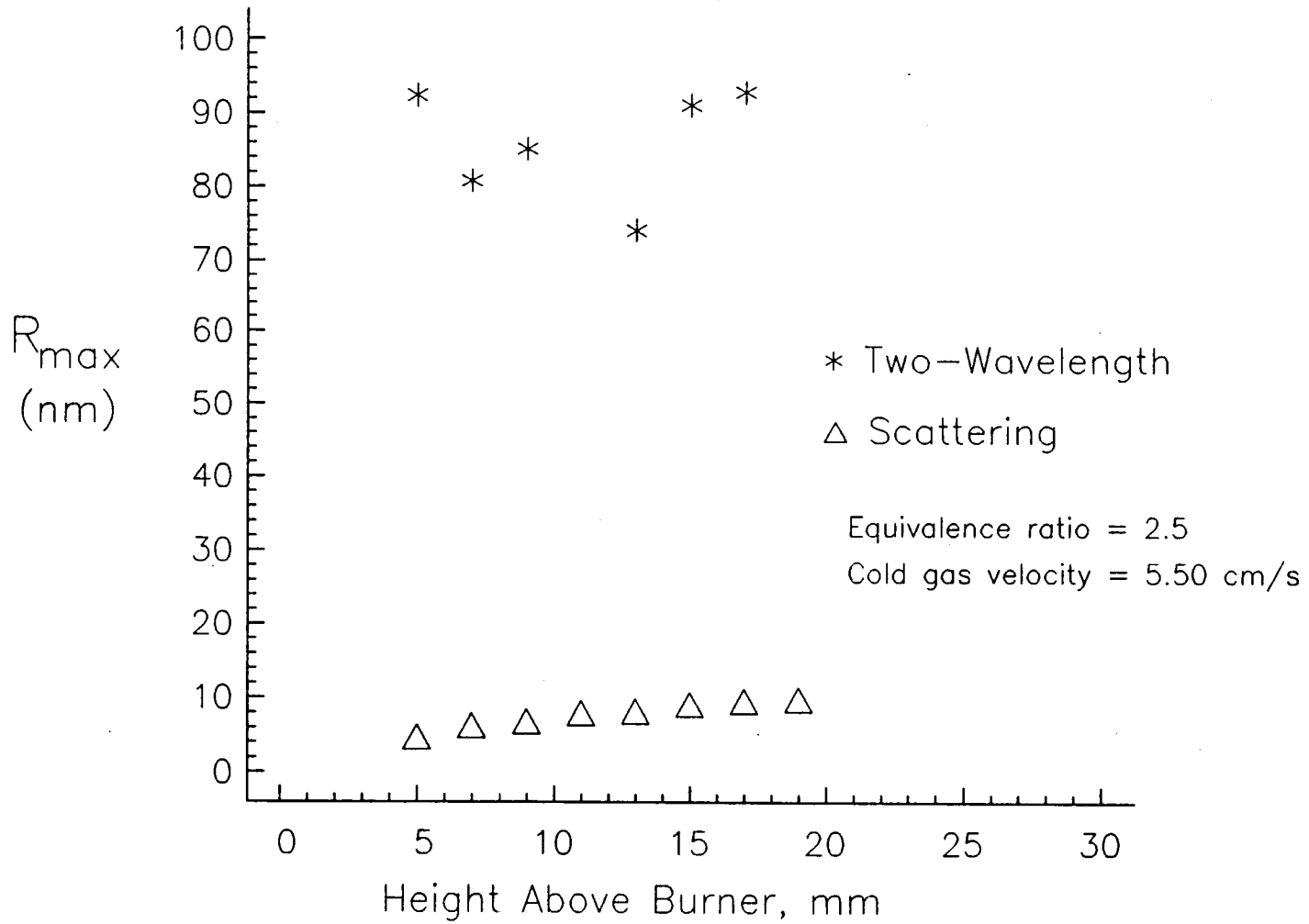

Figure 8.9 Soot Number Density Versus Height Above Burner

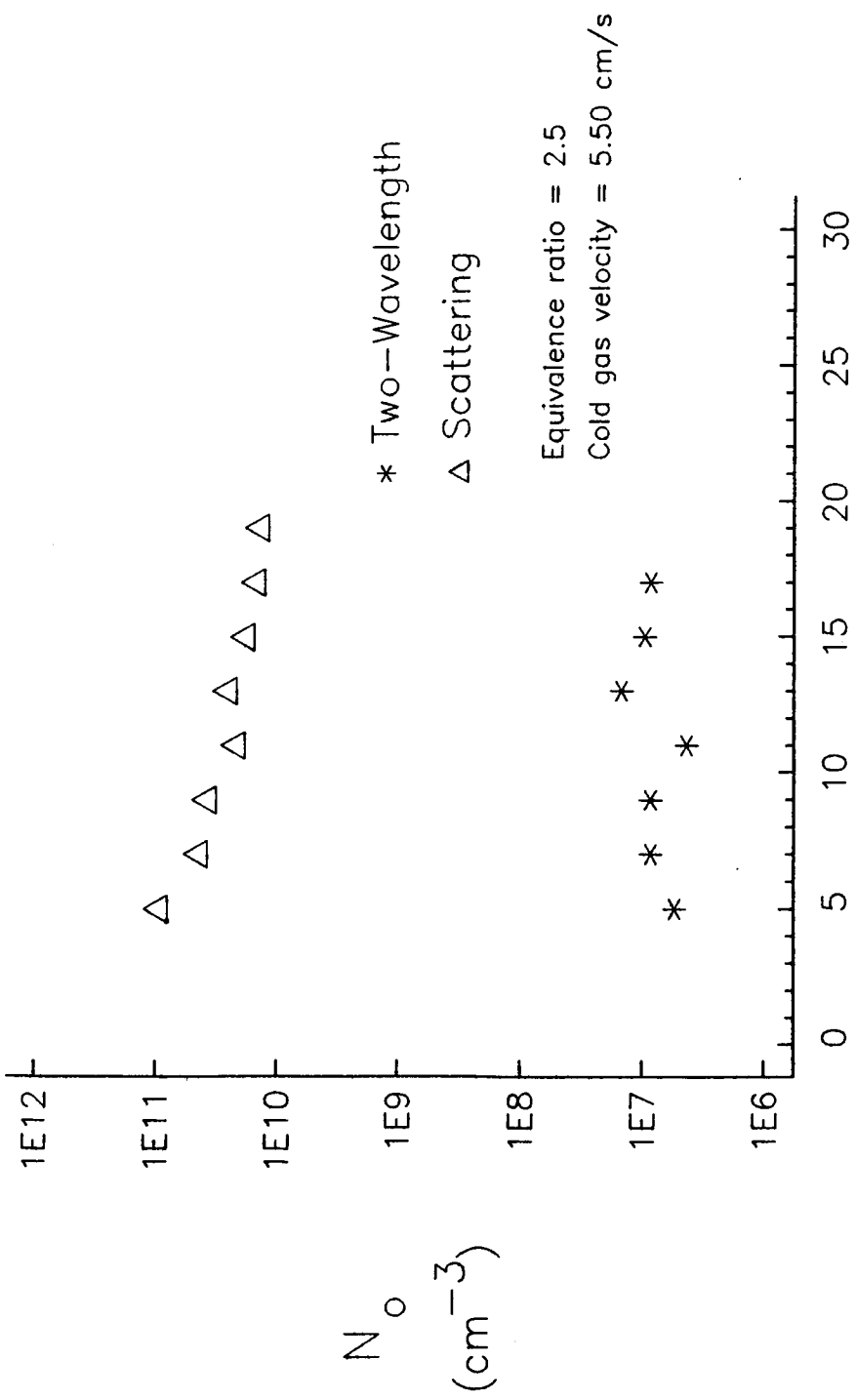

equivalence ratio at a height above the burner of 15 mm for cold gas velocities of 3.4, 3.92 and 4.71 cm/s. All three velocities produced excellent agreement between the two techniques for measuring the soot volume fractions wherever there were results for both techniques (see figures 8.10, 8.11, and 8.12). However, the two-wavelength technique was not able to measure a volume fraction (or particle size, or number density) below an equivalence ratio of 2.25 for velocities of 3.4 and 3.92, or below 2.5 for a velocity of 4.71 cm/s.

A comparison of the results of soot particle size measurements as a function of equivalence ratio for the three cold gas velocities (3.4, 3.92, and 4.71 cm/s) is shown in figures 8.13, 8.14, and 8.15. The agreement between the two-wavelength and scattering/extinction methods is good where a comparison can be made. The agreement begins to break down at lower equivalence ratios (below 2.3 for 3.4 and 3.92 cm/s, and below 2.5 for 4.72 cm/s). At the lower equivalence ratios, the two-wavelength technique predicts larger particles than the scattering/extinction technique. For very sooty flames (equivalence ratios over 2.6), the two-wavelength technique begins to predict smaller particle sizes than the scattering technique for the 3.4 and 3.92 cm/s velocities.

The number densities are shown in figures 8.16, 8.17, and 8.18 as functions of equivalence ratio for the three gas velocities (3.4, 3.92, and 4.71 cm/s). Similar trends in agreement, found for the particle sizes, are seen for the number densities. However, when the two-wavelength technique predicted a larger (or smaller) particle size than the scattering technique, it predicted a corresponding lower (or higher) number density at the given equivalence ratio, resulting in a good agreement in volume fractions.

Figure 8.10 Soot Volume Fraction Versus Equivalence Ratio

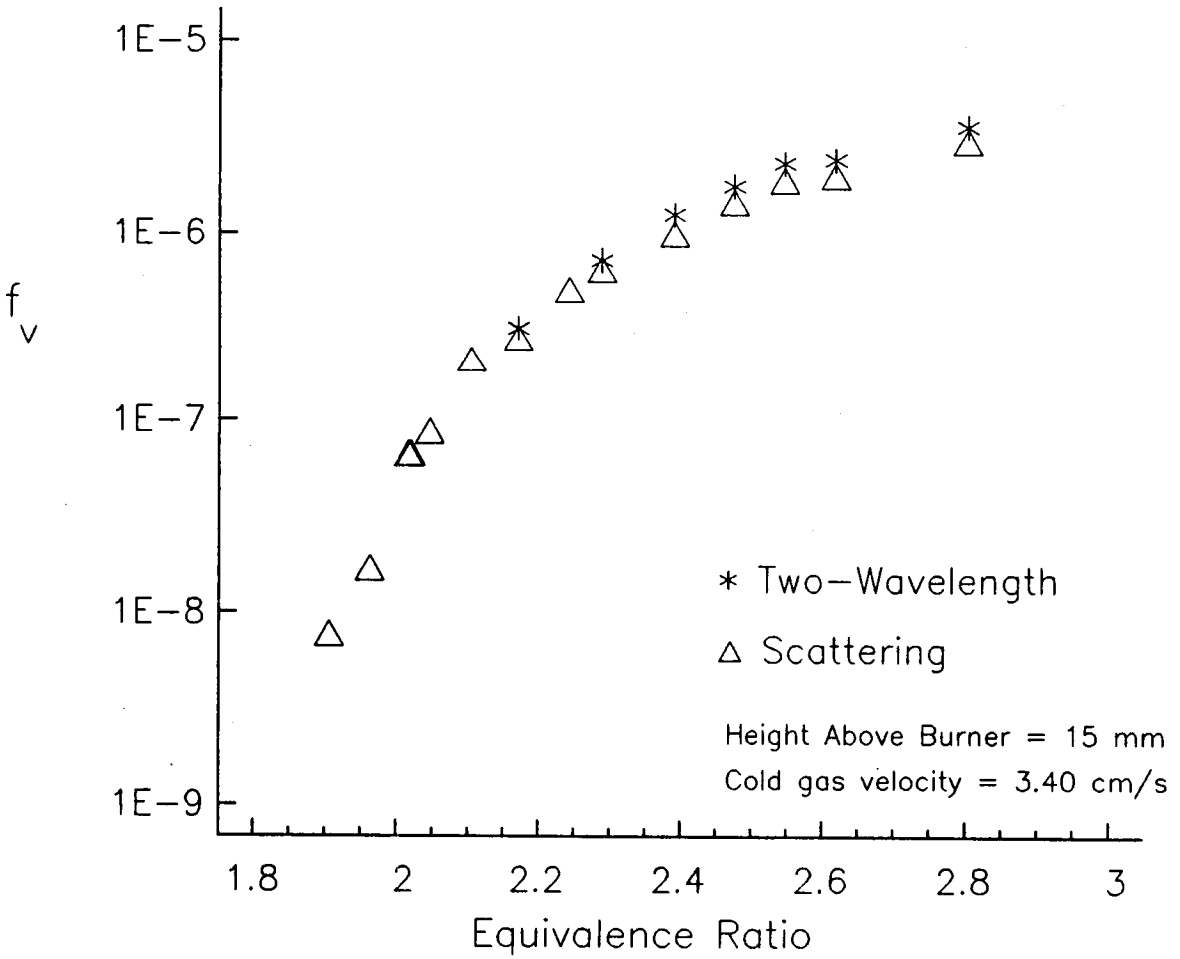

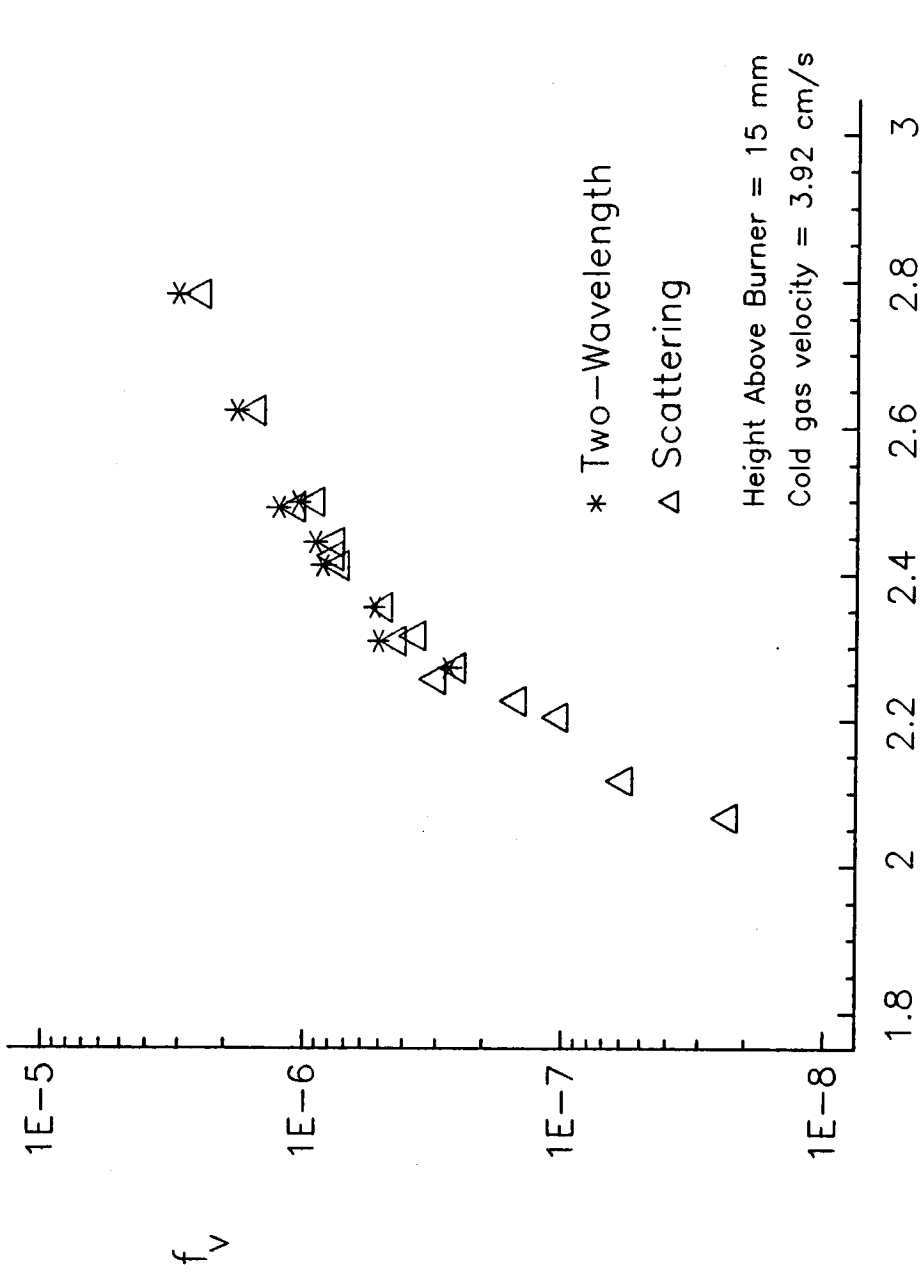
Soot Volume Fraction Versus Equivalence Ratio
f_v
1E-5
1E-6
1E-7
1E-8
1.8
2
2.2
2.4
2.6
2.8
3
Equivalence Ratio
* Two-Wavelength
Δ Scattering
Height Above Burner = 15 mm
Cold gas velocity = 3.92 cm/s

Figure 8.11

Figure 8.12 Soot Volume Fraction Versus Equivalence Ratio

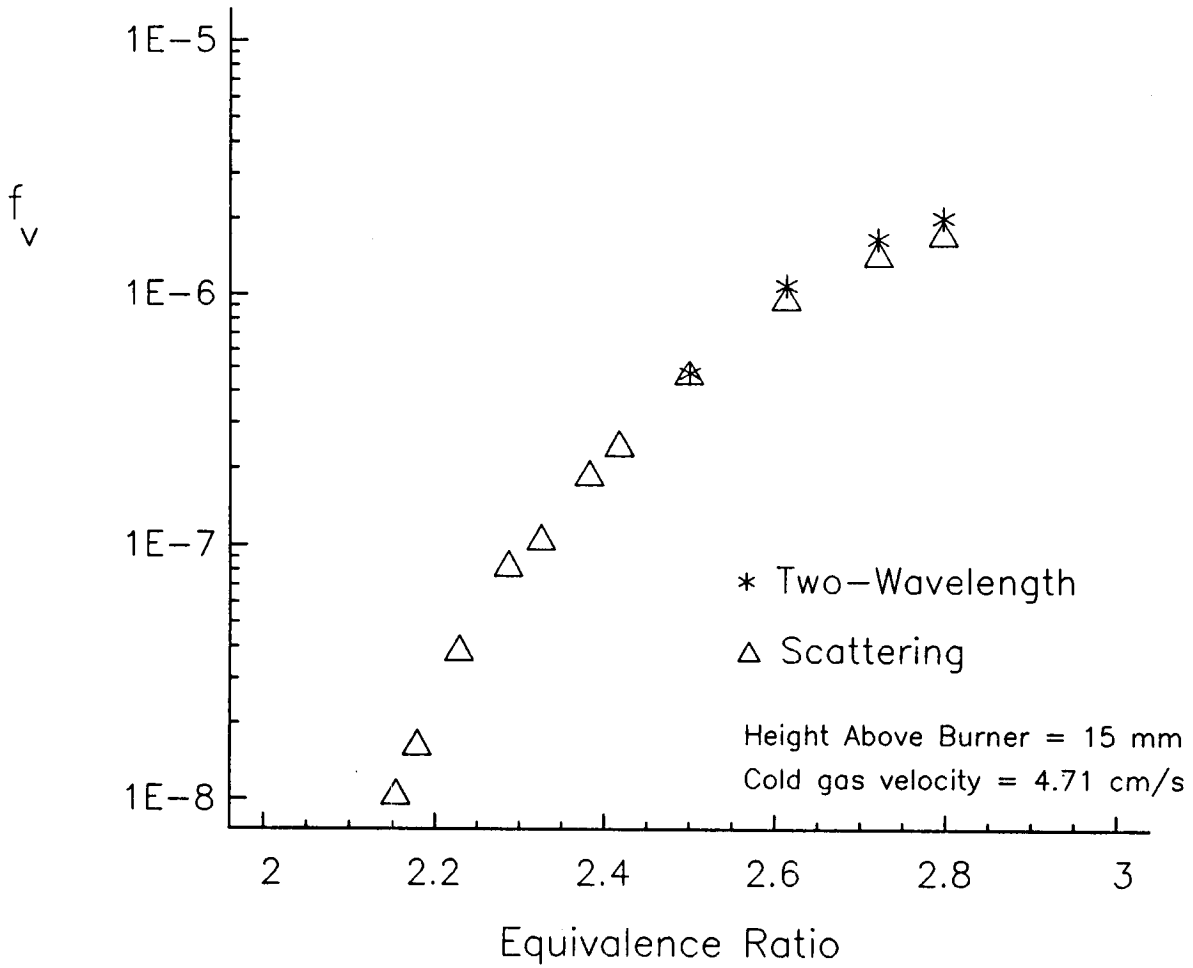

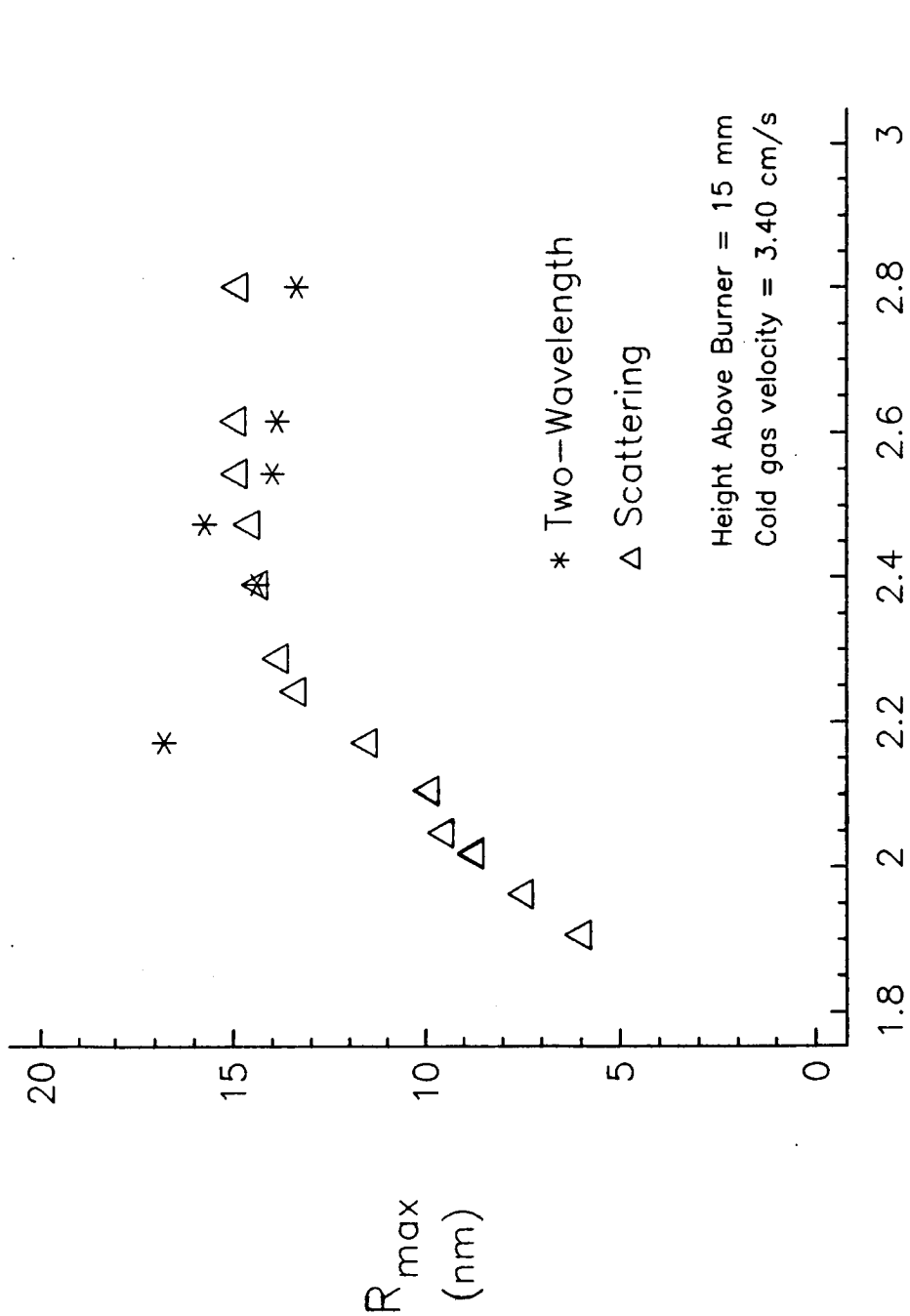

Figure 8.13 Soot Radius Versus Equivalence Ratio

Figure 8.14 Soot Radius Versus Equivalence Ratio

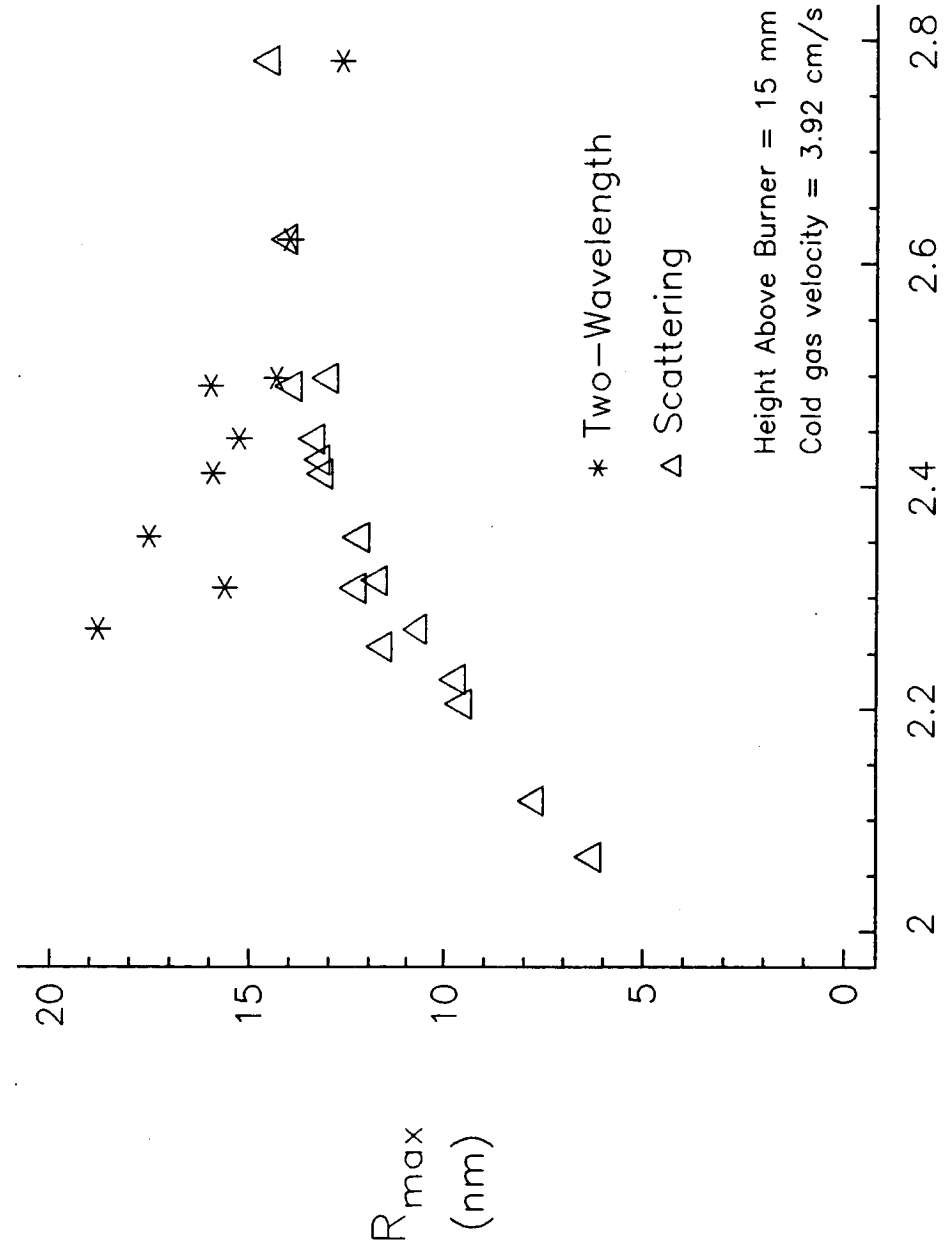

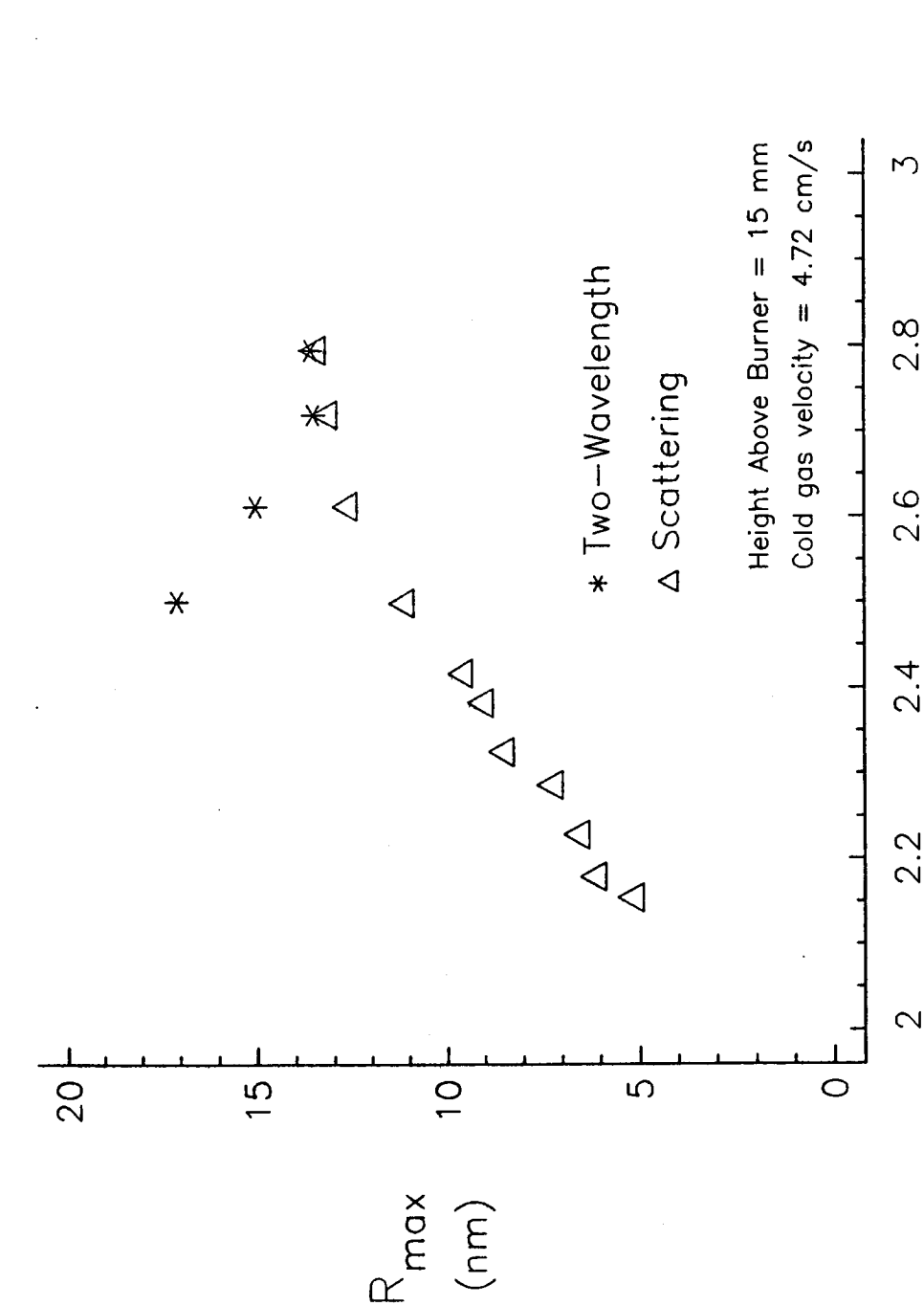

Figure 8.15 Soot Radius Versus Equivalence Ratio

Figure 8.16 Soot Number Density Versus Equivalence Ratio

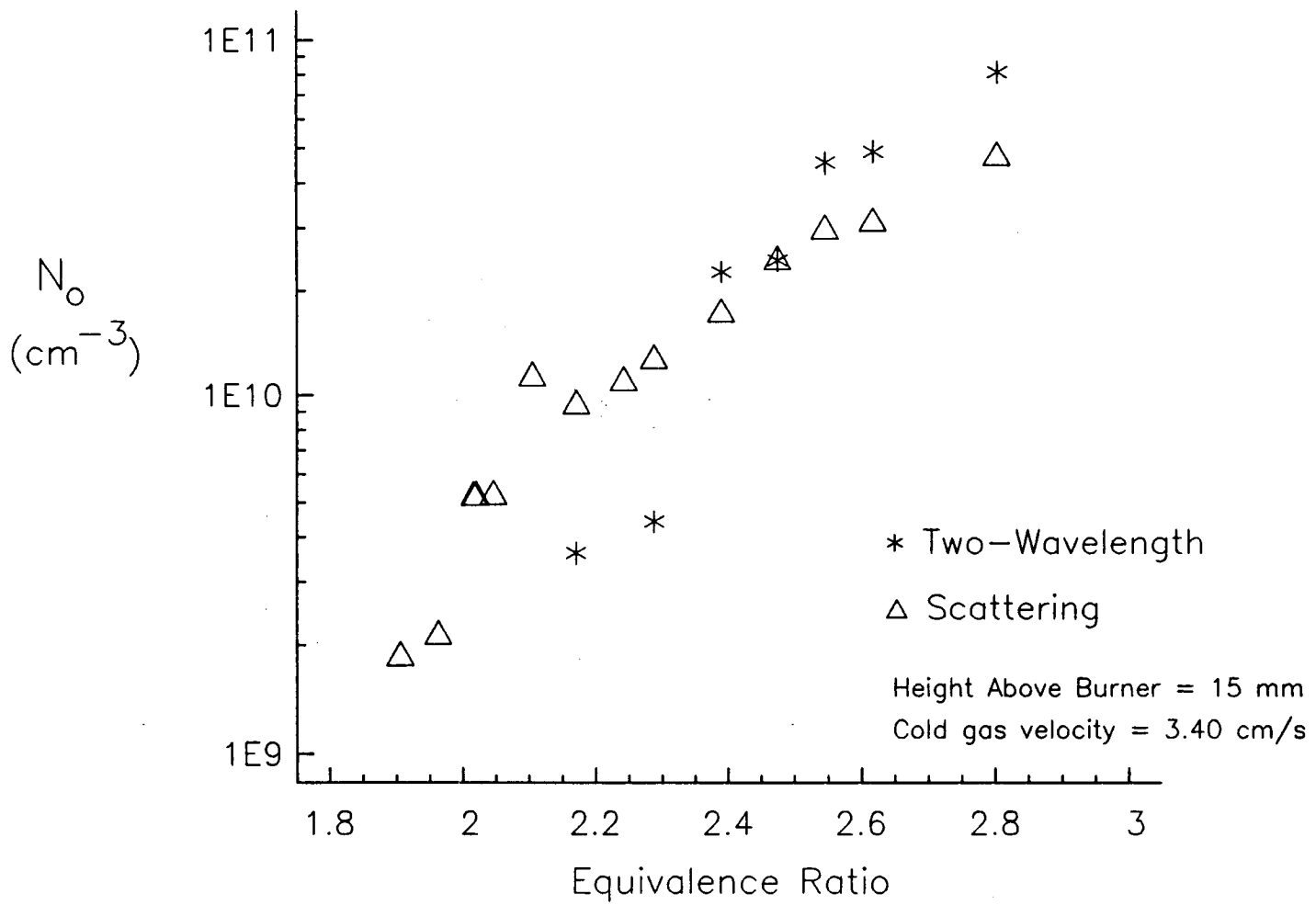

Figure 8.17 Soot Number Density Versus Equivalence Ratio

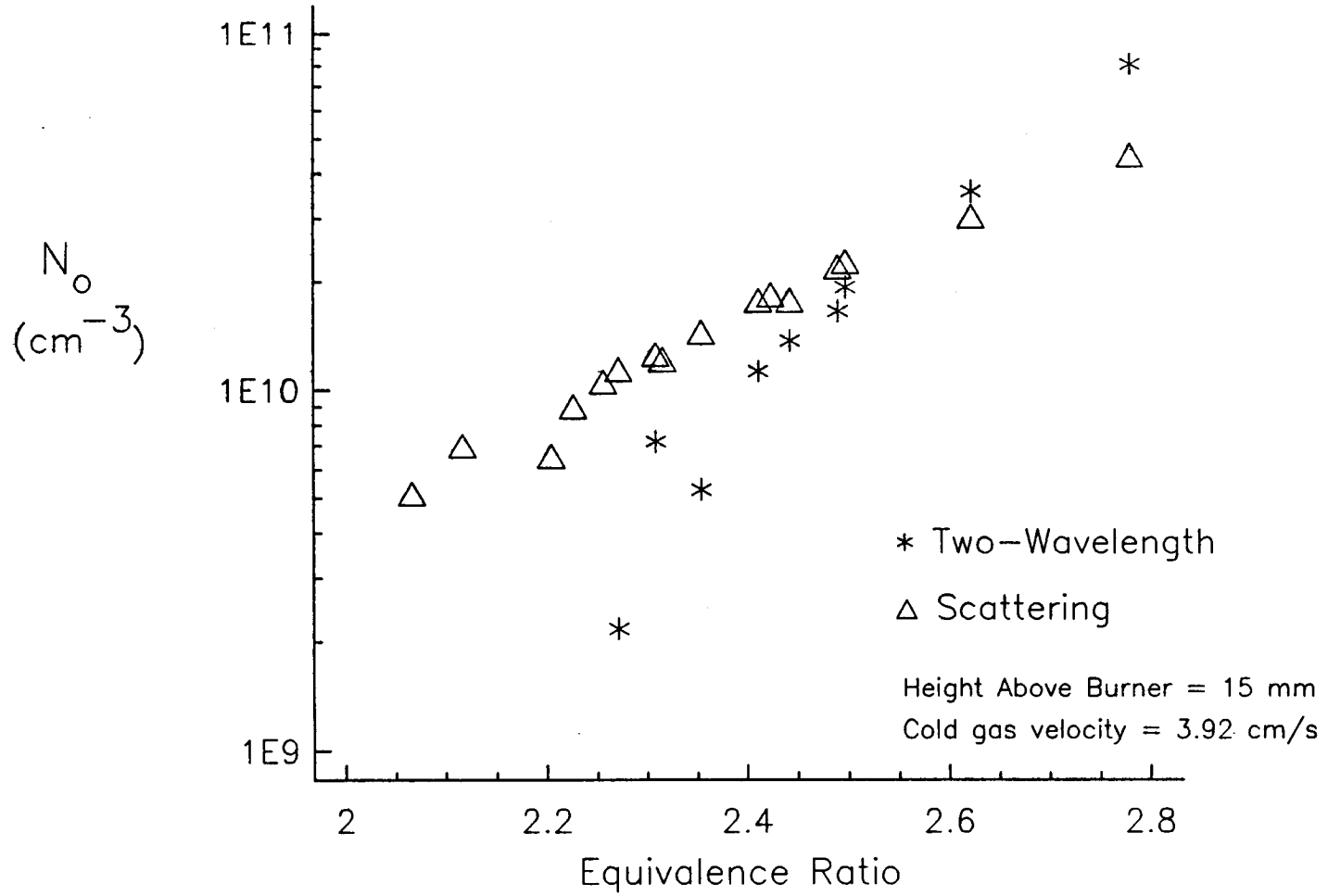

Figure 8.18 Soot Number Density Versus Equivalence Ratio

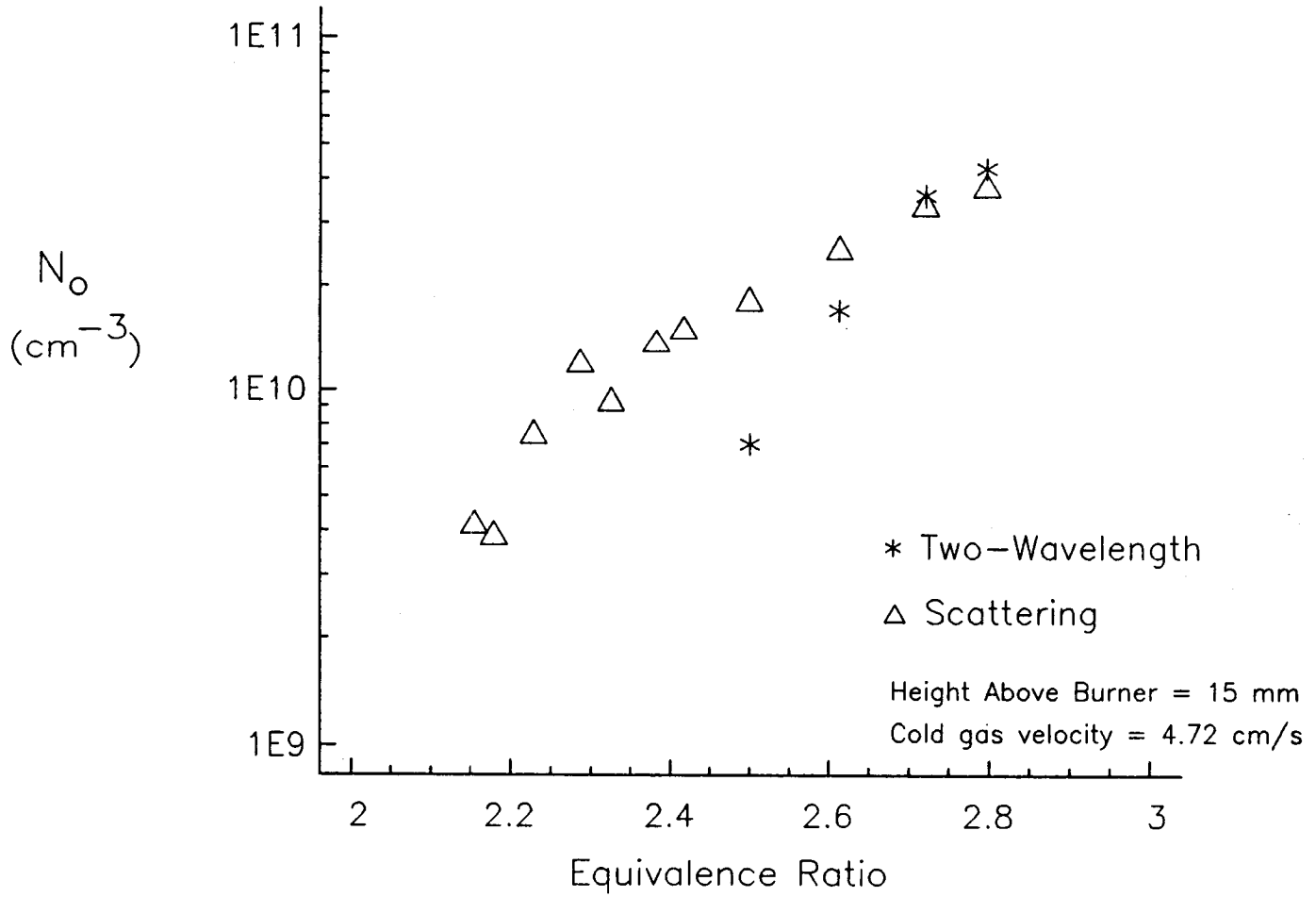

Chapter 9: Discussion of Results

In order to compare results with previous studies, two experimental conditions were chosen to be the same as those studied by Prado, et.al.[11] in a similar burner. These conditions were cold gas flow velocities of 3.92 and 5.5 cm/s at an equivalence ratio of 2.5. Soot volume fractions, f_v, particle radii, R_{max}, and number densities, N_o, were measured at various heights above the burner for these conditions and for a velocity of 4.71 cm/s. Also, at a fixed height above the burner of 15 mm, the equivalence ratio was varied from 2.0 to 2.8, while keeping the cold gas velocity fixed for each of the three chosen velocities. Measurements were made simultaneously using the two-wavelength method and the scattering/extinction method.

9.1 A Function of Height Above Burner

The f_v, R_{max}, and N_o obtained from the scattering/extinction measurements at various heights above the burner are shown in figure 5.3 for the three cold gas velocities and an equivalence ratio of 2.5. The soot particle sizes and number densities compare reasonably with Prado's[11] results, when he also assumed spherical particles. However, the agglomerated particles that Prado measured with sampling probes were larger in diameter and lower in number density. Prado's results are

not shown on figure 5.3 due to the use of different refractive indices in these two studies. There is still controversy over the choice of a refractive index for soot[62]. Prado's results used Dalzell and Sarofim's[63] value of m=1.57-i 0.56 for a wavelength of 514.5 nm. This would lead to a larger expected soot size than for the refractive index recommended by Lee and Tien[60-61] of m=1.93-i 0.52 used here. This smaller particle size leads to a slightly smaller volume fraction than Prado's results. However, similar trends in the relative amounts of soot at a particular height above the burner and cold gas flow rate are seen in both studies.

The scattering/extinction method and the two-wavelength method are compared in flames having an equivalence ratio of 2.5 and cold gas velocities of 3.92, 4.71 and 5.50 cm/s. These conditions provided sufficient amounts of soot to produce strong signals for both the scattering and extinction measurements.

Soot particle size, number density and volume fractions as predicted by both the scattering/extinction and the two-wavelength techniques are presented in figures 8.1 through 8.9 as a function of height above the burner. For a cold gas velocity of 3.92 cm/s, there is some discrepancy below a height above the burner of 10 mm when measuring size and number density as seen in figures 8.2

and 8.3. The two-wavelength technique appears less sensitive to the change in particle sizes for the small (less than 10 nm radius) particles near the burner surface (below 10 mm) and so predicts the same size (or even slightly larger particles) here. Since this particle size is used to determine the number density, the number density predicted by the two-wavelength technique is lower than the scattering technique for measurements below the 10 mm height above the burner. However, there is excellent agreement between the two techniques when measuring volume fraction (figure 8.1) since the over-prediction of particle size by the two-wavelength method is compensated by its under-prediction of number density. It is interesting to note that the agreement between the two methods for size and number density was best for soot volume fractions above $1x10^{-6}$. The experimental results for the cold gas velocity of 3.92 cm/s and an equivalence ratio of 2.5 are shown in Table 5. The measured intensity ratio I/I_o is given for each of the wavelengths as a function of the height above the burner, along with the resulting soot volume fractions, radii and number densities. The calculated error (see Appendix A) in each of these values is shown in Table 6. As previously seen by Bard[33] and Beier[36], the best results for the two-wavelength technique were produced when both wavelengths had I/I_o values less than 0.75. This occurred for heights above the burner greater than 7 mm. Good agreement

Table 5 Soot Volume Fractions, Radii and Number Densities as a Function of H.A.B.

Cold Gas Velocity = 3.92 cm/s
Equivalence Ratio = 2.5

HAB (mm)	L (cm)	I/I_o			Two-Wavelength*			Scattering/Extinction		
		0.4579	0.5145	0.6328	f_v $\times 10^7$	R_{max} (nm)	N_o $\times 10^{-9}/cm^3$	f_v $\times 10^7$	R_{max} (nm)	N_o $\times 10^{-9}/cm^3$
2	5.69	0.902	0.944	0.948	2.06	17.0	2.24	0.48	1.09	1976
3	5.65	0.806	0.890	0.898	2.59	19.1	2.00	2.65	3.11	474
4	5.46	0.724	0.833	0.847	4.47	18.0	4.11	4.47	5.36	156
5	5.36	0.662	0.786	0.804	6.37	16.1	8.23	6.15	7.26	86.3
7	5.09	0.579	0.723	0.749	8.68	15.8	11.9	8.52	10.1	44.5
9	4.74	0.542	0.681	0.714	11.28	13.4	25.4	10.35	11.3	38.3
11	4.61	0.508	0.651	0.691	13.19	13.8	27.2	11.44	12.6	31.1
13	4.45	0.471	0.628	0.666	14.56	14.6	25.0	12.76	13.2	29.8
15	4.35	0.469	0.363	0.675	13.67	17.3	14.3	12.36	13.8	25.3
18	4.06	0.451	0.609	0.651	14.68	14.7	27.7	14.41	14.1	27.4
21	4.19	0.389	0.554	0.605	20.05	15.5	29.0	16.34	14.5	29.1

* .4579 and .6328

Table 6 Experimental Results as a Function of H.A.B. Showing the Percent Deviation in Soot Volume Fractions, Radii and Number Densities

Cold Gas Velocity = 3.92 cm/s
Equivalence Ratio = 2.5

	Two-Wavelength*						Scattering/Extinction					
HAB (mm)	f_v $\times 10^7$	%Δ	R_{max} (nm)	%Δ	N_o $\times 10^{-9}/cm^3$	%Δ	f_v $\times 10^7$	%Δ	R_{max} (nm)	%Δ	N_o $\times 10^{-9}/cm^3$	%Δ
2	2.06	2.6	17.0	37	2.24	164	0.48	250	1.09	13	1976	326
4	4.47	5.2	18.0	33	4.11	87	4.47	21	5.36	4.1	156	34
5	6.37	2.7	16.1	19	8.23	52	6.15	21	7.26	3.8	86.3	33
7	8.68	2.0	15.8	19	11.9	54	8.52	19	10.1	3.9	44.5	31
9	11.28	5.1	13.4	12	25.4	32	10.35	22	11.3	4.1	38.3	34
11	13.19	4.9	13.8	14	27.2	38	11.44	18	12.6	4.1	31.1	31
13	14.56	1.4	14.6	22	25.0	66	12.76	26	13.2	4.9	29.8	41
15	13.67	0.8	17.3	24	14.3	68	12.36	19	13.8	4.3	25.3	32
18	14.68	3.2	14.7	16	27.7	45	14.41	24	14.1	4.7	27.4	38
21	20.05	2.5	15.5	16	29.0	45	16.34	22	14.5	4.4	29.1	35

* .4579 and .6328

NOTE: %Δ = 100 x (Max. − Min.)/ Mean

between the techniques and greater measurement accuracy began to be seen above this point also.

The results of measurements taken with a cold gas velocity of 4.71 and 5.50 cm/s, seen in figures 8.4 through 8.9, show increasing disagreement between the two techniques as the cold gas velocity is increased. This is mainly due to the decrease in the amount of soot at the chosen height above the burner (15 mm). The reduced residence time in the flame and the increased flame temperature at increased flow velocities (see figure 3.4a) produces less soot. As seen in figures 8.4 and 8.7, the soot volume fractions are all below $1x10^{-6}$, less than the amount of soot seen (in figures 8.1-8.3) to produce good agreement between the techniques.

9.2 A Function of Equivalence Ratio

A comparison of the two techniques was made as a function of equivalence ratio at a height above the burner of 15 mm for 3.40, 3.92, and 4.71 cm/s cold gas velocities. Figures 8.10 through 8.18 show the results for the soot particle radius, number density and volume fraction for equivalence ratios from 1.8 to 2.8. The tabulated results for the 3.92 cm/s cold gas velocity are seen in Table 7. The two-wavelength method calculated impossible (negative or too-large positive) values for X_{ij}, resulting in no measurements until an equivalence

Table 7 Soot Volume Fractions, Radii and Number Densities as a Function of Equivalence Ratio

Cold Gas Velocity = 3.92 cm/s
Height Above Burner = 15 mm

Φ	L (cm)	I/I_o			Two-Wavelength *			Scattering/Extinction		
		0.4579	0.5145	0.6328	f_v $\times 10^7$	R_{max} (nm)	N_o $\times 10^{-9}/cm^3$	f_v $\times 10^7$	R_{max} (nm)	N_o $\times 10^{-9}/cm^3$
2.07	4.09	0.966	0.993	0.988	--	--	--	0.22	6.33	4.72
2.13	4.13	0.931	0.983	0.978	--	--	--	0.58	7.73	6.79
2.20	4.15	0.899	0.968	0.963	--	--	--	1.04	9.52	6.48
2.27	4.28	0.859	0.920	0.925	2.77	18.8	2.24	2.55	10.7	11.29
2.31	4.39	0.770	0.860	0.870	5.17	15.6	7.29	4.26	12.3	12.23
2.35	4.35	0.748	0.845	0.860	5.39	17.5	5.37	4.83	12.2	14.19
2.41	4.38	0.644	0.768	0.793	8.51	15.9	11.30	7.31	13.2	17.23
2.44	4.38	0.632	0.755	0.783	9.07	15.3	13.70	7.68	13.4	17.28
2.49	4.38	0.520	0.672	0.708	12.65	16.0	16.60	10.82	13.9	21.42
2.62	4.39	0.416	0.568	0.620	19.11	14.0	37.40	16.70	14.0	29.81
2.78	4.43	0.242	0.385	0.454	31.05	12.7	81.70	25.06	14.5	44.10

* .4579 and .6328

ratio of 2.27. Below this equivalence ratio, the I/I_o (extinction measurement) values for the three wavelengths used were nearly 1.0. Measurement of the slight variations from this value was difficult due to a small signal to noise ratio. This problem was not as evident in the scattering/extinction measurements since the scattering intensity varies by a much greater amount for small changes in equivalence ratio (for example from 2.11 to 2.17, the scattering intensity doubles). The extinction measurement plays a lesser role in the final results for the scattering/extinction method, although the accuracy of the results is affected, as seen by the large errors below an equivalence ratio of 2.3 in Table 8. For longer pathlengths (larger burner), or more densely sooting flames, the extinction measurement would be more accurate. Table 8 shows large errors below an equivalence ratio of 2.1, evidence that there was too little soot to allow repeatable measurements for the scattering-extinction technique.

The agreement between the two techniques begins to be good near an equivalence ratio of 2.5 (where the I/I_o for all the wavelengths was below 0.75). The two techniques begin to disagree slightly in the very rich (near equivalence ratio 2.8) flames. For the very sooty flames, a change in the equivalence ratio will produce a smaller relative change in the extinction intensity than in the

scattering intensity. The differences between the two techniques in prediction of soot particle size and number density for the very rich flames are fairly small. There is excellent agreement in the prediction of soot volume fractions by both techniques where measurements could be taken. At equivalence ratios higher than 2.8, the flame was beginning to be unsteady,[64] making it difficult to measure L.

Table 8 Experimental Results as a Function of Equivalence Ratio Showing the Percent Deviation in Soot Volume Fractions, Radii and Number Densities

Cold Gas Velocity = 3.92 cm/s
Height Above Burner = 15 mm

	Two-Wavelength*						Scattering/Extinction					
Φ	f_v $\times 10^7$	%Δ	R_{max} (nm)	%Δ	N_o $\times 10^{-9}/cm^3$	%Δ	f_v $\times 10^7$	%Δ	R_{max} (nm)	%Δ	N_o $\times 10^{-9}/cm^3$	%Δ
2.07	--		--		--		0.22	199	6.33	45.0	4.72	636
2.13	--		--		--		0.58	80	7.73	19.0	6.79	156
2.20	--		--		--		1.04	41	9.52	10.0	6.48	75
2.27	2.77	0.8	18.8	59	2.24	375	2.55	33	10.7	8.0	11.29	60
2.31	5.17	0.3	15.6	31	7.29	93	4.26	28	12.3	5.6	12.23	45
2.35	5.39	0.9	17.5	30	5.37	123	4.83	20	12.2	4.0	14.19	33
2.41	8.51	3.1	15.9	16	11.30	43	7.31	23	13.2	4.6	17.23	37
2.44	9.07	3.4	15.3	15	13.70	41	7.68	21	13.4	4.3	17.28	34
2.49	12.65	1.4	16.0	20	16.60	57	10.82	21	13.9	4.6	21.42	35
2.62	19.11	4.6	14.0	12	37.40	31	16.70	18	14.0	4.0	29.81	30
2.78	31.05	3.5	12.7	17	81.70	47	25.06	25	14.5	4.4	44.10	38

* .4579 and .6328

NOTE: %Δ = 100 x (Max. - Min.)/ Mean

Chapter 10: Conclusions

10.1 Relative Merits of the Two Techniques

Two laser diagnostic techniques, scattering-extinction and two-wavelength methods, have been shown to be capable of measuring soot volume fractions, radii, and number densities in premixed, propane-oxygen flames. The two methods agree very well for some of the flow conditions, but increasingly disagree as the soot concentration decreases.

One benefits of the two-wavelength method is the ease of alignment of the optical system. Especially in the uniform flow field of the premixed flat flame, there is no very strict alignment procedure required. The two laser beams from the helium-neon and argon ion lasers must be reasonably closely superimposed, but this is much more critical in other flames (such as a boundary layer flame[36]). The photodiodes collecting the laser light must be placed so that all the light falls on the detector, but with a detector surface 12 mm in diameter, this is not a critical procedure. Care must be taken to completely separate the wavelengths so that only the wavelength of interest falls on the corresponding detector, however. Care must also be taken to prevent any beam stops or apertures from blocking the beams when the flame flickers, or erroneously low signals will result. The photodetectors are easily saturated when making extinction

measurements, so neutral density filters are needed to prevent this. Care must be taken in selecting good quality neutral density filters so that spatial variation of the density of the filter is minimized. If poor filters are used, the flickering of the flame will produce varying signals which are characteristic of the filter, not of the flame. The electronic readouts for the detectors must also be set at a proper range to avoid over-scale readings, or lack of resolution. Another possible problem can arise due to electronic drift of the lasers and the various electronic readouts and amplifiers for the system. A sufficiently short data-sampling time, coupled with continual updating of the calibration of the equipment can minimize this. Despite these precautions, the two-wavelength method is fairly straight-forward to set up. As previously discussed (Chapter 9), this technique is limited to flames where the resulting I/I_o is less than 0.75. One frustration involved in using this method is the lack of any calculated values of volume fraction, radius, or number density until there is enough soot to provide a strong extinction signal. There is no evidence of any problem and there appears to be a "reasonable" amount of soot in the flame, however, the calculated X_{ij} value is out of range. For the short (4-6 cm) pathlengths of this flat flame burner, this "reasonable" amount of soot was not enough to produce I/I_o's below 0.75, although it was enough to produce

strong signals for the light scattering measurements. This allowed the scattering/extinction method to make measurements where the two-wavelength method could not.

The scattering/extinction method was more "user-friendly" in that it would produce results whenever a slight amount of soot was seen in the flame. However, some of the results were later seen to be relatively inaccurate (see error bars on Figures A.1 through A.8) The scattering-extinction method required a more sophisticated optical set-up and more critical alignment procedure than the two-wavelength method. Besides all the precautions mentioned for the two-wavelength technique, the scattering optics had their own set of special problems. First of all, the detector (photomultiplier tube) required to measure the weakly scattered light from the soot particles was more sophisticated (expensive and fragile) than those required for the extinction measurements. It was also necessary to protect this sensitive detector from the bright light from the flame while not diminishing the signal from the soot particles. This required a very narrow-band line filter (514.5 ± 1 nm) and a beam chopper/lock-in amplifier system as well as a very small pin-hole (1 mm diameter). It then became necessary to very carefully align the laser beam so the image of the probe volume fell on this 1 mm pin-hole. Also, the positioning of the photomultiplier, in all three

axes as well as pitch and yaw, was critical. This positioning had to be checked using the calibration procedures with two known scattering cross-sections (nitrogen and methane). Care had to be taken to be sure the polarization of the laser beam was correct also.

10.2 Recommendations

Although the scattering-extinction method was more difficult to set up than the two-wavelength method, it was able to measure soot volume fractions, radii and number densities in a greater range of flames. In the flames where a good comparision could be made, the two-wavelength technique determined the soot volume fractions with greater accuracy (see Tables 6 and 8), while the scattering-extinction method determined the soot radii and number densities with greater accuracy. If the goal of a future research project is to determine a soot volume fraction, and the flame is such as to allow adjustment of either the pathlength or the equivalence ratio to produce I/I_o values below 0.75, the two-wavelength technique would be the simplest method to use. However, if it was necessary to determine the soot radii and number densities as well as the volume fractions and the flame was not heavily sooting and/or was relatively small (allowing a short pathlength), the increased complexity of the scattering/extinction technique would be justified and highly recommended.

In conclusion, soot volume fractions, particle sizes and number densities were measured in various propane/oxygen premixed flames by two laser techniques. The two methods compared favorably in flames where the extinction intensity ratios (I/I_o) were between 0.1 and 0.75. Within this range, the two techniques produced good agreement in prediction of R_{max}, N_o and f_v. The two methods agreed in the prediction of f_v alone for intensity ratios up to 0.95. The good agreement between the two techniques affirms the analysis performed and gives credence to the size distribution and soot optical properties chosen.

References

1. Wey, C.,"Soot Formation in Gaseous Laminar Diffusion Flames", Ph.D. Thesis, Georgia Institute of Technology, 1984.

2. Stark, S., *Wiedem Ann.*, **62**, 353, 1897.

3. Becker, A., *Ann. Physik*, **28**, 1017, 1909.

4. Hottel, H.C. and Broughton, F.P., Ind. Eng. Chem. (Anal. Ed.), **4**, 166, 1932.

5. Millikan, R.C., Temperature--Its Measurement and Control in Science and Industry, Vol. 3, Part 2, 497, Reinhold Pu. Co., N.Y., 1962

6. Bonne, U. and Wagner H.Gg., Ber. Bersenges, Physik Chem., **69**, 1965.

7. Pagni, P.J and Bard, S., Seventeenth Symposium (International) on Combustion, Combustion Institute, 1017, 1978.

8. Senftleben, H. and Benedict, B., *Ann. Phys. Lpz.*, **61**, 297, 1919.

9. Dalzell, W.H., Williams, G.C., and Hottel, H.C., *Comb. and Flame*, **14**, 161, 1970.

10. D'Allesio, A., Beretta, F. and Venitozzi, C., *Comb. Sci. and Tech.*, **5**, 263, 1972.

11. Prado, G., Jagoda, J., Neoh, K., and Lahaye, J., Eighteenth Symposium (International) on Combustion, Combustion Institute, 1127, 1980.

12. Bockhorn, H., Fetting, F., Meyer, U., Reck, R., and Wannemacher, G., Eighteenth Symposium (International) on Combustion, The Combustion Institute, 1137, 1981.

13. Santoro, R.J., Semerjian, R.A., and Dobbins, R.A., *Comb. Flame*, **51**, 203, 1983a.

14. Santoro, R.J., Semerjian, R.A., and Dobbins, R.A., AIAA 18th Thermophysics Conference, Paper AIAA-83-1516, Montreal, Canada, 1983.

15. Dobbins, R.A. and Mulholland, G.W., Comb. Sci. Tech., **40**, 175, 1984.

16. Mie, G. *Ann. Physik (IV)*, **25**, 377, 1908.

17. Pepperhoff, W., *Optik*, **8**, 354, 1951.

18. Rossler, F., *Optik*, **10**, 531, 1953.

19. Stull, V.R. and Plass, G.M., *J. Opt. Soc. Am.*, **50**, 121, 1960.

20. Glassman, I. and Yaccarino, P., The Eighteenth Symposium (International) on Combustion, The Combustion Institute, 1175, 1980.

21. Glassman, I. and Yaccarino, P., *Comb. Sci. and Tech.*, **24**, 107, 1980.

22. Kadota, T., Hiroyasu, H. and Farazandehmehr, A., *Comb. and Flame*, **29**, 67, 1977.

23. Chakraborty, B.B. and Long, R., *Comb. and Flame*, **12**, 237, 1968.

24. Jagoda, I.J., Prado, G., and Lahaye, J., *Comb. and Flame*, **37**, 261, 1980.

25. D'Allesio, A., Di Lorenzo, A., Sarofim, A.F., Beretta, F., Masi, S., and Venitozzi, C., Fifteenth Symposium (International) on Combustion, The Combustion Institute, 1427, 1974.

26. D'Allesio, A., Di Lorenzo, A., Borghese, A., Beretta, F., and Masi, S., Sixteenth Symposium (International) on Combustion, The Combustion Institute, 695, 1977.

27. Kent, J.H., Jander, H., and Wagner, H.Gg., Eighteenth Symposium (International) on Combustion, The Combustion Institute, 1117, 1980.

28. Haynes, B.S. and Wagner, H.Gg., Ber. Bunsenges. Phys. Chem., **84**, 499, 1980.

29. Haynes, B.S., Jander, H., and Wagner, H.Gg., Ber. Bunsenges. Phys. Chem., **84**, 585, 1980.

30. Chang, P.H.P. and Penner, S.S., *J. Quant. Spectrosc. Radiat. Transfer*, **25**, 105, 1981.

31. Pagni, P.J and Bard, S., Seventeenth Symposium (International) on Combustion, Combustion Institute, 1017, 1978.

32. Bard, S. and Pagni, P.J., *J. Quant. Spec. Rad. Trans.*, **25**, 453, 1981.

33. Bard, S., "Diffusion Flame Particulate Volume Fractions," Ph.D. Dissertation, Mechanical Engineering Dept., University of California, Berkeley, 1980.

34. Bard, S. and Pagni, P.J., *ASME Journal of Heat Transfer*, **103**, 357, 1981.

35. Bard, S. and Pagni, P.J., "Spatial Variation of Soot Volume Fractions in Pool Fire Diffusion Flames", Fire Safety Science-Proceedings of the 1st International Symposium, 1986.

36. Beier, R.A., "Soot and Radiation in Combusting Boundary Layers," Ph.D. Dissertation, Mechanical Engineering Dept., University of California, Berkeley, 1981.

37. Beier, R.A. and Pagni, P.J., J.Ht. Trans., **105**, 159, 1983.

38. Beier, R.A. and Pagni, P.J., Twentieth ASME/AIChE National Heat Transfer Conference, ASME Paper No. 81 -HT-1, 1981.

39. Asano, S. and Yamamato, G., *Applied Optics*, **14**, No. 1, 29, 1975.

40. Palmer, H.B. and Cullis, C.F., The Chemistry and Physics of Carbon (Editor Walker, P.L.), **1**, Marcel Dekker, New York, p.265, 1965.

41. Wagner, H.Gg., Seventeenth Synposium (International) on Combustion, The Combustion Institute, 3, 1979.

42. Bittner, J.D. and Howard, J.B., Alternative Hydrocarbon Fuels: Combustion and Kinetics, Progress in Astronautics and Aeronautics, **62**, 335, A.I.A.A., New York, 1978.

43. Haynes, B.S. and Wagner, H.G., Progr. Energy Comb. Sci., **7**, 229, 1981.

44. Baumgärtner, L., Hesse, D., Jander, H., and Wagner, H.G., Twentieth Symposium (International) on Combustion, The Combustion Institute, 959, 1984.

45. Pagni, P.J., Ortega, A., Toosi, R., Western States Section of the Combustion Institute, Paper 79-47, 1979.

46. Tourin, R.H., Temperature-Its Measurement and Control in Science and Industry, Vol. 3, Part 2, p.455, Reinhold Publishing Corp., 1962.

47. Barnes Radiometer Instruction Manual, Barnes Engineering Company, Stamford, Connecticut, 1977.

48. Schmidt, H., Ann.Physik, Vol. 29, p.971, 1909.

49. Kreith, F., Principles of Heat Transfer, Harper & Row, 1973.

50. Jakob, M., Heat Transfer, Vol. 1, John Wiley & Sons, 1949.

51. Siegel, R. and Howell, J.R., Thermal Radiation Heat Transfer, McGraw-Hill, New York, 1972.

52. Ang, J.A., Pagni, P.J., Mataga, T.G., Margle, J.M. and Lyons, V.J., AIAA 24th Aerospace Sciences Meeting, Paper 86-0575, 1986.

53. Ang, J.A., "Perturbed Boundary Layer Diffusion Flames", Ph.D Dissertation, Mechanical Engineering Dept. University of California, Berkeley, 1986.

54. Rudder, R.R. and Bach, D.R., *J. Optical Soc. of Am.*, **58**, 1260, 1968.

55. Hottel, H.C. and Sarofim, A.F., Radiative Transfer, McGraw-Hill, New York, 1967.

56. Kerker, M., The Scattering of Light and Other Electromagnetic Radiation, Academic Press, New York, 1969.

57. Wersborg, B.L., Howard, J.B., and Williams, G.C., Fourteenth Symposium (International) on Combustion, 929, 1972.

58. Bohren, C.F. and Huffman, D.R., Absorption and Scattering of Light by Small Particles, John Wiley and Sons, New York, 1983.

59. Hildebrand, F.B., Introduction to Numerical Analysis, McGraw-Hill, New York, 1956.

60. Lee, S.C. and Tien, C.L., Eighteenth Symposium (International) on Combustion, Combustion Institute, 1159, 1980.

61. Tien, C.L. and Lee, S.C., Prog. Energy Comb. Sci., **8**, 41, 1982.

62. Charalampopoulos, T.T. and Felske, J.D., Comb. and Flame, **68**, 283, 1987.

63. Dalzell, W.H. and Sarofim, A.F., Trans. A.S.M.E., J. Ht. Trans., **91**, 100, 1969.

64. Gaydon, A.G. and Wolfhard, H.G., Flames, Their Structure, Radiation and Temperature (3rd ed.), p. 32, Chapman and Hall, London, 1970.

65. Kiernan, C.L., Spencer, J.M. and Turner, J.R., APL*PLUS System, STSC, Inc., Rockville, Md., 1985.

Appendix A ERROR ANALYSIS

A.1 Two-Wavelength Technique

A detailed error analysis of the multiwavelength technique has been given by Bard[33]. This error analysis showed that a 10% uncertainty in n or nk gives a 10% uncertainty in the soot volume fraction, f_v. In Bard and Pagni's pool fire experiments[31-35], the fluctuations in beam pathlength were much larger than those found in Beier and Pagni's boundary layer flames[36-38], or in the pathlengths found in the flat flame burner: ±5% maximum deviation. The uncertainty in f_v, r_{max}, and N_o, depends also on the accuracy of the measured beam intensities.

The fractional uncertainty in a quantity $S = F(x_1, x_2, \ldots, x_n)$ is given by:

$$\left(\frac{\Delta S}{S} \right)^2 = \left(\frac{\delta F}{\delta x_1} \frac{\Delta x_1}{S} \right)^2 + \left(\frac{\delta F}{\delta x_2} \frac{\Delta x_2}{S} \right)^2 + \ldots + \left(\frac{\delta F}{\delta x_n} \frac{\Delta x_n}{S} \right)^2 \quad (A.1)$$

Applying equation A.1 to equations 7.1 and 7.8 gives the fractional uncertainties in K_{ext} and K_i/K_j as:

$$\frac{\Delta K_{ext}}{K_{ext}} = \left[\left(\frac{\Delta I}{I \ln \frac{I}{I_o}} \right)^2 + \left(\frac{\Delta Io}{I_o \ln \frac{I}{I_o}} \right)^2 + \left(\frac{\Delta L}{L} \right)^2 \right]^{1/2} \quad (A.2)$$

and

$$\frac{\Delta K_{ij}}{K_{ij}} = \left[\left(\frac{\Delta I_i}{I_i \ln \frac{I}{I_o}} \right)^2 + \left(\frac{\Delta I_j}{I_j \ln \frac{I}{I_o}} \right)^2 + \left(\frac{\Delta I_{oi}}{I_{oi} \ln \frac{I}{I_o}} \right)^2 + \left(\frac{\Delta I_{oj}}{I_{oj} \ln \frac{I}{I_o}} \right)^2 \right]^{1/2} \quad (A.3)$$

where $K_{ij} = K_i/K_j$. Equation (A.3) is used along with applying equation (A.1) to equation 7.7 to find the uncertainty in X_{ij}:

$$\Delta X_{ij} = \frac{\left[\frac{\Delta K_{ij}}{K_{ij}} \right] K_{ij}}{[\, K_{ij} - 1]_{abs}} \quad (A.4)$$

A.2 Scattering Technique

Equation (A.1) is applied to equation (4.21) to give the uncertainty in the volumetric scattering cross section:

$$\frac{\Delta Q_{vv}}{Q_{vv}} = \left[\left(\frac{\Delta I_{s,s}}{I_{s,s}} \right)^2 + \left(\frac{\Delta I_{s,N}}{I_{s,N}} \right)^2 + \left(\frac{\Delta I_o}{I_o} \right)^2 + \left(\frac{\Delta I}{I} \right)^2 \right]^{1/2} \quad (A.5)$$

where $I_{s,s}$ is the intensity of light scattered from soot particles and $I_{s,N}$ is the intensity of light scattered from nitrogen molecules. Dividing equation (4.21) by (4.20) gives an expression for the experimental Q_{vv}/K_{ext}:

$$\frac{Q_{vv}}{K_{ext}} = \frac{(\sigma_o N_o)_{N_2}}{-L} \left(\frac{I_{s,s}}{I_{s,N}}\right)\left(\frac{I_o}{I}\right)\left(\ln \frac{I}{I_o}\right)^{-1} \qquad (A.6)$$

Applying equation (A.1) to equation (A.6) gives an expression for the uncertainty in Q_{vv}/K_{ext} (renamed QK for simplicity):

$$\frac{\Delta QK}{QK} = \left[\left(\frac{\Delta I_{s,s}}{I_{s,s}}\right)^2 + \left(\frac{\Delta I_{s,N}}{I_{s,N}}\right)^2 + \left\{\frac{\Delta I}{I}\left[1+\left(\ln \frac{I}{I_o}\right)^{-1}\right]\right\}^2 + \left\{\frac{\Delta I_o}{I_o}\left[1+\left(\ln \frac{I}{I_o}\right)^{-1}\right]\right\}^2 + \left(\frac{\Delta L}{L}\right)^2\right]^{1/2} \qquad (A.7)$$

The extreme values for the ratio Q_{vv}/K_{ext} are found from:

$$\left(\frac{Q_{vv}}{K_{ext}}\right)_{max,min} = QK \pm \frac{\Delta QK}{QK} QK \qquad (A.8)$$

where $QK = Q_{vv}/K_{ext}$ is determined experimentally. These extreme values for this ratio are used to determine the extreme values for R_{max}. These R_{max} values are then used, along with the extreme values for Q_{vv}, ($= Q_{vv} \pm \Delta Q_{vv}$) using equation (A.5), to find extremes for N_o and f_v.

Figures A.1a through A.7b show the extreme values for f_v, R_{max}, and N_o shown as error bars about the mean value for both the two-wavelength and scattering-extinction methods as functions of equivalence ratio and height above the burner.

Figure A.1a Soot Volume Fraction Versus Equivalence Ratio

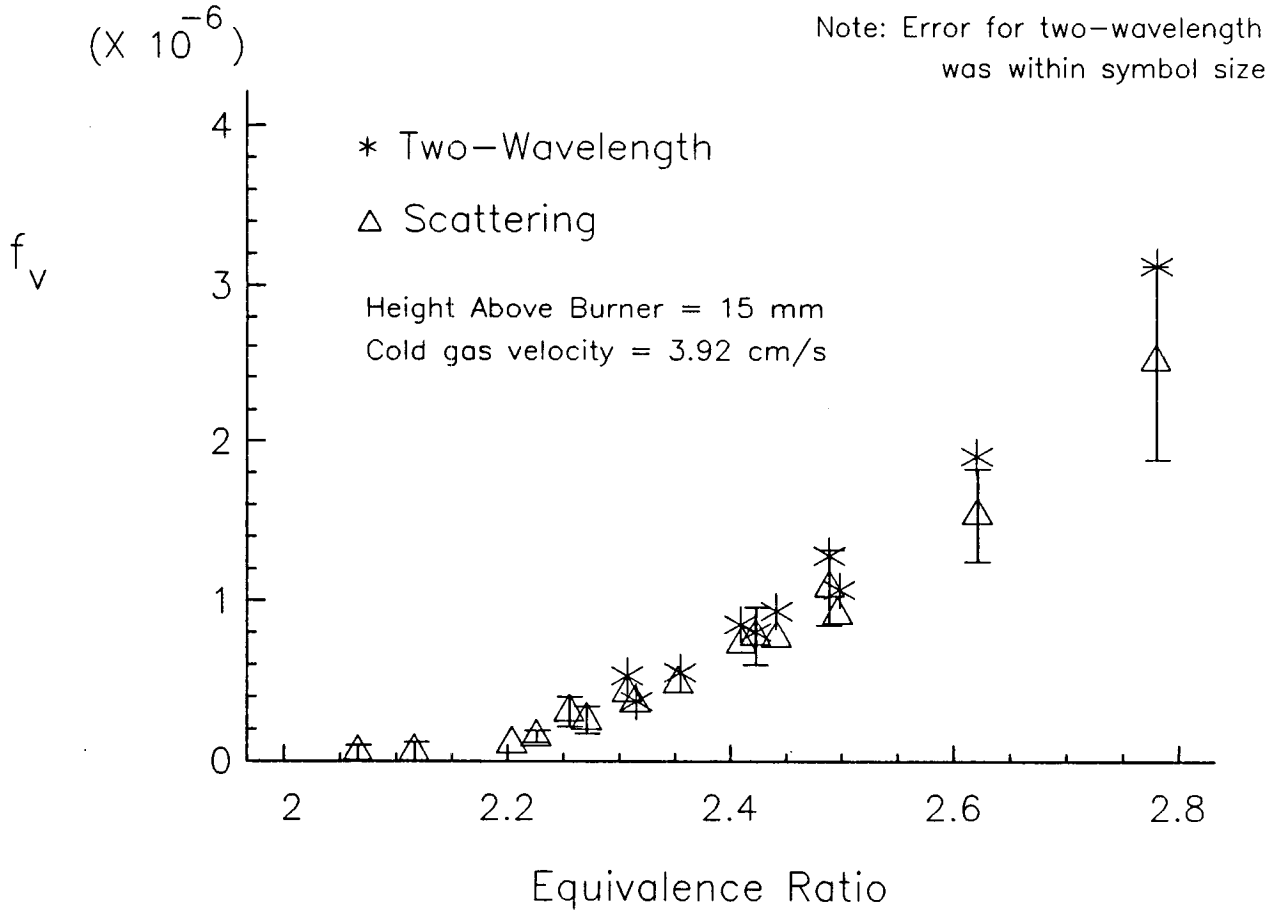

Figure A.1b Soot Volume Fraction Versus Equivalence Ratio

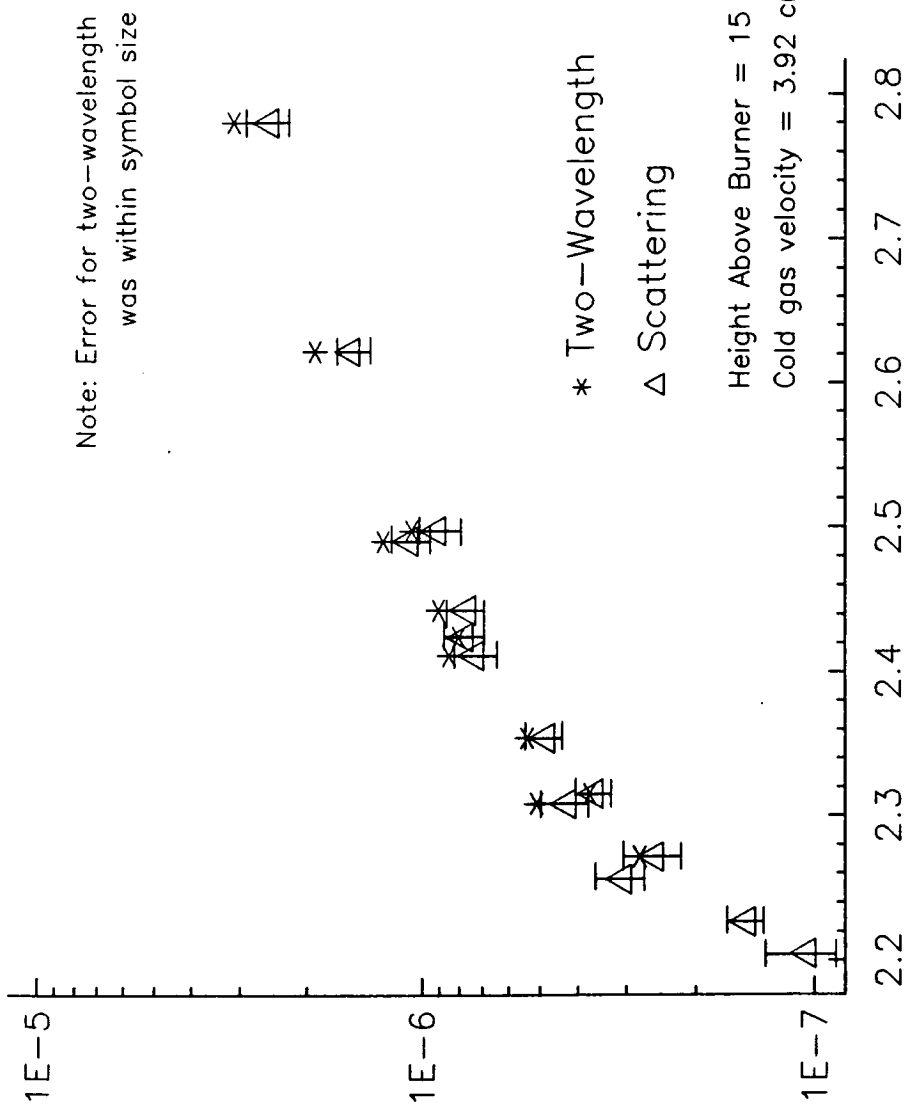

Figure A.2a Soot Volume Fraction Versus Height Above Burner

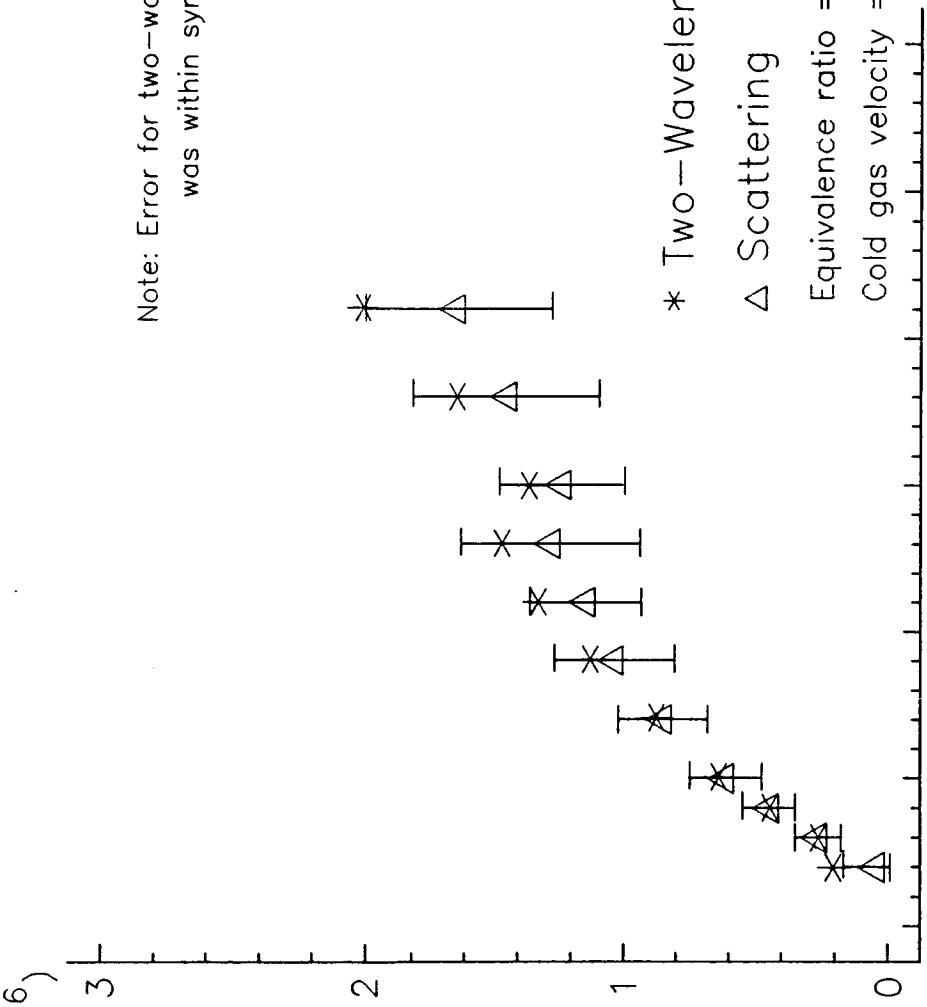

Figure A.2b Soot Volume Fraction Versus Height Above Burner

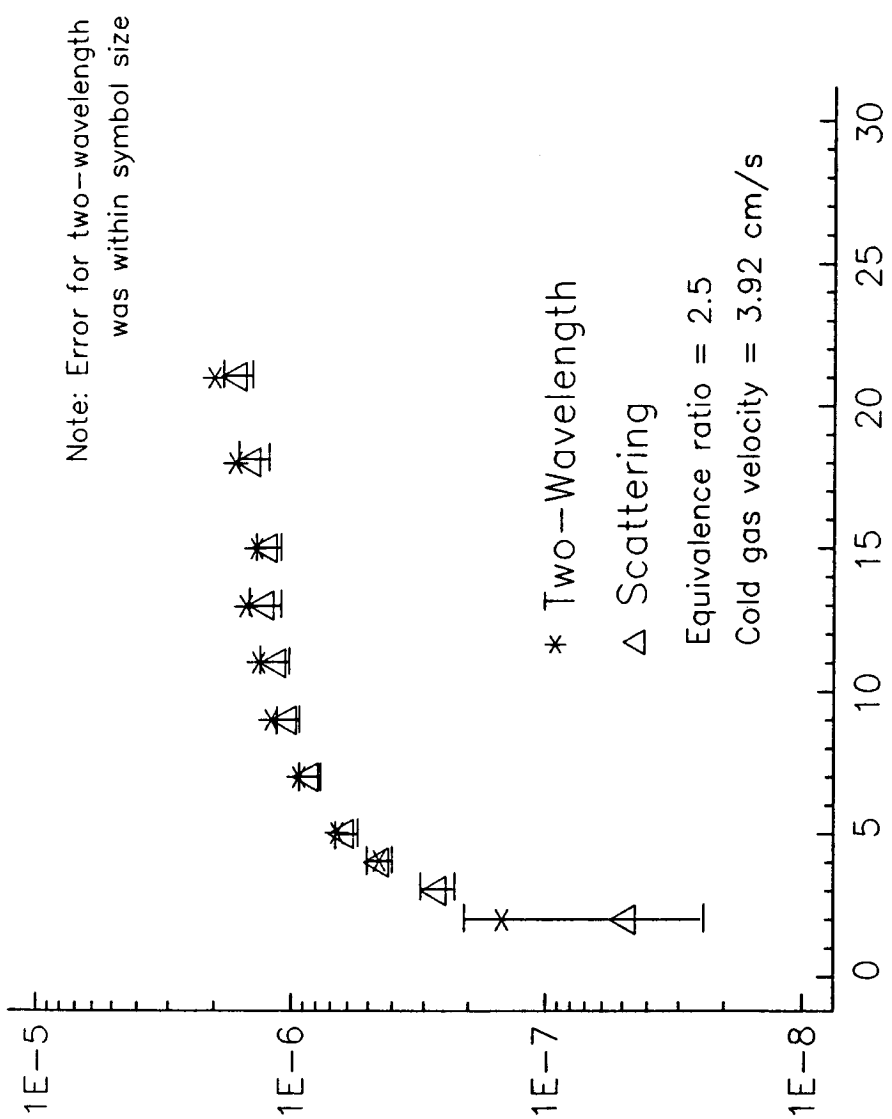

Figure A.3 Soot Radius Versus Equivalence Ratio

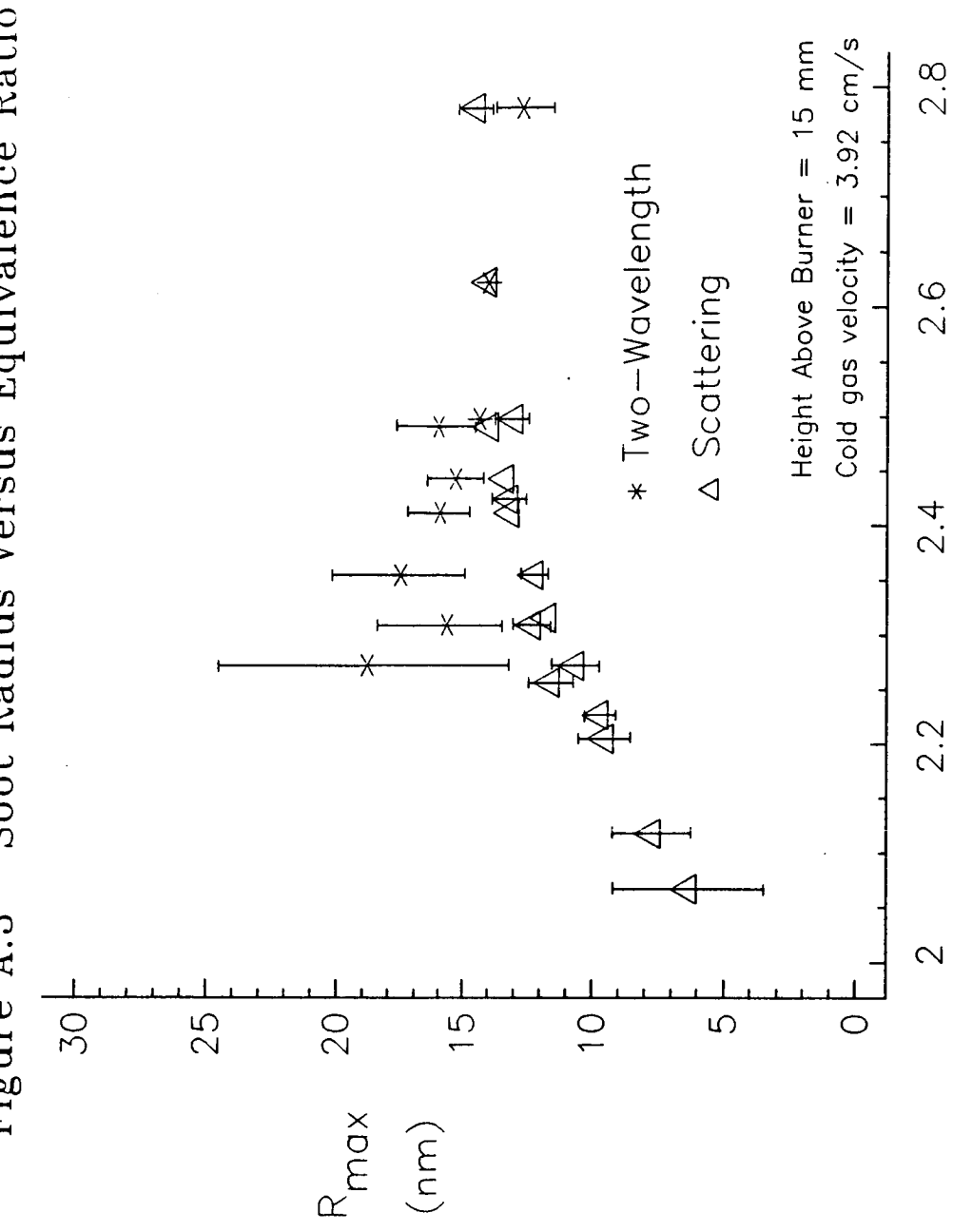

Figure A.4 Soot Radius Versus Height Above Burner

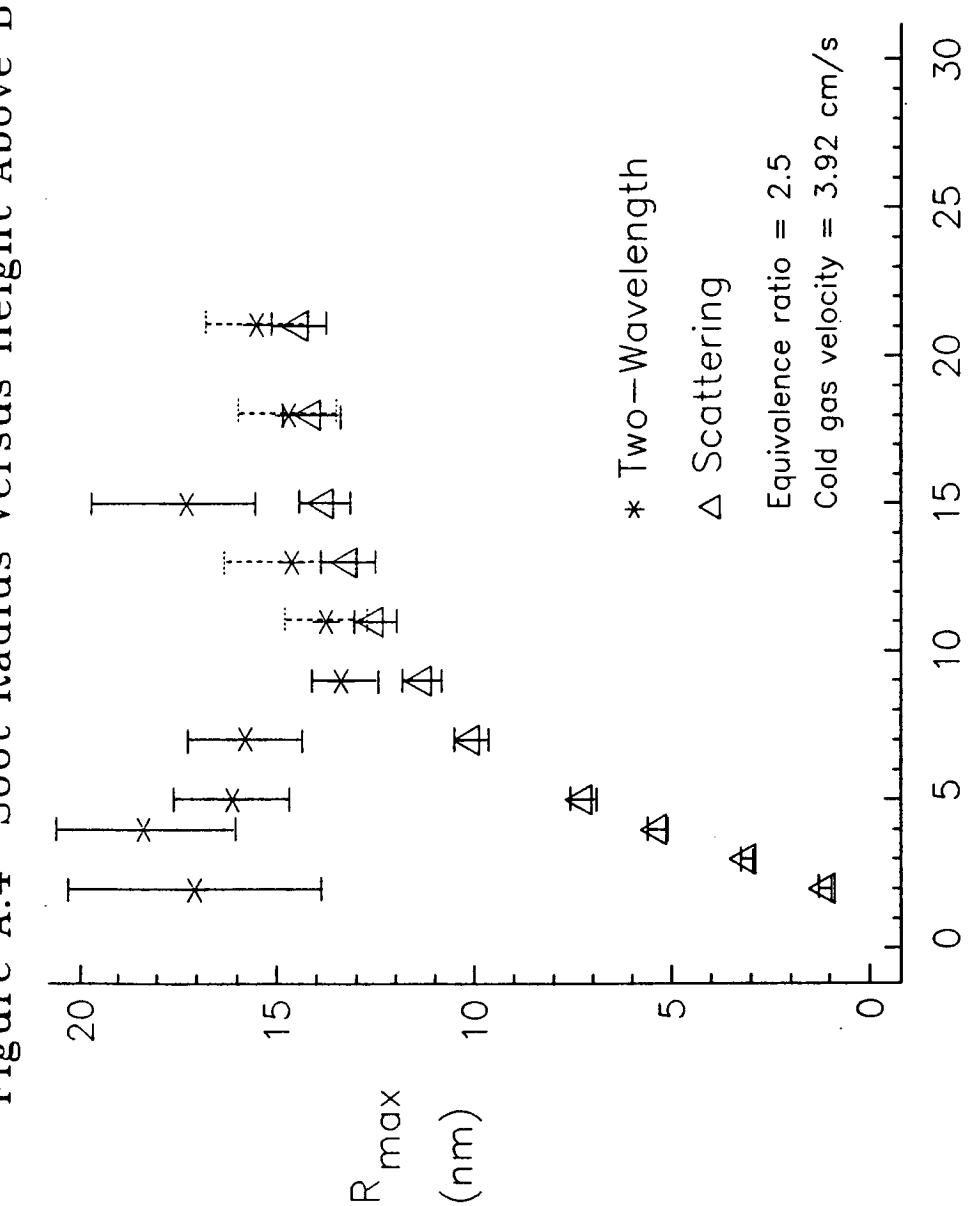

Figure A.5 Soot Radius Versus Equivalence Ratio

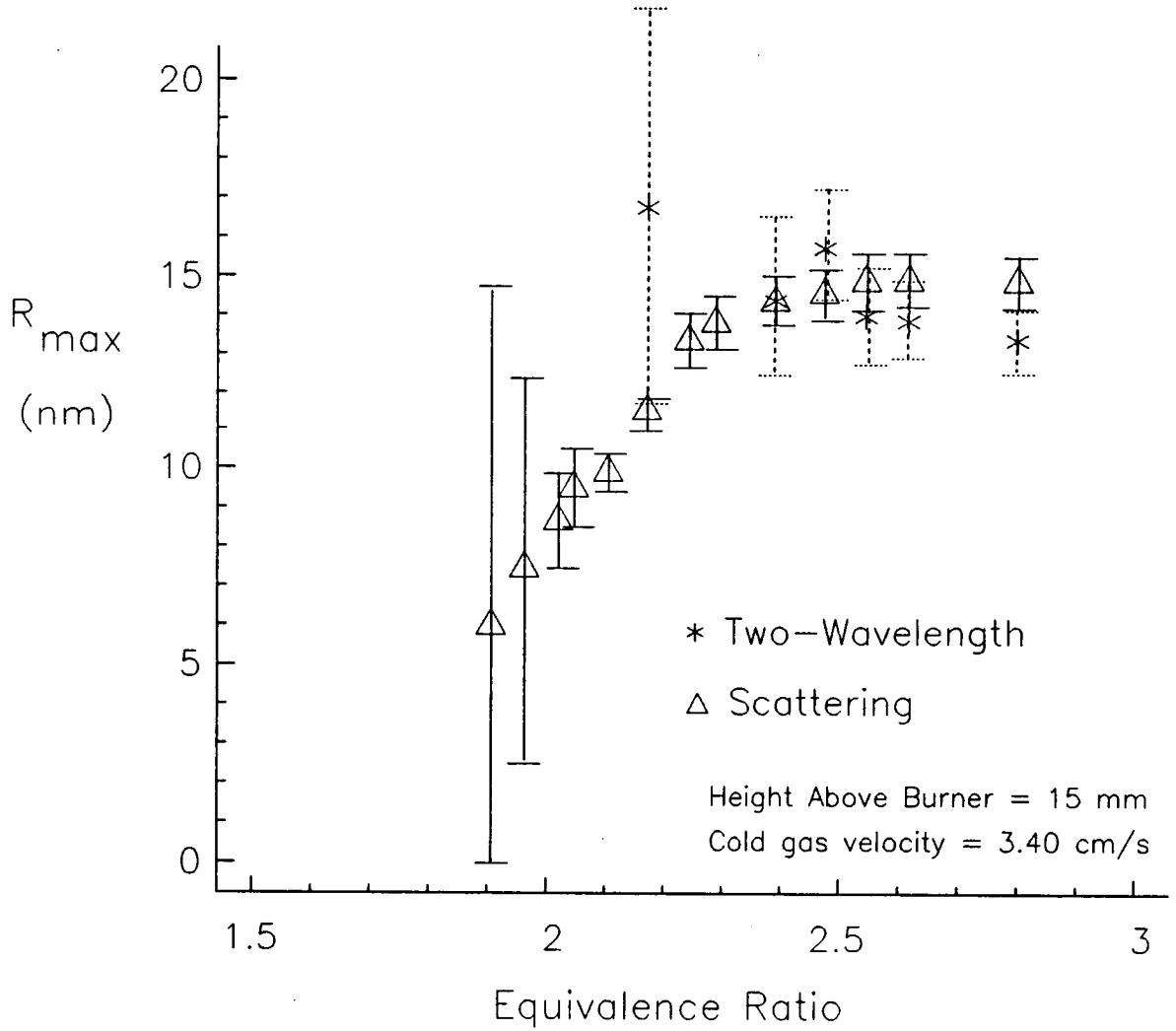

Figure A.6a Soot Number Density Versus Equivalence Ratio

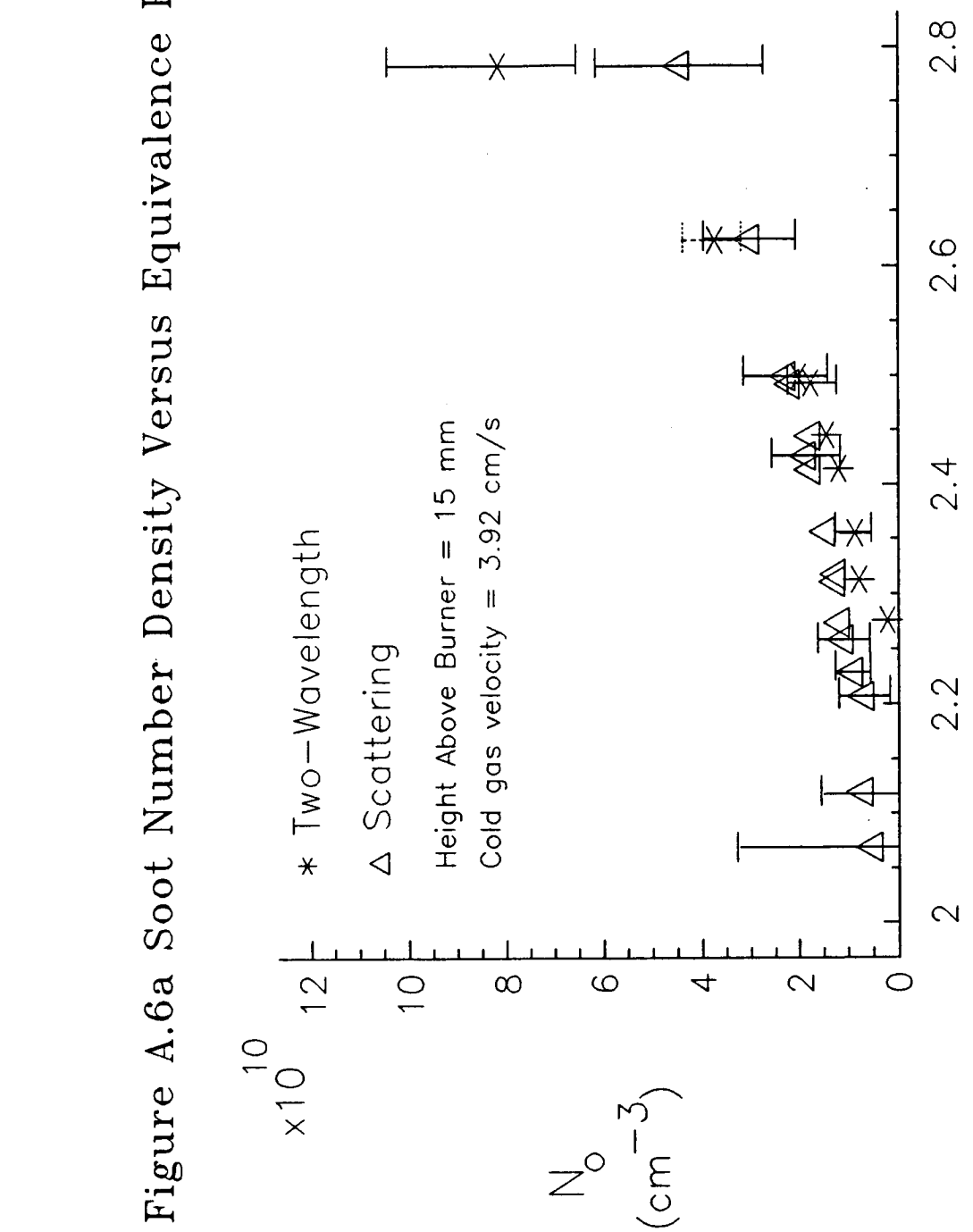

Figure A.6b Soot Number Density Versus Equivalence Ratio

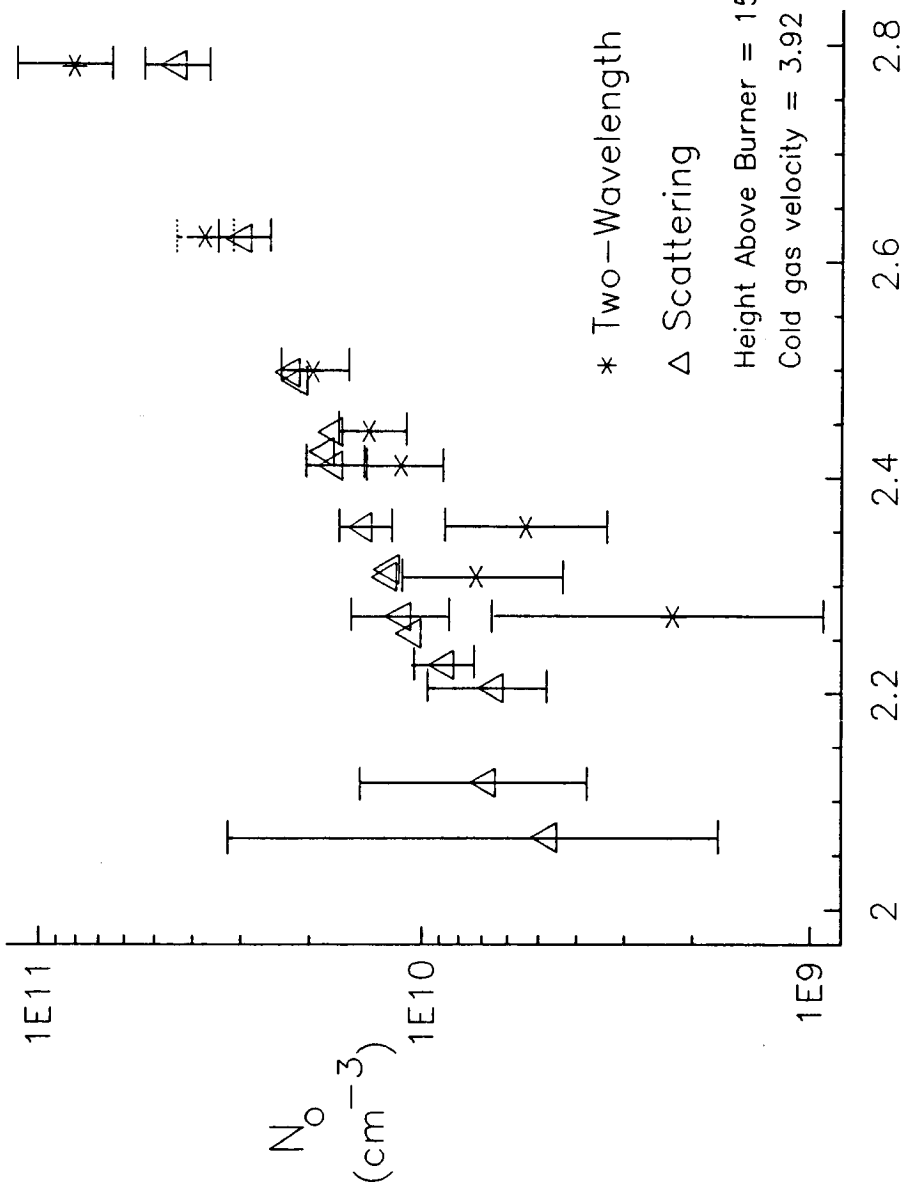

Figure A.7a Soot Number Density Versus Height Above Burner

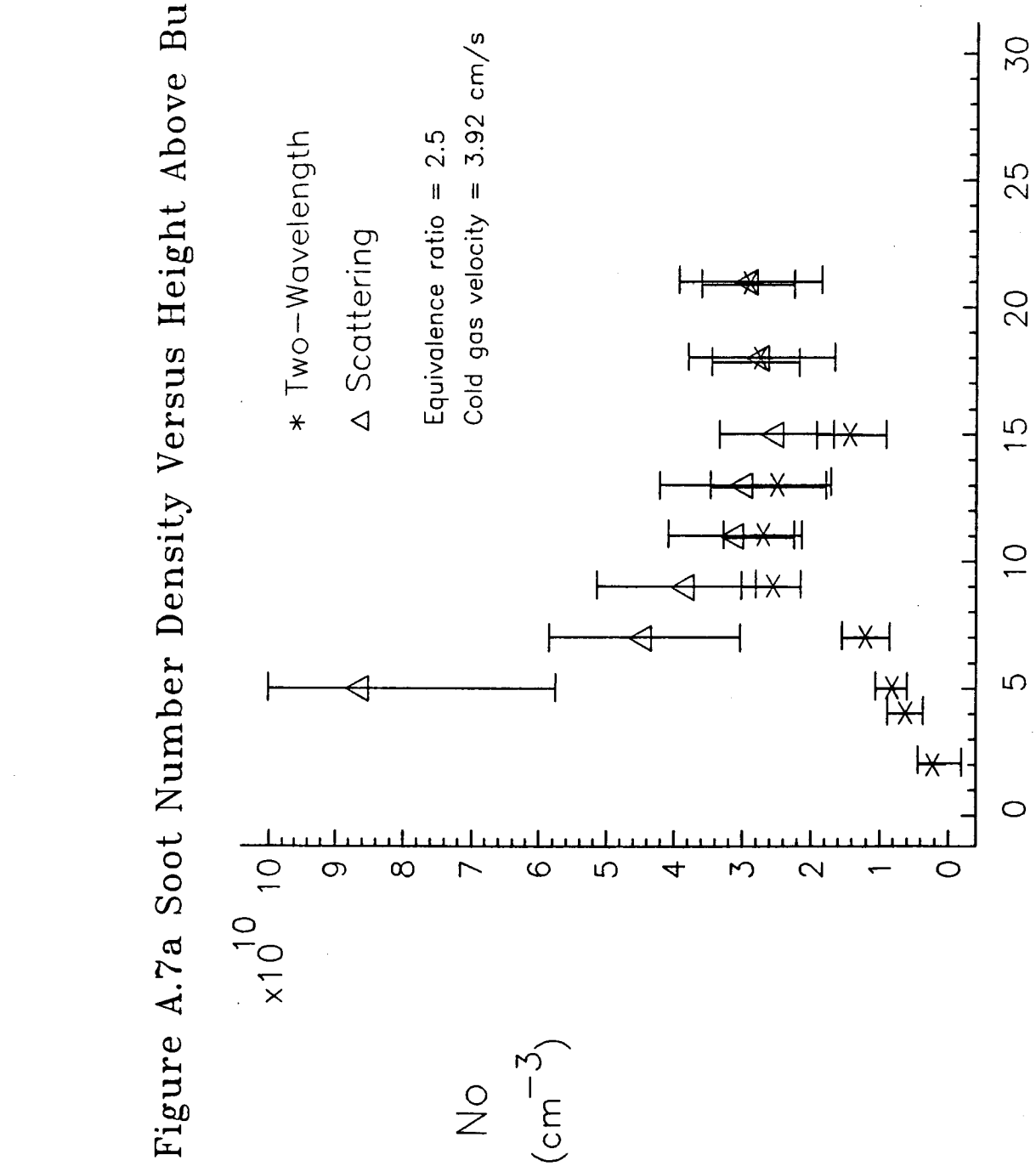

Figure A.7b Soot Number Density Versus Height Above Burner

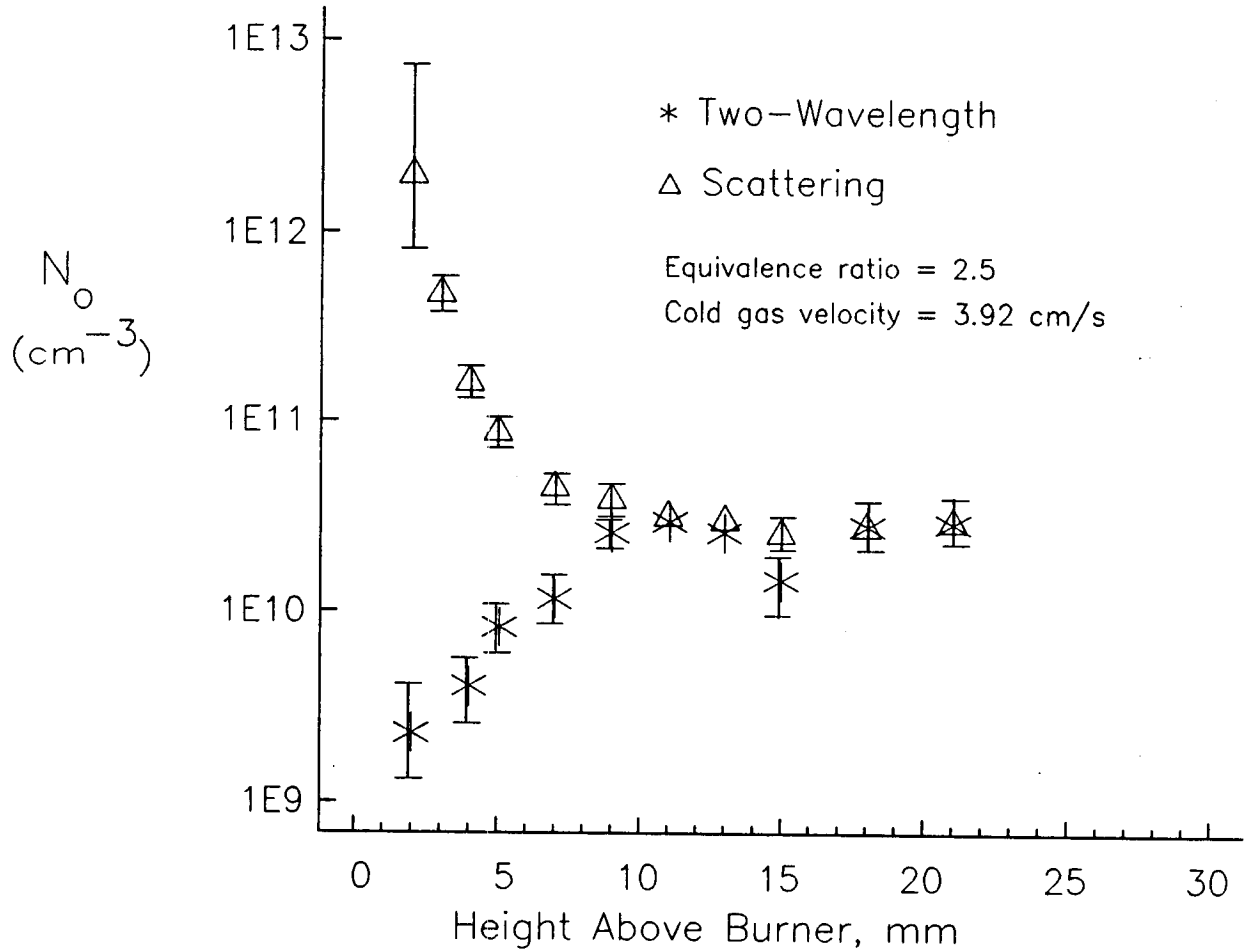

Appendix B COMPUTER PROGRAMS

The programs listed on the following pages are written in the APL language, using the APL*Plus/PC[65] system Version 7.0 for the IBM PC/AT. The programs used for the data analysis are given in Part I. The error analysis programs are given in Part II and the thermocouple correction program is in Part III.

APPENDIX B-- PART I: COMPUTER PROGRAMS FOR DATA ANALYSIS

FUNCTION: ANALYZE

```
    ∇ ANALYZE RNS;I;Z;RUN;WAT;TIN;TOUT;EQUIV;NEWCH0;PUR;GR
      E;RED;WL1;WL2;WL3;WW;MPARAM;A;XK;QVV;W1RATIO;W2RATIO
      ;W3RATIO;ZERO;X;WBB;WOBB;VBB;WAT;TIN;TOUT;IWL;WL;GI0
      ;GI;GREO;IWL1;IWL2;IWL3
[1]   ⍝ MAIN FUNCTION TO ANALYZE RUNS
[2]    →(0=1↑⍴RNS)/0 ⍝ LEAVE IF NO MORE RUNS
[3]    →(1<⍴⍴RNS)/NXT ⍝ IF RNS IS VECTOR, RESHAPE TO A MATR
       IX
[4]    RNS←(1,⍴RNS)⍴RNS
[5]   NXT:→(0=1↑⍴RNS)/0 ⍝ LEAVE IF NO MORE RUNS
[6]    RUN←DEB,(1,1↓⍴RNS)⍴RNS ⍝ TAKE ONE SET OF RUN NUMBERS
[7]    RNS← 1 0 ↓RNS
[8]    I←I/(⍳⍴I)×I←RUN='R'
[9]
[10]  ⍝  FIRST SET ZERO CONDITIONS (NO SOOT)
[11]
[12]   →(1=⍴I)/SAME ⍝ IF NO ZERO RUN IS SPECIFIED USE PREVI
       OUS ZERO
[13]   Z←(-/ΦI)↓RUN
[14]   CALZERO Z
[15]
[16]  ⍝ SHOWS TEST CONDITIONS AND PRINTS MEAN AND STD DEV O
       F DATA
[17]  SAME:RUN←(-0⌈(1≠⍴I)×(⍴RUN)--/ΦI)↓RUN
[18]   ⎕TCNL,'BE SURE PRINTER IS ON',⎕TCNL
[19]
[20]   I←INPUT RUN
[21]   AN I
[22]
[23]  ⍝ CALCULATE EQUIVALENCE RATIO
[24]   FLOWMETER
[25]
[26]  ⍝ PERFORM TWO WAVELENGTH ANALYSIS
[27]
[28]  ⍝ PURPLE-GREEN  ---- NOT USED BECAUSE TOO CLOSE IN WA
       VELENGTH
[29]  ⍝IWL←IWL1,IWL2
[30]  ⍝WL←0.4579,0.5145,PUR,GRE
[31]  ⍝IWL TWOWAVE WL
[32]
[33]  ⍝ PURPLE-RED
[34]   WL←0.4579,0.6328,PUR,RED
[35]   TWOWAVE WL
[36]
[37]   DELTAUIJ WL ⍝ CALCULATES THE UPPER AND LOWER LIMITS
       OF RESULTS
```

```
[38]
[39] ⍝ GREEN-RED
[40]  WL←0.5145,0.6328,GRE,RED
[41]  TWOWAVE WL
[42]
[43]  DELTAUIJ WL ⍝ CALCULATES UPPER AND LOWER LIMITS
[44]
[45] ⍝ PERFORM ERROR ANALYSIS ON SCATTERING RESULTS:
[46]
[47]  SCATTER
[48]
[49]  SAVEPHI←SAVEPHI,EQUIV ⍝ SAVE EQUIVALENCE RATIO VALUE
      S
[50]  SAVECGV←SAVECGV,CGV ⍝ SAVE COLD GAS VELOCITY
[51]
[52]  →NXT ⍝→0
[53]  I←⍳0 ⍝ ZERO I TO SAVE MEMORY
[54]  WHICH ANALYZE RNS ⍝ RECURSIVE CALL TO SELF UNTIL ALL
       RUNS ANALYZED
    ∇
```

FUNCTION: FIRST

```
    ∇ FIRST RUN;I
[1]  ⍝ CALIBRATION (NO FLAME) RUN, SETS I/I0 REFERENCE VAL
      UES
[2]  ⍝ SHOWS TEST CONDITIONS AND PRINTS MEAN AND STD DEV O
      F DATA
[3]   ⎕TCNL,'BE SURE PRINTER IS ON',⎕TCNL
[4]   I←INPUT RUN
[5]   AN I
[6]  ⍝ INITIALIZE VARIABLE FOR MEAN VALUES
[7]   AA←PUR
[8]   BB←GRE
[9]   CC←RED
[10]  SAVEPHI←0⍴0
[11]  SAVERSPR←0⍴0
[12]  SAVERSGR←0⍴0
[13]  SAVEREPR←0⍴0
[14]  SAVEREGR←0⍴0
[15]  SAVENOSPR←0⍴0
[16]  SAVENOSGR←0⍴0
[17]  SAVENOEPR←0⍴0
[18]  SAVENOEGR←0⍴0
[19]  SAVEFVSPR←0⍴0
[20]  SAVEFVSGR←0⍴0
[21]  SAVEFVEPR←0⍴0
[22]  SAVEFVEGR←0⍴0
[23]  SAVEHPR←0⍴0
[24]  SAVEHGR←0⍴0
[25]  SAVECH0←0⍴0
[26]  SAVEFIPR←0⍴0
[27]  SAVEFIGR←0⍴0
[28]  SAVEW←0⍴0
[29]  SAVEIN←0⍴0
[30]  SAVEOUT←0⍴0
[31]  SAVESC←0⍴0
[32]  HMSC←0⍴0
[33]  FIMSC←0⍴0
[34]  SAVET←0⍴0
[35]  WBB←0
[36]  WOBB←0
[37]  VBB←0
[38]  SAVEN2←0⍴0
[39]  N2CONC←0⍴0
[40]  SAVECGV←0⍴0
[41]  RmM←0⍴0
[42]  No←0⍴0
[43]  Fv←0⍴0
    ∇
```

FUNCTION: INPUT

```
    ∇ N←INPUT RUN;A;B;I;N;NSIZE
[1]  ⍝ PRINTS RUN INFO AND GETS DATA FOR ANALYZE FUNCTION
[2]   PRINT RUN
[3]
[4]   A←⎕CMD 'A:'
[5]   RUN ⎕NTIE ¯10
[6]   NSIZE←⎕NSIZE ¯10
[7]   A←⎕NREAD ¯10 82 ,NSIZE ⍝ READ IN FILE
[8]   I←A⍳'→' ⍝ FIND INDEX WHERE DATA END OF FILE MARKER I
      S
[9]   A←(~B←A∈⎕TCNL,⎕TCLF)/A ⍝ REMOVE ALL ⎕TCNL AND ⎕TCLF
[10]  N←⍎(I-1++/B)↑A ⍝ CONVERT TO NUMBERS
[11]
[12] ⍝ REMOVE AND PRINT OUT RUN INFO APPENDED TO END OF TH
      E DATASET
[13] ⍝    THIS ASSUMES MAXIMUM FIELD WIDTH IN mask IS 6
[14]  INFO←((⌊(⍴A)÷6),6)⍴A←(-NSIZE-I)↑A
[15]  RUN PRINTINFO INFO
[16]  ⎕NUNTIE ¯10
[17]
    ∇
```

FUNCTION: AN

```
    ∇ AN X;MEANX;SDEVX;P;Y;R;PURSD;PURPD;GRESD;GREPD;REDSD
      ;REDPD
[1]  ⍝ FINDS MEAN AND STD DEV OF RAW DATA AND INTENSITY RA
      TIOS
[2]   X←((⌊(⍴X)÷8),8)⍴X
[3]   MEANX←MEAN X
[4]
[5]   GREF←MEANX[4]
[6]   GI←MEANX[5]
[7]
[8]   SDEVX←SDEV X
[9]   P←(SDEVX÷MEANX)×100
[10]
[11] ⍝ ARRANGE I/IO RATIOS AND SCATTERING DATA INTO AN 8 B
      Y ? MATRIX AND          CASTOUT BAD DATA
[12]  Y←(X[;3]÷PUR0),(X[;5]÷GRE0),(X[;8]÷RED0),[1.5]X[;6]
[13]  R←CASTOUT Y
[14]
[15] ⍝ 'WAVELENGTH .4579'
[16]  PUR←MEAN R[;1] ⍝ FINDS MEAN OF GOOD I/IO
[17]  PURSD←SDEV R[;1] ⍝ FINDS STANDARD DEVIATION OF GOOD
      I/IO
```

```
[18]  PURPD←(PURSD÷PUR)×100
[19]
[20] ⍝ 'WAVELENGTH .5145'
[21]  GRE←MEAN R[;2] ⍝ FINDS MEAN OF GOOD I/IO
[22]  GRESD←SDEV R[;2] ⍝ FINDS STANDARD DEVIATION OF GOOD
      I/IO
[23]  GREPD←(GRESD÷GRE)×100
[24]
[25] ⍝ 'WAVELENGTH .6328'
[26]  RED←MEAN R[;3] ⍝ FINDS MEAN OF GOOD I/IO
[27]  REDSD←SDEV R[;3] ⍝ FINDS STANDARD DEVIATION OF GOOD
      I/IO
[28]  REDPD←(REDSD÷RED)×100
[29]
[30] ⍝ PRINT OUT RAW DATA
[31]  '   '
[32]  PRINT '   '
[33] ⍝ PRINT RUN
[34]  RUN
[35] ⍝ TEMPORARILY LEAVE OUT PRINTING OF RAW DATA WHEN COM
      MENT ON NEXT LINE
[36]
[37]  SHOW MEANX[2 3 4 5 7 8],SDEVX[2 3 4 5 7 8],P[2 3 4 5
       7 8],PUR,PURSD,PURPD,GRE,GRESD,GREPD,RED,REDSD,REDP
      D
[38]
[39]  ''
[40]  '   '
[41]  PRINT '   '
[42]  SCAT←((MEAN R[;4])÷409.5)×⍎INFO[20;] ⍝ SCATTERED LIG
      HT INTENSITY IN VOLTS
[43] ⍝ WHERE INFO[20;] IS THE LOCK-IN AMPLIFIER RANGE FACT
      OR
[44]  PRINT 'SCATTERED INTENSITY MEAN ',⍕SCAT
[45]  SDSCAT←(((SDEV R[;4])÷409.5)×⍎INFO[20;])
[46]  PRINT 'STD. DEV. ',⍕SDSCAT
[47]  PRINT '% STD DEV ',⍕(SDSCAT÷SCAT×100)
[48]  PRINT '   '
[49]
[50]  ''
[51]  '   '
[52]  'SCATTERED INTENSITY MEAN ',⍕SCAT
[53]  'STD DEV ',⍕SDSCAT
[54]  '% STD DEV ',⍕(SDSCAT÷SCAT×100)
[55]  '   '
[56]  ''
[57]
[58]  SDP←SDEVX[3]
[59]  SDG←SDEVX[5]
[60]  SDR←SDEVX[8]
[61]  PV←MEANX[3]
```

```
[62]  GV←MEANX[5]
[63]  RV←MEANX[8]
    ∇
```

FUNCTION: SHOW

```
    ∇ SHOW Z;E;F;G;H;J
[1]  ⍝ DISPLAYS MEAN AND STANDARD DEVIATION OF RAW DATA AN
      D INTEN. RATIOS
[2]  ⍝ CALL FUNCTION TO FIND MEANS AND STD DEVIATION
[3]  ⍝ TURN ON PRINTER
[4]   PON
[5]   '-------------------------------------------------'
[6]   '         MEAN          STD. DEV.       PERCENT SD'
[7]   '-------------------------------------------------'
[8]   '    '
[9]   '    '
[10]  '  RAW DATA FROM CHANNELS 1 THROUGH 4, 6 AND 7   '
[11]  '    '
[12]  'F14.3' ⎕FMT⍉ 3 6 ⍴Z[⍳18]
[13]  '      '
[14]  F←'F14.3' ⎕FMT Z[19 20 21]
[15]  W1RATIO←⌽F[1;]
[16]  'WAVELENGTH .4579 I/I0 '
[17]  ' '
[18]  F[1;],F[2;],F[3;]
[19]  '      '
[20]  'WAVELENGTH .5145 I/I0'
[21]  '    '
[22]  E←'F14.3' ⎕FMT Z[22 23 24]
[23]  E[1;],E[2;],E[3;]
[24]  W2RATIO←⌽E[1;]
[25]  '    '
[26]  'WAVELENGTH .6328 I/IO'
[27]  '    '
[28]  J←'F14.3' ⎕FMT Z[25 26 27]
[29]  J[1;],J[2;],J[3;]
[30]  W3RATIO←⌽J[1;]
[31]  POFF
    ∇
```

FUNCTION: FLOWMETER

```
    ∇ FLOWMETER;C;D;E;PROP;O2;N2B;N2R;O2R;PROPR;ARR;AR;AIR
      ;MOLFA;MTOT;MO2;MN2;MAR;QWATER;HLOSS;SNVEL
[1]   PROP←0
[2]   O2←0
[3]   N2B←0
[4]   N2CONC←0
[5]   PRINT '  '
[6]   '  '
[7]  ⍝ CALLS FMETER TO CONVERT FROM HZ TO SCCM (OR GPM)
[8]
[9]   C←1000×⍕INFO[1;]
[10]  →(C=0)/OXYGEN
[11] ⍝ D←⍕INFO[3;]
[12]  D←((⍕INFO[3;])×0.9807)-2.88 ⍝ ADJUSTING FOR NEW P TR
      ANSDUCER CALIB.
[13]  E←⍕INFO[5;]
[14]  C←(C,D,E)
[15]  D←C FMETER 1
[16]  PRINT 'PROPANE FLOWRATE IN SCCM: ',⍕D
[17]  'PROPANE FLOWRATE IN SCCM: ',⍕D
[18]  PROP←D
[19]
[20] OXYGEN:C←1000×⍕INFO[6;]
[21]  →(C=0)/BN2
[22]  D←((⍕INFO[7;])×0.9378)+0.882
[23]  E←⍕INFO[8;]
[24]  C←(C,D,E)
[25]  D←C FMETER 2
[26]  PRINT 'OXYGEN FLOWRATE IN SCCM: ',⍕D
[27]  'OXYGEN FLOWRATE IN SCCM: ',⍕D
[28]  O2←D
[29]
[30] BN2:C←2000×⍕INFO[9;] ⍝ CHANGE TO 1000 IF USE 1.6 KHZ
      SCALE ON ANADEX,2000 FOR 3.2 KHZ SCALE.
[31] ⍝--
[32]  →(C=0)/NON2
[33]  D←((⍕INFO[10;])×0.9155)-0.307
[34]  E←⍕INFO[11;]
[35]  C←(C,D,E)
[36]  D←C FMETER 3
[37]  N2B←D
[38]  PRINT 'BURNER NITROGEN FLOWRATE IN SCCM: ',⍕D
[39]  'BURNER NITROGEN FLOWRATE IN SCCM: ',⍕D
[40]
[41] ⍝ START HERE FOR O2+N2+PROPANE CONDITIONS
[42] ⍝ FIND N2 VOLUME FRACTION
[43]  N2CONC←N2B÷(PROP+O2+N2B)
[44]  '**********************************'
[45]  'N2 VOLUME FRACTION = ',⍕N2CONC
```

```
[46]
[47]  →(C>0)/MOLE
[48] NON2:N2B←0
[49]  →(N2B=0)/CHECK
[50] MOLE:N2R←N2B÷(N2B+O2)
[51]  '   '
[52]  PRINT ' '
[53]  'N2 MOLE FRAC = ',⍕N2R
[54]  PRINT 'N2 MOLE FRAC = ',⍕N2R
[55]  O2R←O2÷(N2B+O2)
[56]  PRINT 'O2 MOLE FRAC = ',⍕O2R
[57]  'O2 MOLE FRAC = ',⍕O2R
[58] CHECK:MOLFA←PROP+O2+N2B ⍝ TOTAL VOLUME OF GASES, FUEL
      +O2+N2
[59]  PRINT '  '
[60]
[61] ⍝ THE FOLLOWING EQUATIONS APPLY WHEN USING AIR+FUEL
[62]
[63] ⍝ NON2:AIR←N2B ⍝ AIR FLOWS THROUGH FORMER N2 LINE
[64] ⍝ MOLE:MTOT←(5+18.64+0.223)
[65] ⍝ MO2←(5÷MTOT)×AIR
[66] ⍝ MN2←(18.64÷MTOT)×AIR
[67] ⍝ MAR←(0.223÷MTOT)×AIR
[68] ⍝ MOLFA←PROP+MO2+MN2+MAR ⍝ TOTAL VOLUME OF GASES, FUE
      L+AIR
[69] ⍝ MOLE FRACTIONS
[70] ⍝ PROPR←PROP÷MOLFA
[71] ⍝ O2R←MO2÷MOLFA
[72] ⍝ N2R←MN2÷MOLFA
[73] ⍝ ARR←MAR÷MOLFA
[74]  '  '
[75]  PRINT ' '
[76]  'TOTAL NUMBER OF MOLES (PER MINUTE) = ',⍕(MOLFA÷2240
      0) ⍝ CC/MOLE @ STP
[77]  PRINT 'TOTAL NUMBER OF MOLES (PER MINUTE) = ',⍕(MOLF
      A÷22400)
[78]  'PROPANE MOLES = ',⍕(PROP÷22400)
[79]  PRINT 'PROPANE MOLES = ',⍕(PROP÷22400)
[80] ⍝ FOR AIR:
[81] ⍝ ' N2 MOLES = ',⍕(MN2÷22400)
[82] ⍝ PRINT 'N2 MOLES = ',⍕(MN2÷22400)
[83] ⍝ PRINT 'O2 MOLES = ',⍕(MO2÷22400)
[84] ⍝ 'O2 MOLES = ',⍕(MO2÷22400)
[85] ⍝ PRINT 'ARGON MOLES = ',⍕(MAR÷22400)
[86]
[87] ⍝ FOR PROP/O2+N2:
[88]  ' N2 MOLES = ',⍕(N2B÷22400)
[89]  PRINT 'N2 MOLES = ',⍕(N2B÷22400)
[90]  PRINT 'O2 MOLES = ',⍕(O2÷22400)
[91]  'O2 MOLES = ',⍕(O2÷22400)
[92]  →(O2=0)/COLD
```

```
[93]  '    '
[94]  PRINT '   '
[95]  EQUIV←((PROP÷0.53)÷(O2÷0.755))÷0.275 ⍝ PROP,O2 SPECI
      FIC VOL'S IN M*3/KG
[96] ⍝  .275 IS THE STOICHIOMETRIC FUEL/O2 MASS RATIO
[97] ⍝ EQUIV←((PROP÷0.53)÷(AIR÷0.83))÷0.06384 ⍝ FOR AIR
[98]  PRINT 'Φ =   ',⍕EQUIV
[99]  'Φ = ',⍕EQUIV
[100]  '    '
[101]  PRINT '   '
[102] COLD:CGV←(PROP+O2+N2B)÷(28.3×60)
[103]  PRINT 'COLD GAS VEL.(CM/S)= ',⍕CGV
[104]  'COLD GAS VELOCITY (CM/S) = ',⍕CGV
[105]  PRINT '-----------------------------------'
[106]  '-----------------------------------'
[107] SN2:C←2000×⍎INFO[12;]
[108]  →(C=0)/WATER
[109]  D←⍎INFO[13;]
[110]  E←⍎INFO[14;]
[111]  C←(C,D,E)
[112]  D←C FMETER 4
[113]  PRINT 'SHROUD NITROGEN FLOWRATE IN SCCM: ',⍕D
[114]  'SHROUD NITROGEN FLOWRATE IN SCCM: ',⍕D
[115]  SNVEL←D÷(10.524×60)
[116]  PRINT 'SHROUD N2 VELOCITY (CM/S): ',⍕SNVEL
[117]  'SHROUD N2 VEL. (CM/S): ',⍕SNVEL
[118]
[119] WATER:CONST←2000 ⍝ FOR DATA AFTER 1/6/87
[120]  C←CONST×⍎INFO[17;] ⍝ BEFORE 11/14/86 CONST=20,FOR 1
      1/14-1/6, CONST=250
[121]  →(C=0)/END
[122]  D←20
[123]  E←⍎INFO[19;]
[124]  C←(C,D,E)
[125]  D←C FMETER 6
[126]  '    '
[127]  PRINT '   '
[128]  PRINT 'WATER FLOWRATE IN GPM: ',⍕D
[129]  'WATER FLOW (GPM): ',⍕D
[130]  WAT←D
[131]  TIN←⍎INFO[18;]
[132]  TOUT←⍎INFO[19;]
[133] ⍝PRINT 'WATER TEMP IN  (deg F): ',⍕TIN
[134] ⍝PRINT '              OUT (deg F): ',⍕TOUT
[135]  HLOSS←0.555×(TOUT-TIN)
[136]  PRINT 'HEAT LOSS IN CAL/GM: ',⍕HLOSS
[137]  'HEAT LOSS (CAL/GM) :',⍕HLOSS
[138]
[139]  PRINT '    '
[140] END:→0
    ∇
```

FUNCTION: FMETER

```
    ∇ SCCM←C FMETER N;A;P;T
[1]  ⍝ CONVERTS ACFM TO SCCM FOR FLOW METER N
[2]  ⍝ C[1] IS HZ , C[2] IS PSIG , C[3] IS ACTUAL TEMP. F
[3]  ⍝ CONVERT TEMP. TO RANKINE
[4]   P←C[2]+14.7
[5]   T←C[3]+460
[6]   →(N=1)/PROPANE
[7]   →(N=2)/OXYGEN
[8]   →(N=3)/BN2
[9]   →(N=4)/SN2
[10]  →(N=5)/TOTAL
[11]  →(N=6)/WATER
[12]  →END
[13] PROPANE:A←(C[1]∘.* 0 1 2 3)+.× 28.0157 1.06411 5.8895
      1E¯4 ¯3.03572E¯7
[14]  A←A÷28317 ⍝ CONVERT FROM ACCM TO ACFM
[15]  →END
[16]
[17] TOTAL:A←(C[1]∘.* 0 1 2 3)+.× 0.0234884 2.64592E¯4 ¯6.
      95705E¯8 4.80248E¯11
[18]  →END
[19] ⍝ FOR AIR THROUGH THE N2 LINE, USE EQN. BELOW
[20] ⍝IN ACFM-- BN2:A←(C[1]∘.* 0 1 2 3)+.× 0.0233532 1.964
      16E¯4 7.07235E¯8 ¯3.52441E¯11
[21] BN2:A←(C[1]∘.* 0 1)+.× 538.957 6.64635
[22]  A←A÷28317 ⍝ CONVERT FROM ACCM TO ACFM, FOR N2 ALONE
      ONLY
[23]  →END
[24]
[25] SN2:A←(C[1]∘.* 0 1 2 3)+.× 0.0137138 1.27508E¯4 5.889
      69E¯8 ¯3.95535E¯11
[26]  →END
[27]
[28] OXYGEN:A←(C[1]∘.* 0 1)+.× 176.008 4.07573
[29]  A←A÷28317 ⍝ CONVERT FROM ACCM TO ACFM
[30]  →END
[31]
[32] WATER:SCCM←(C[1]∘.* 0 1)+.× 5.2433E¯3 6.8434E¯5
[33] ⍝ (WATER  IS IN GPM)
[34]  →0
[35]
[36] END:SCCM←A×(P÷T)×(530×28317)÷14.7
    ∇
```

FUNCTION: TWOWAVE

```
    ∇ TWOWAVE WL;L;H;PRAT1;PRAT2;TAU1;TAU2;TAUABS;RMAXEPR;
      RMAXEGR;RMAXSPR;RMAXSGR;TAUPRIMEE;TAUPRIMES;TAUP1S;T
      AUP2S;TAUP1E;TAUP2E;FVSPR;FVSGR;FVEPR;FVEGR;NOSPR;NO
      SGR;NOEPR;NOEGR;RPRINT;XIJ;RS;N;RE
[1]   □PP←3
[2]   ⍝  ANALYZES DATA FROM TWO-WAVELENGTH LASER EXTINCTION
       TECHNIQUE FOR PURPLE-GREEN, THEN PURPLE-RED, THEN G
      REEN-RED
[3]   ⍝FINDS SOOT VOLUME FRACTIONS FROM TWO WAVELENGTH LIGH
      T EXTINCTION
[4]   ⍝ 'ENTER WAVELENGTH 1 (MICRONS) : '
[5]   ⍝ 'ENTER WAVELENGTH 2 (MICRONS) : '
[6]   ⍝ PUR0 CAME FROM CALZERO, WL[3] (eg. W1RATIO÷PUR0) FR
      OM     SHOW
[7]   ⍝ RED0 CAME FROM CALZERO, WL[4] (eg. W2RATIO÷RED0) FR
      OM     SHOW
[8]   ⍝ LASER PATHLENGTH THROUGH FLAME, L in CM.:
[9]    L←(⍎INFO[4;])
[10]  TAU1←(¯1÷(L×10000))×⍟WL[3] ⍝ CONVERT L FROM cm TO um
[11]  TAU2←(¯1÷(L×10000))×⍟WL[4]
[12]  'TAU1 = ',(⍕TAU1),'    TAU2 = ',(⍕TAU2)
[13]  →(TAU2=0)/END
[14]
[15]  ⍝ CALCULATE EXPERIMENTAL XIJ
[16]   PRINT '  '
[17]   TAUABS←(WL[2]×FA WL[1])÷(WL[1]×FA WL[2])
[18]   XIJ←((TAU1÷TAU2)-1)÷(TAUABS-1)
[19]   '  '
[20]   'EXPERIMENTAL XIJ FOR WAVELENGTHS ',(⍕WL[1]),' AND '
       ,(⍕WL[2]),' = ',⍕XIJ
[21]
[22]   PRINT 'EXPERIMENTAL XIJ FOR WAVELENGTHS ',(⍕WL[1]),'
        AND ',(⍕WL[2]),' = ',⍕XIJ
[23]
[24]   →(XIJ≤0)/END
[25]
[26]  ⍝ GO TO XIJ TABLE WITH EXPERIMENTAL XIJ VALUE AND WAV
      ELENGTHS USED
[27]  ⍝ '1ST LETTERS OF WAVELENGTHS--  PR  GR : '
[28]   →(∧/((WL[1]),WL[2])=0.4579,0.6328)/PR
[29]   →(∧/((WL[1]),WL[2])=0.5145,0.6328)/GR
[30]  GR:WW←'GR'
[31]   →CONTINUE
[32]  PR:WW←'PR'
[33]  CONTINUE:PRINT ' '
[34]   '  '
[35]   PRINT ' WAVELENGTHS :    ',⍕WW
[36]  ⍝ GET RMAX VALUES AND TAUPRIME VALUES FROM TABLE
[37]   XIJTABLE WW
```

```
[38]  PRINT ' '
[39]  '   '
[40]  ⍎('RMAXS',WW,'←RS')
[41]  →(RS<0)/RME
[42]  TAUPRIMES←TAUP1S
[43] ⍝ CALCULATE SOOT PARTICLE NUMBER DENSITY FOR FIRST RM
      AX AND TAU'
[44]  ⍎('NOS',WW,'←(TAU1÷(TAUPRIMES×RMAXS',WW,'*2))') ⍝ NO
      S IN um
[45]  PRINT '   '
[46]  ⍎('RPRINT←1000×RMAXS',WW) ⍝ RMAXS IN um, RPRINT IN n
      m
[47]  '  '
[48]  'RMAX (S) FOR WAVELENGTHS ',(⍕WL[1]),' AND ',(⍕WL[2]
      ),' = ',(⍕RPRINT),' nm '
[49]  PRINT 'RMAX (S) FOR WAVELENGTHS ',(⍕WL[1]),' AND ',(
      ⍕WL[2]),' = ',(⍕RPRINT),' nm'
[50]  'NO, SOOT PARTICLE NO. DENSITY (S) FOR WAVELENGTHS '
      ,(⍕WL[1]),' AND ',(⍕WL[2]),' = ',(⍕(⍎('NOS',WW,'×10*
      12'))),' cm¯3'
[51]  PRINT 'NO, SOOT PARTICLE NO. DENSITY (S) FOR WAVELEN
      GTHS ',(⍕WL[1]),' AND ',(⍕WL[2]),' = ',(⍕(⍎('NOS',WW
      ,'×10*12'))),' cm¯3'
[52] ⍝ CALCULATE SOOT VOLUME FRACTION FOR FIRST RMAX AND T
      AU'
[53]  ⍎('FVS',WW,'←18.62×NOS',WW,'×RMAXS',WW,'*3')
[54]  'FV, SOOT VOLUME FRACTION (S) FOR WAVELENGTHS ',(⍕WL
      [1]),' AND ',(⍕WL[2]),' = ',(⍕(⍎('FVS',WW))),' '
[55]  PRINT 'FV, SOOT VOLUME FRACTION (S) FOR WAVELENGTHS
      ',(⍕WL[1]),' AND ',(⍕WL[2]),' = ',(⍕(⍎('FVS',WW))),'
       '
[56]  PRINT '    '
[57]  '  '
[58]  PRINT '   '
[59]  '  '
[60] RME:⍎('RMAXE',WW,'←RE')
[61]  →(RE<0)/END
[62]  TAUPRIMEE←TAUP1E
[63] ⍝ CALCULATE SOOT PARTICLE NO. DENSITY FOR SECOND RMAX
       AND TAU'
[64]  ⍎('NOE',WW,'←(TAU1÷(TAUPRIMEE×RMAXE',WW,'*2))') ⍝ NO
      E IN um
[65]  PRINT '    '
[66]  ⍎('RPRINT←1000×RMAXE',WW) ⍝ RMAXE IN um, RPRINT IN n
      m
[67]  '   '
[68]  'RMAX (E) FOR WAVELENGTHS ',(⍕WL[1]),' AND ',(⍕WL[2]
      ),' = ',(⍕RPRINT),' nm'
[69]  PRINT 'RMAX (E) FOR WAVELENGTHS ',(⍕WL[1]),' AND ',(
      ⍕WL[2]),' = ',(⍕RPRINT),' nm'
[70]  'NO, SOOT PARTICLE NO. DENSITY (E) FOR WAVELENGTHS '
```

```
      ,(⍕WL[1]),' AND ',(⍕WL[2]),' = ',(⍕(⍎('NOE',WW,'×10*
      12'))),' cm¯3'
[71]  PRINT 'NO, SOOT PARTICLE NO. (E) FOR WAVELENGTHS ',(
      ⍕WL[1]),' AND ',(⍕WL[2]),' = ',(⍕(⍎('NOE',WW,'×10*12
      '))),' cm¯3'
[72] ⍝ CALCULATE SOOT VOLUME FRACTION FOR SECOND RMAX AND
      TAU'
[73]  ⍎('FVE',WW,'←18.62×NOE',WW,'×RMAXE',WW,'*3')
[74]  'FV, SOOT VOLUME FRACTION (E) FOR WAVELENGTHS ',(⍕WL
      [1]),' AND ',(⍕WL[2]),' = ',(⍕(⍎('FVE',WW))),' '
[75]  PRINT 'FV, SOOT VOLUME FRACTION (E) FOR WAVELENGTHS
      ',(⍕WL[1]),' AND ',(⍕WL[2]),' = ',(⍕(⍎('FVE',WW))),'
       '
[76]  PRINT '  '
[77]  '  '
[78]  →(XIJ≤0)/END
[79] ⍝ INITIALIZE N FOR SAVER PROGRAM
[80]  H←⍎(INFO[2;]) ⍝ HEIGHT ABOVE BURNER
[81]  →(∧/((WL[1]),WL[2])=0.4579,0.6328)/N1
[82]  →(∧/((WL[1]),WL[2])=0.5145,0.6328)/N2
[83] N1:N←1
[84]  →SAVE
[85] N2:N←2
[86] SAVE:SAVER ⍝  RUN PROGRAM TO SAVE VALUES FOR ALL THE
      RUNS
[87]  PRINT '  '
[88] END:→0
[89]
    ∇
```

FUNCTION: FA

```
    ∇ R←FA WAVE;N;K;BK;A;B;C
[1]  ⍝ FUNCTION USED TO DETERMINE XIJ, IS A FCN OF SOOT OP
      TICAL PROPERTIES
[2]   →(WAVE=1.06)/YAG
[3]   →(WAVE=0.488)/BLUE
[4]   →(WAVE=0.5145)/GRN
[5]   →(WAVE=0.6328)/RED
[6]   →(WAVE=0.4579)/PURPLE
[7]   →END
[8]  YAG:K←0.6
[9]   N←1.9
[10]  →END
[11] BLUE:K←0.54
[12]  N←1.94
[13]  →END
[14] GRN:K←0.52
[15]  N←1.93
```

```
[16]  →END
[17] RED:K←0.48
[18]  N←1.89
[19]  →END
[20] PURPLE:K←0.58
[21]  N←1.94
[22]  →END
[23] END:BK←K÷N
[24]  A←((N*2)×(1-(K*2)))-1
[25]  B←2×(N*2)×K
[26]  C←A+3
[27]  MPARAM←((A*B)-(B*C))÷((C*2)+(B*2))
[28]  R←((N*2)×BK)÷(4×(N*4)×(BK*2))+((2+N*2)-((N×BK)*2))*2
[29]
    ∇
```

FUNCTION: SAVER

```
    ∇ SAVER
[1]  ⍝ SAVES MEAN VALUES OF VARIABLES FROM VARIOUS RUN NUM
      BERS
[2]  ⍝ ×1000 = IN nm ---- ×10*12 = IN cm¯3
[3]
[4]   →(N=1)/SAVEPR
[5]   →(N=2)/SAVEGR
[6]   AA←AA,PUR ⍝ WAVELENGTH 1 MEAN VALUE
[7]   BB←BB,GRE ⍝ WAVELENGTH 2 MEAN VALUE
[8]   CC←CC,RED ⍝ WAVELENGTH 3 MEAN VALUE
[9]  ⍝  BURNER COOLING WATER FLOWRATE AND TEMPERATURES, IN
      & OUT: SAVED IN PROGRAM 'ANALYZE'
[10]
[11] ⍝ SAVE PURPLE-RED VALUES
[12] SAVEPR:→(∧/(RMAXSPR,RMAXEPR)≤0,0)/END
[13] ⍝ BEGINNING OF TABLE VALUES
[14]  SAVEHPR←SAVEHPR,H ⍝   SAVES HEIGHT ABOVE BURNER PURP
      LE-RED
[15]  SAVEFIPR←SAVEFIPR,EQUIV ⍝ SAVES EQUIVALENCE RATIO PU
      RPLE-RED
[16]  →(RMAXSPR≤0)/RSPR
[17]  SAVERSPR←SAVERSPR,(RMAXSPR×1000) ⍝ SAVES RMAX PURPLE
      -RED
[18]  SAVENOSPR←SAVENOSPR,(NOSPR×10*12) ⍝ SAVES NUMBER DEN
      SITY PURPLE-RED
[19]  SAVEFVSPR←SAVEFVSPR,FVSPR ⍝ SAVES VOLUME FRACTION PU
      RPLE-RED
[20]  →(RMAXEPR>0)/OTHERPR
[21]  SAVEREPR←SAVEREPR,0
[22]  SAVENOEPR←SAVENOEPR,1
[23]  SAVEFVEPR←SAVEFVEPR,1
```

```
[24]  →END
[25]
[26] RSPR:SAVERSPR←SAVERSPR,0
[27]  SAVENOSPR←SAVENOSPR,1
[28]  SAVEFVSPR←SAVEFVSPR,1
[29]
[30] ⍝ END OF TABLE VALUES
[31] OTHERPR:SAVEREPR←SAVEREPR,(RMAXEPR×1000) ⍝ SAVES RMAX
       PURPLE-RED
[32]  SAVENOEPR←SAVENOEPR,(NOEPR×10*12) ⍝ SAVES NUMBER DEN
      SITY PURPLE-RED
[33]  SAVEFVEPR←SAVEFVEPR,FVEPR ⍝ SAVES VOLUME FRACTION PU
      RPLE-RED
[34]  →END
[35]
[36] ⍝ SAVE GREEN-RED VALUES
[37] SAVEGR:→(∧/(RMAXSGR,RMAXEGR)≤0,0)/END
[38] ⍝ BEGINNING OF TABLE VALUES
[39]  SAVEHGR←SAVEHGR,H ⍝   SAVES HEIGHT ABOVE BURNER GREE
      N-RED
[40]  SAVEFIGR←SAVEFIGR,EQUIV ⍝ SAVES EQUIVALENCE RATIO GR
      EEN-RED
[41]  →(RMAXSGR≤0)/RSGR
[42]  SAVERSGR←SAVERSGR,(RMAXSGR×1000) ⍝ SAVES RMAX GREEN-
      RED
[43]  SAVENOSGR←SAVENOSGR,(NOSGR×10*12) ⍝ SAVES NUMBER DEN
      SITY GREEN-RED
[44]  SAVEFVSGR←SAVEFVSGR,FVSGR ⍝ SAVES VOLUME FRACTION GR
      EEN-RED
[45]  →(RMAXEGR>0)/OTHERGR
[46]  SAVEREGR←SAVEREGR,0
[47]  SAVENOEGR←SAVENOEGR,1
[48]  SAVEFVEGR←SAVEFVEGR,1
[49]  →END
[50]
[51] RSGR:SAVERSGR←SAVERSGR,0
[52]  SAVENOSGR←SAVENOSGR,1
[53]  SAVEFVSGR←SAVEFVSGR,1
[54]
[55] ⍝ END OF TABLE VALUES
[56] OTHERGR:SAVEREGR←SAVEREGR,(RMAXEGR×1000) ⍝ SAVES RMAX
       GREEN-RED
[57]  SAVENOEGR←SAVENOEGR,(NOEGR×10*12) ⍝ SAVES NUMBER DEN
      SITY GREEN-RED
[58]  SAVEFVEGR←SAVEFVEGR,FVEGR ⍝ SAVES VOLUME FRACTION GR
      EEN-RED
[59]
[60] END:→0
[61]
    ∇
```

FUNCTION: POLYMIE

```
    ∇ POLYMIE;XIO;XIT;XL;S;SM;Rmax;QKR;NoMT;QFACM;KFACM;QV
      V;XK;C2;C3
[1]   ⍝ ANALYZES 514.5 NM LASER LIGHT SCATTER FROM POLYDISP
      ERSE SOOT
[2]   ⍝ PARTICLES IN A LAMINAR PROPANE FLAT FLAME
[3]   ⍝
[4]   ⍝ HERE WE MUST GET VALUES FROM THE RAW DATA ANALYSIS
      PROGRAMS
[5]   ⍝ WRITTEN FOR THE TWO WAVELENGTH TECHNIQUE:
[6]   ⍝ USE THE I/IO RATIO FOR GREEN WAVELENGTH = GRE, FROM
       ¨AN¨
[7]
[8]   ⍝ 'PATHLENGTH IN CM. :'
[9]    XL←⍞INFO[4;]
[10]
[11]   XK←(¯1×⍟(GRE))÷XL ⍝ EXPERIMENTAL VALUE
[12]  ⍝ SCATTERED INTENSITY FROM N2 ≡  SN2←SCAT   FROM ¨CAL
      ZERO¨
[13]  ⍝ MEASURED SCATTERED INTENSITY FROM SOOT = SCAT
[14]
[15]   QVV←1.729E¯8×(SCAT÷SN2)×(GRE)*¯1 ⍝  ×(1+d)÷XL  WHEN
      NOT IN CENTER
[16]  ⍝FACTOR: 7.03E¯28×2.46E19 = SCAT.CROSS SECT. N2× NoM,
      N2 @ T=298K P=1 ATM
[17]  ⍝ NOTE THAT 7.03E¯28=SIGMA, RUDDER & BACH BUT CORRECT
      ED FOR 514.5 LIGHT
[18]
[19]   '   '
[20]   PRINT 'MIE SCATTERING DATA'
[21]   'MIE SCATTERING DATA'
[22]   'EXPERIMENTAL Qvv/Kext FOR MIE = ',⍕(QVV÷XK)
[23]
[24]  ⍝ CALCULATE MOST PROBABLE RADIUS, Rmo
[25]  ⍝ GET VALUES FROM Qvv/Kext TABLE
[26]   PAGNI(QVV÷XK)
[27]  ⍝ CHECK FOR OUT OF RANGE VALUES
[28]   →(QVV≤0)/END
[29]   →(XK≤0)/END
[30]   →((QVV÷XK)<0)/END
[31]
[32]   RNM←RmaxM×1000 ⍝ CONVERT TO RADIUS IN nm
[33]   PRINT '
       '
[34]   ''
[35]   ' '
[36]   PRINT '   '
[37]   'MOST PROBABLE RADIUS = ',(⍕RNM),' nm'
[38]   PRINT 'MOST PROBABLE RADIUS = ',(⍕RNM),' nm'
[39]   PRINT '   '
```

```
[40]  '  '
[41] ⍝ FIND NoM FROM TRANSMISSION, XK
[42]
[43]  NoMT←(2÷27)×XK÷(KFACM×10*¯8) ⍝ CONVERTING FROM uM¯2
      TO CM¯2
[44] ⍝ 'Kext = ',⍕XK
[45]
[46] ⍝ 'NUMBER DENSITY  NoMT = ',(⍕(NoMT)),' CM¯3 '
[47]  'NUMBER DENSITY  NoMT = ',(⍕(NoMT)),' CM¯3 '
[48] ⍝ PRINT 'NUMBER DENSITY  NoMT = ',(⍕(NoMT)),' CM¯3 '
[49]
[50] ⍝ FIND NoM FROM SCATTERING MEASUREMENT, Qvv
[51]  NoM←(2÷27)×QVV÷(QFACM×10*¯8)
[52] ⍝ 'NUMBER DENSITY  NoM = ',(⍕(NoM)),' CM¯3 '
[53]  'NUMBER DENSITY  NoM = ',(⍕(NoM)),' CM¯3 '
[54] ⍝ PRINT 'NUMBER DENSITY  NoM = ',(⍕(NoM)),' CM¯3 '
[55]  PRINT '  '
[56]  PRINT '  '
[57]
[58] ⍝ FIND Fv
[59]  FvM←18.62×NoM×(RmaxM×10*¯4)*3 ⍝ RmaxM WAS IN uM, NOW
       IN CM
[60]  PRINT '   '
[61]  '  '
[62]  'VOLUME FRACTION  FvM = ',⍕(FvM)
[63]  PRINT 'VOLUME FRACTION  FvM = ',⍕(FvM)
[64]  '  '
[65]  ''
[66]  PRINT '
      '
[67]  '  '
[68]  PRINT '  '
[69]  '  '
[70] END:MSCAVE ⍝ SAVE SCATTER RESULTS
    ∇
```

FUNCTION: PAGNI

```
    ∇ PAGNI QKR
[1]  ⍝ THIS FUNCTION REFERS TO A LIST OF THEORETICAL Qvv/K
      ext VALUES AND CORRESPONDING VALUES OF Rmax, SIGMA (
      USED WITH Qvv TO FIND No), AND TAU (USED  WITH Kext
       TO FIND No).
[2]  ⍝ THE FUNCTION INT IS CALLED WHICH PERFORMS INTERPOLA
      TION.
[3]   RmaxM←BE[;2 1]INT QKR
[4]   QFACM←BE[;2 3]INT QKR
[5]   KFACM←BE[;2 4]INT QKR
    ∇
```

FUNCTION: INT

```
    ∇ R←XY INT G;I;X;Y
[1]   ⍝ LINEAR INTERPOLATES G INTO XY
[2]   ⍝ SORT XY INTO ASCENDING ORDER WITH RESPECT TO X
[3]    X←XY[;1] ◇ Y←(XY[;2])[⍋X] ◇ X←X[⍋X]
[4]   ⍝ CHECK IF G IS OUT OF RANGE OF XY
[5]    →((G>⌈/X)∨(G<⌊/X))/OUTRANGE
[6]   ⍝ FIND INDEX I OF FIRST OCCURANCE OF G≥X
[7]    I←I/(⍳⍴I)×I←I>((-⍴⍴I)↑¯1)↓0,I←X≥G
[8]   ⍝ DO LINEAR INTERPOLATION
[9]    R←Y[I-1]+(Y[I]-Y[I-1])×(G-X[I-1])÷(X[I]-X[I-1])
[10]   →0
[11] OUTRANGE:'X VALUE OUT OF RANGE IN INTERPOLATION FUNCT
       ION INT'
[12]   R←¯1
    ∇
```

FUNCTION: MSCAVE

```
    ∇ MSCAVE
[1]   ⍝ SAVES RESULTS OF SCATTERED LIGHT ANALYSIS PROGRAM
[2]    HMSC←HMSC,⍪(INFO[2;])
[3]    FIMSC←FIMSC,EQUIV
[4]    →(RNM≤0)/ZEROS
[5]    RmM←RmM,RNM
[6]    No←No,NoM
[7]    Fv←Fv,FvM
[8]    →END
[9]   ZEROS:RmM←RmM,0
[10]   No←No,1
[11]   Fv←Fv,1
[12] END:→0
    ∇
```

FUNCTION: CO2TEMP

```
    ∇ X CO2TEMP Y;ALN;AT;EMM;NTBB;NTF;VOLT;NREF;SAT;TAU;TC
      ALC;KSCALC;NDFN;FN
[1]   ⍝ W/O BB TO LEFT OF CO2TEMP AND W/ BB TO RIGHT OF CO2
      TEMP
[2]   ⍝ THIS PROGRAM CALCULATES THE SPECTRAL TRANSMITTANCE
      (TAU) AND SPECTRAL EMITTANCE OF A FLAME USING THE IN
      FRARED SPECTROMETER FILTER #13 AND THE NEUTRAL DENSI
      TY FILTER #3.
[3]   ⍝ THIS PROGRAM WILL CALCULATE A CALIBRATION CONSTANT
      KS, BASED ON THE VOL-TAGE READING FOR THE BLACK BODY
       SOURCE AT 1000 DEGREES C.
[4]   ⍝ FOUR READINGS OF VOLTAGE ARE REQUIRED:  V[1]=V0, V[
      2]=VBB, V[3]=VF1,    V[4]=VF2
[5]    NTBB←0.051064 ⍝ NT FOR BBS AT 1000 DEGREES C.
[6]    NREF←4.442E¯5 ⍝ NREF FOR CO2 FILTER.
[7]    AT←33 ⍝ CONSTANT ATTENTUATION VALUE.
[8]    SAT←44.6 ⍝ SENSITIVITY FOR ATTENUATION VALUE OF 33.
[9]    FN←13 ⍝ INFRARED SPECTROMETER FILTER #13.
[10]   NDFN←3 ⍝ NEUTRAL DENSITY FILTER #3.
[11]  ⍝ CALCULATION OF THE CALIBRATION CONSTANT KS FROM THE
       VOLTAGE READING FOR THE BLACK BODY SOURCE AT 1000 C
      .
[12]   KSCALC←(SAT×VBB)÷(NTBB-NREF)
[13]   'KSCALC =',(⍕KSCALC)
[14]   VOLT←0,VBB,X,Y
[15]   TAU←((VOLT[4]×SAT)-(VOLT[3]×SAT))÷((VOLT[2]×SAT)-(VO
      LT[1]×SAT))
[16]   EMM←1-TAU
[17]   'TAU =',(⍕TAU),' EMM =',(⍕EMM)
[18]   'FN =',(⍕FN),' NDFN =',(⍕NDFN),' VOLTAGES (1 TO 4) =
      ',(⍕VOLT),' ATT =',(⍕AT)
[19]  ⍝ .964 IS A TRANSMISSION CORRECTION FACTOR, SINCE FLA
      ME IS <60' FROM RAD
[20]   NTF←NREF+((SAT×VOLT[3])÷(KSCALC×EMM×0.964))
[21]   ALN←⍟NTF
[22]   'NTF =',(⍕NTF)
[23]   TCALC←6379+(5072.53×ALN)+(2267.85×(ALN*2))+(659.18×(
      ALN*3))+(127.59×(ALN*4))+(16.23×(ALN*5))+(1.295×(ALN
      *6))+(0.0584×(ALN*7))+(1.129E¯3×(ALN*8))
[24]   TCALC←TCALC+273 ⍝ CONVERT TO KELVIN.
[25]   'FLAME TEMPERATURE (DEG. K) =',(⍕TCALC)
[26]   SAVET←SAVET,TCALC ⍝ STORE TEMPERATURE VALUES.
[27]   WOBB←0
[28]   WBB←0
[29]  DONE:'DONE'
[30]
    ∇
```

APPENDIX B- PART II: COMPUTER PROGRAMS FOR ERROR ANALYSIS

FUNCTION: ANALYZE

```
    ∇ ANALYZE RNS;I;Z;RUN;WAT;TIN;TOUT;EQUIV;NEWCH0;PUR;GR
      E;RED;WL1;WL2;WL3;WW;MPARAM;A;XK;QVV;W1RATIO;W2RATIO
      ;W3RATIO;ZERO;X;WBB;WOBB;VBB;WAT;TIN;TOUT;IWL;WL;GI0
      ;GI;GREO;IWL1;IWL2;IWL3
[1]   ⍝ MAIN FUNCTION TO ANALYZE RUNS
[2]    →(0=1↑⍴RNS)/0 ⍝ LEAVE IF NO MORE RUNS
[3]    →(1<⍴⍴RNS)/NXT ⍝ IF RNS IS VECTOR, RESHAPE TO A MATR
      IX
[4]    RNS←(1,⍴RNS)⍴RNS
[5]   NXT:→(0=1↑⍴RNS)/0 ⍝ LEAVE IF NO MORE RUNS
[6]    RUN←DEB,(1,1↓⍴RNS)⍴RNS ⍝ TAKE ONE SET OF RUN NUMBERS
[7]    RNS← 1 0 ↓RNS
[8]    I←I/(⍳⍴I)×I←RUN='R'
[9]
[10]  ⍝  FIRST SET ZERO CONDITIONS (NO SOOT)
[11]
[12]   →(1=⍴I)/SAME ⍝ IF NO ZERO RUN IS SPECIFIED USE PREVI
      OUS ZERO
[13]   Z←(-/ΦI)↓RUN
[14]   CALZERO Z
[15]
[16]  ⍝ SHOWS TEST CONDITIONS AND PRINTS MEAN AND STD DEV O
      F DATA
[17]  SAME:RUN←(-0⌈(1≠⍴I)×(⍴RUN)--/ΦI)↓RUN
[18]   ⎕TCNL,'BE SURE PRINTER IS ON',⎕TCNL
[19]
[20]   I←INPUT RUN
[21]   AN I
[22]
[23]  ⍝ CALCULATE EQUIVALENCE RATIO
[24]   FLOWMETER
[25]
[26]  ⍝ PERFORM TWO WAVELENGTH ANALYSIS
[27]
[28]  ⍝ PURPLE-GREEN  ---- NOT USED BECAUSE TOO CLOSE IN WA
      VELENGTH
[29]  ⍝IWL←IWL1,IWL2
[30]  ⍝WL←0.4579,0.5145,PUR,GRE
[31]  ⍝IWL TWOWAVE WL
[32]
[33]  ⍝ PURPLE-RED
[34]   WL←0.4579,0.6328,PUR,RED
[35]   TWOWAVE WL
[36]
[37]   DELTAUIJ WL ⍝ CALCULATES THE UPPER AND LOWER LIMITS
      OF RESULTS
```

```
[38]
[39] ⍝ GREEN-RED
[40]  WL←0.5145,0.6328,GRE,RED
[41]  TWOWAVE WL
[42]
[43]  DELTAUIJ WL ⍝ CALCULATES UPPER AND LOWER LIMITS
[44]
[45] ⍝ PERFORM ERROR ANALYSIS ON SCATTERING RESULTS:
[46]
[47]  SCATTER
[48]
[49]  SAVEPHI←SAVEPHI,EQUIV ⍝ SAVE EQUIVALENCE RATIO VALUE
      S
[50]  SAVECGV←SAVECGV,CGV ⍝ SAVE COLD GAS VELOCITY
[51]
[52]  →NXT ⍝→0
[53]  I←⍳0 ⍝ ZERO I TO SAVE MEMORY
[54]  WHICH ANALYZE RNS ⍝ RECURSIVE CALL TO SELF UNTIL ALL
       RUNS ANALYZED
    ∇
```

FUNCTION: AN

```
     ∇ AN X;MEANX;SDEVX;P;Y;R;PURSD;PURPD;GRESD;GREPD;REDSD
       ;REDPD
[1]   ⍝ FINDS MEAN AND STD DEV OF RAW DATA AND INTENSITY RA
       TIOS
[2]    X←((⍳(⍴X)÷8),8)⍴X
[3]    MEANX←MEAN X
[4]
[5]    GREF←MEANX[4]
[6]    GI←MEANX[5]
[7]
[8]    SDEVX←SDEV X
[9]    P←(SDEVX÷MEANX)×100
[10]
[11]  ⍝ ARRANGE I/IO RATIOS AND SCATTERING DATA INTO AN 8 B
       Y ? MATRIX AND          CASTOUT BAD DATA
[12]   Y←(X[;3]÷PUR0),(X[;5]÷GRE0),(X[;8]÷RED0),[1.5]X[;6]
[13]   R←CASTOUT Y
[14]
[15]  ⍝ 'WAVELENGTH .4579'
[16]   PUR←MEAN R[;1] ⍝ FINDS MEAN OF GOOD I/IO
[17]   PURSD←SDEV R[;1] ⍝ FINDS STANDARD DEVIATION OF GOOD
       I/IO
[18]   PURPD←(PURSD÷PUR)×100
[19]
[20]  ⍝ 'WAVELENGTH .5145'
[21]   GRE←MEAN R[;2] ⍝ FINDS MEAN OF GOOD I/IO
[22]   GRESD←SDEV R[;2] ⍝ FINDS STANDARD DEVIATION OF GOOD
       I/IO
[23]   GREPD←(GRESD÷GRE)×100
[24]
[25]  ⍝ 'WAVELENGTH .6328'
[26]   RED←MEAN R[;3] ⍝ FINDS MEAN OF GOOD I/IO
[27]   REDSD←SDEV R[;3] ⍝ FINDS STANDARD DEVIATION OF GOOD
       I/IO
[28]   REDPD←(REDSD÷RED)×100
[29]
[30]  ⍝ PRINT OUT RAW DATA
[31]   '   '
[32]   PRINT '   '
[33]  ⍝ PRINT RUN
[34]   RUN
[35]  ⍝ TEMPORARILY LEAVE OUT PRINTING OF RAW DATA WHEN COM
       MENT ON NEXT LINE
[36]
[37]   SHOW MEANX[2 3 4 5 7 8],SDEVX[2 3 4 5 7 8],P[2 3 4 5
        7 8],PUR,PURSD,PURPD,GRE,GRESD,GREPD,RED,REDSD,REDP
       D
[38]
[39]   ''
```

```
[40]  '    '
[41]  PRINT '    '
[42]  SCAT←((MEAN R[;4])÷409.5)×⍎INFO[20;] ⍝ SCATTERED LIG
      HT INTENSITY IN VOLTS
[43] ⍝ WHERE INFO[20;] IS THE LOCK-IN AMPLIFIER RANGE FACT
      OR
[44]  PRINT 'SCATTERED INTENSITY MEAN ',⍕SCAT
[45]  SDSCAT←(((SDEV R[;4])÷409.5)×⍎INFO[20;])
[46]  PRINT 'STD. DEV. ',⍕SDSCAT
[47]  PRINT '% STD DEV ',⍕(SDSCAT÷SCAT×100)
[48]  PRINT '    '
[49]
[50]  ''
[51]  '    '
[52]  'SCATTERED INTENSITY MEAN ',⍕SCAT
[53]  'STD DEV ',⍕SDSCAT
[54]  '% STD DEV ',⍕(SDSCAT÷SCAT×100)
[55]  '    '
[56]  ''
[57]
[58]  SDP←SDEVX[3]
[59]  SDG←SDEVX[5]
[60]  SDR←SDEVX[8]
[61]  PV←MEANX[3]
[62]  GV←MEANX[5]
[63]  RV←MEANX[8]
    ∇
```

FUNCTION: CALZERO

```
    ∇ CALZERO RUN;I
[1]  ⍝ CALIBRATION (NO FLAME) RUN, SETS I/I0 REFERENCE VAL
      UES
[2]  ⍝ SHOWS TEST CONDITIONS AND PRINTS MEAN AND STD DEV O
      F DATA
[3]   ⎕TCNL,'BE SURE PRINTER IS ON',⎕TCNL
[4]   I←INPUT RUN
[5]   PUR0←1
[6]   GRE0←1
[7]   RED0←1
[8]   AN I
[9]   PUR0←PUR
[10]  GRE0←GRE
[11]  RED0←RED
[12]  SDP0←SDP
[13]  SDG0←SDG
[14]  SDR0←SDR
[15]  ISN←SCAT
[16]  DELISN←SDSCAT
```

```
[17]  GV0←GV
[18]  SDGV0←SDG
      ∇
```

FUNCTION: CASTOUT

```
      ∇ I←CASTOUT H;B
[1]   ⍝ REMOVES POINTS THAT ARE OUTSIDE OF TWICE STANDARD D
        EVIATION
[2]     I←(|H-(⍴H)⍴MEAN H)>2×(⍴H)⍴SDEV H
[3]   ⍝ REMOVE ROW OF DATA WHERE ANY CHANNEL = ZERO
[4]
[5]   ⍝ REMOVE ROW OF DATA WHERE ANY CHANNEL DEVIATES
[6]     I←(~B←∨/I)/[1]H
[7]     'NUMBER OF BAD DATA POINTS: ',⍕+/B
      ∇
```

FUNCTION: DELTAUIJ

```
      ∇ DELTAUIJ WAVES;IRAT2;I2N2;I2SOOT;SD2N2;SD2SOOT
[1]   ⍝ FINDS THE ERROR IN TAUij/TAU FOR VARIOUS INTENSITY
        RATIOS I/Io
[2]     →(WAVES[1]=0.5145)/GREENRED
[3]   ⍝ 'ENTER I/Io, WAVELENGTH 1: '
[4]     IRAT1←PUR
[5]   ⍝ 'ENTER I/Io, WAVELENGTH 2: '
[6]     IRAT2←RED
[7]   ⍝ 'ENTER I1, THROUGH N2: ' ◇
[8]     I1N2←PUR0
[9]   ⍝ '    ENTER STD. DEV. OF I1 THROUGH N2: ' ◇
[10]    SD1N2←SDP0
[11]  ⍝ 'ENTER I1, THROUGH SOOT: ' ◇
[12]    I1SOOT←PV
[13]  ⍝ '     ENTER STD. DEV. OF I1 THROUGH SOOT: ' ◇
[14]    SD1SOOT←SDP
[15]  ⍝ '      '
[16]  ⍝ 'ENTER I2, THROUGH N2: ' ◇
[17]    I2N2←RED0
[18]  ⍝ '    ENTER STD. DEV. OF I2 THROUGH N2: ' ◇
[19]    SD2N2←SDR0
[20]  ⍝ 'ENTER I2, THROUGH SOOT: ' ◇
[21]    I2SOOT←RV
[22]  ⍝ '     ENTER STD. DEV. OF I2 THROUGH SOOT: ' ◇
[23]    SD2SOOT←SDR
[24]  ⍝ 'ENTER WL1, MICRONS: ' ◇
[25]    WL1←0.4579
[26]  ⍝ 'ENTER WL2, MICRONS: ' ◇
```

```
[27]  WL2←0.6328
[28]  →(WL1=0.4579)/CALC
[29] GREENRED:IRAT1←GRE
[30]  IRAT2←RED
[31]  I1N2←GRE0
[32]  SD1N2←SDG0
[33]  I1SOOT←GV
[34]  SD1SOOT←SDG
[35]  I2N2←RED0
[36]  SD2N2←SDR0
[37]  I2SOOT←RV
[38]  SD2SOOT←SDR
[39]  WL1←0.5145
[40]  WL2←0.6328
[41]
[42] ⍝ CALCULATE ΔTAUij/TAUij:
[43]
[44] CALC:TAURATIO←(((SD1SOOT÷(I1SOOT×⊛(IRAT1)))*2)+((SD2S
      OOT÷(I2SOOT×⊛(IRAT2)))*2)+((SD1N2÷(I1N2×⊛(IRAT1)))*2
      )+((SD2N2÷(I2N2×⊛(IRAT2)))*2))
[45]  TAURATIO←TAURATIO*0.5
[46]  'TAURATIO = ',⍕TAURATIO
[47]
[48] ⍝ CALCULATE ΔTAU/TAU FOR EACH WAVLENGTH, 1 AND 2:
[49]
[50]  TAUWL1←(((SD1SOOT÷(I1SOOT×⊛(IRAT1)))*2)+((SD1N2+(I1N
      2×⊛(IRAT1)))*2)+((0.05)*2))
[51]  TAUWL1←TAUWL1*0.5
[52]  TAUWL2←(((SD2SOOT÷(I2SOOT×⊛(IRAT2)))*2)+((SD2N2÷(I2N
      2×⊛(IRAT2)))*2)+((0.05)*2))
[53]  TAUWL2←TAUWL2*0.5
[54]
[55] ⍝ CALCULATE ΔXij
[56]  DELXIJ
[57]  OLDXIJ←XIJ
[58]  UPPER OLDXIJ+DELXij ⍝ CALCULATES UPPER VALUE FOR Xij
       AND Rmax, No, Fv
[59]  LOWER OLDXIJ-DELXij ⍝ CALCULATES LOWER VALUE FOR Xij
       AND Rmax, No, Fv
    ∇
```

FUNCTION: DELXIJ

```
    ∇ DELXIJ;ABS
[1]  ⍝ CALCULATES THE ERROR IN Xij
[2]
[3]  ⍝ CALCULATE THE ABSORPTION LIMIT:
[4]  CALC:ABS←(WL2×(FA WL1))÷(WL1×(FA WL2))
[5]
```

```
[6]   ⍝ CALCULATE ΔXij
[7]    DELXij←(TAURATIO÷ABS)×(⍎IRAT1)÷(⍎IRAT2)
[8]    'ΔXij = ',⍕DELXij
      ∇
```

FUNCTION: LOWER

```
     ∇ LOWER NEW;H;PRAT1;PRAT2;TAU1;TAU2;TAUABS;RMAXEPR;RMA
       XEGR;RMAXSPR;RMAXSGR;TAUPRIMEE;TAUPRIMES;TAUP1S;TAUP
       2S;TAUP1E;TAUP2E;FVSPR;FVSGR;FVEPR;FVEGR;NOSPR;NOSGR
       ;NOEPR;NOEGR;RPRINT;RS;N;RE
[1]   ⍝  ANALYZES DATA FROM TWO-WAVELENGTH LASER EXTINCTION
       TECHNIQUE FOR PURPLE-RED, THEN GREEN-RED FOR MINIMU
      M VALUE OF Xij
[2]   ⍝FIND LOWEST VALUES FOR TAUS  FOR EACH WAVELENGTH:
[3]
[4]    ⎕PP←5
[5]    TAU1←(¯1÷(L×10000))×⍟WL[3] ⍝ CONVERT L FROM CM TO MI
      CRONS
[6]    TAU1←TAU1-(TAU1×TAUWL1)
[7]    TAU2←(¯1÷(L×10000))×⍟WL[4]
[8]    TAU2←TAU2-(TAU2×TAUWL2)
[9]    →(TAU2=0)/END
[10]
[11]   XIJ←NEW
[12]   '  '
[13]   'LOWER LIMIT  XIJ FOR WAVELENGTHS ',(⍕WL[1]),' AND '
      ,(⍕WL[2]),' = ',⍕XIJ
[14]
[15]   PRINT 'LOWER LIMIT XIJ FOR WAVELENGTHS ',(⍕WL[1]),'
      AND ',(⍕WL[2]),' = ',⍕XIJ
[16]
[17]   →(XIJ≤0)/END
[18]
[19] ⍝ GO TO XIJ TABLE WITH XIJ VALUE AND WAVELENGTHS USED
[20] ⍝ '1ST LETTERS OF WAVELENGTHS--  PR  GR : '
[21]   →(∧/((WL[1]),WL[2])=0.4579,0.6328)/PR
[22]   →(∧/((WL[1]),WL[2])=0.5145,0.6328)/GR
[23] GR:WW←'GR'
[24]   →CONTINUE
[25] PR:WW←'PR'
[26] CONTINUE:PRINT ' '
[27]   '  '
[28]   PRINT ' WAVELENGTHS :   ',⍕WW
[29] ⍝ GET RMAX VALUES AND TAUPRIME VALUES FROM TABLE
[30]   XIJTABLE WW
[31]   PRINT ' '
[32]   '  '
[33]   ⍎('RMAXS',WW,'←RS')
[34]   →(RS<0)/RME
[35]   TAUPRIMES←TAUP1S
[36] ⍝ CALCULATE SOOT PARTICLE NUMBER DENSITY FOR FIRST RM
      AX AND TAU'
[37]   ⍎('NOS',WW,'←(TAU1÷(TAUPRIMES×RMAXS',WW,'*2))') ⍝ NO
      S IN um
[38]   PRINT '  '
```

```
[39]  ⍎('RPRINT←1000×RMAXS',WW) ⍝ RMAXS IN um, RPRINT IN n
      m
[40]  '  '
[41]  'RMAX (S) FOR WAVELENGTHS ',(⍕WL[1]),' AND ',(⍕WL[2]
      ),' = ',(⍕RPRINT),' nm '
[42]  PRINT 'RMAX (S) FOR WAVELENGTHS ',(⍕WL[1]),' AND ',(
      ⍕WL[2]),' = ',(⍕RPRINT),' nm'
[43]  'N0, SOOT PARTICLE NO. DENSITY (S) FOR WAVELENGTHS '
      ,(⍕WL[1]),' AND ',(⍕WL[2]),' = ',(⍕(⍎('NOS',WW,'×10*
      12'))),' cm¯3'
[44]  PRINT 'N0, SOOT PARTICLE NO. DENSITY (S) FOR WAVELEN
      GTHS ',(⍕WL[1]),' AND ',(⍕WL[2]),' = ',(⍕(⍎('NOS',WW
      ,'×10*12'))),' cm¯3'
[45] ⍝ CALCULATE SOOT VOLUME FRACTION FOR FIRST RMAX AND T
      AU'
[46]  ⍎('FVS',WW,'←18.62×NOS',WW,'×RMAXS',WW,'*3')
[47]  'FV, SOOT VOLUME FRACTION (S) FOR WAVELENGTHS ',(⍕WL
      [1]),' AND ',(⍕WL[2]),' = ',(⍕(⍎('FVS',WW))),' '
[48]  PRINT 'FV, SOOT VOLUME FRACTION (S) FOR WAVELENGTHS
      ',(⍕WL[1]),' AND ',(⍕WL[2]),' = ',(⍕(⍎('FVS',WW))),'
       '
[49]  PRINT '    '
[50]  '  '
[51]  PRINT '  '
[52]  '  '
[53] RME:⍎('RMAXE',WW,'←RE')
[54]  →(RE<0)/END
[55]  TAUPRIMEE←TAUP1E
[56] ⍝ CALCULATE SOOT PARTICLE NO. DENSITY FOR SECOND RMAX
       AND TAU'
[57]  ⍎('NOE',WW,'←(TAU1÷(TAUPRIMEE×RMAXE',WW,'*2))') ⍝ NO
      E IN um
[58]  PRINT '    '
[59]  ⍎('RPRINT←1000×RMAXE',WW) ⍝ RMAXE IN um, RPRINT IN n
      m
[60]  '   '
[61]  'RMAX (E) FOR WAVELENGTHS ',(⍕WL[1]),' AND ',(⍕WL[2]
      ),' = ',(⍕RPRINT),' nm'
[62]  PRINT 'RMAX (E) FOR WAVELENGTHS ',(⍕WL[1]),' AND ',(
      ⍕WL[2]),' = ',(⍕RPRINT),' nm'
[63]  'N0, SOOT PARTICLE NO. DENSITY (E) FOR WAVELENGTHS '
      ,(⍕WL[1]),' AND ',(⍕WL[2]),' = ',(⍕(⍎('NOE',WW,'×10*
      12'))),' cm¯3'
[64]  PRINT 'N0, SOOT PARTICLE NO. (E) FOR WAVELENGTHS ',(
      ⍕WL[1]),' AND ',(⍕WL[2]),' = ',(⍕(⍎('NOE',WW,'×10*12
      '))),' cm¯3'
[65] ⍝ CALCULATE SOOT VOLUME FRACTION FOR SECOND RMAX AND
      TAU'
[66]  ⍎('FVE',WW,'←18.62×NOE',WW,'×RMAXE',WW,'*3')
[67]  'FV, SOOT VOLUME FRACTION (E) FOR WAVELENGTHS ',(⍕WL
      [1]),' AND ',(⍕WL[2]),' = ',(⍕(⍎('FVE',WW))),' '
```

```
[68]  PRINT 'FV, SOOT VOLUME FRACTION (E) FOR WAVELENGTHS
      ',(⍕WL[1]),' AND ',(⍕WL[2]),' = ',(⍕(⍎('FVE',WW))),'
       '
[69]  PRINT '  '
[70]  '  '
[71]  →(XIJ≤0)/END
[72] ⍝ INITIALIZE N FOR SAVER PROGRAM
[73]  H←⍎(INFO[2;]) ⍝ HEIGHT ABOVE BURNER
[74]  →(∧/((WL[1]),WL[2])=0.4579,0.6328)/N1
[75]  →(∧/((WL[1]),WL[2])=0.5145,0.6328)/N2
[76] N1:N←1
[77]  →SAVE
[78] N2:N←2
[79] SAVE:SAVER ⍝  RUN PROGRAM TO SAVE VALUES FOR ALL THE
      RUNS
[80]  PRINT '  '
[81] END:→0
[82]
[83]
    ∇
```

FUNCTION: UPPER

```
    ∇ UPPER NEW;H;PRAT1;PRAT2;TAU1;TAU2;TAUABS;RMAXEPR;RMA
      XEGR;RMAXSPR;RMAXSGR;TAUPRIMEE;TAUPRIMES;TAUP1S;TAUP
      2S;TAUP1E;TAUP2E;FVSPR;FVSGR;FVEPR;FVEGR;NOSPR;NOSGR
      ;NOEPR;NOEGR;RPRINT;RS;N;RE
[1]  ⍝  ANALYZES DATA FROM TWO-WAVELENGTH LASER EXTINCTION
      TECHNIQUE FOR PURPLE-RED, THEN GREEN-RED FOR MAXIMU
      M VALUE OF Xij
[2]
[3]  ⍝FIND THE ERROR IN TAU1 AND TAU2:
[4]
[5]   ⎕PP←5
[6]   TAU1←(¯1÷(L×10000))×⍟WL[3] ⍝ CONVERT L FROM CM TO MI
      CRONS
[7]   TAU1←TAU1+(TAU1×TAUWL1)
[8]   TAU2←(¯1÷(L×10000))×⍟WL[4]
[9]   TAU2←TAU2+(TAU2×TAUWL2)
[10]  →(TAU2=0)/END
[11]
[12]  XIJ←NEW
[13]  '  '
[14]  'UPPER LIMIT  XIJ FOR WAVELENGTHS ',(⍕WL[1]),' AND '
      ,(⍕WL[2]),' = ',⍕XIJ
[15]
[16]  PRINT 'UPPER LIMIT XIJ FOR WAVELENGTHS ',(⍕WL[1]),'
      AND ',(⍕WL[2]),' = ',⍕XIJ
[17]
```

```
[18]  →(XIJ≤0)/END
[19]
[20] ⍝ GO TO XIJ TABLE WITH XIJ VALUE AND WAVELENGTHS USED
[21] ⍝ '1ST LETTERS OF WAVELENGTHS--  PR  GR : '
[22]  →(∧/((WL[1]),WL[2])=0.4579,0.6328)/PR
[23]  →(∧/((WL[1]),WL[2])=0.5145,0.6328)/GR
[24] GR:WW←'GR'
[25]  →CONTINUE
[26] PR:WW←'PR'
[27] CONTINUE:PRINT ' '
[28]  '  '
[29]  PRINT ' WAVELENGTHS :    ',⍕WW
[30] ⍝ GET RMAX VALUES AND TAUPRIME VALUES FROM TABLE
[31]  XIJTABLE WW
[32]  PRINT ' '
[33]  '   '
[34]  ⍎('RMAXS',WW,'←RS')
[35]  →(RS<0)/RME
[36]  TAUPRIMES←TAUP1S
[37] ⍝ CALCULATE SOOT PARTICLE NUMBER DENSITY FOR FIRST RM
      AX AND TAU'
[38]  ⍎('NOS',WW,'←(TAU1÷(TAUPRIMES×RMAXS',WW,'⋆2))') ⍝ NO
      S IN um
[39]  PRINT '  '
[40]  ⍎('RPRINT←1000×RMAXS',WW) ⍝ RMAXS IN um, RPRINT IN n
      m
[41]  '  '
[42]  'RMAX (S) FOR WAVELENGTHS ',(⍕WL[1]),' AND ',(⍕WL[2]
      ),' = ',(⍕RPRINT),' nm '
[43]  PRINT 'RMAX (S) FOR WAVELENGTHS ',(⍕WL[1]),' AND ',(
      ⍕WL[2]),' = ',(⍕RPRINT),' nm'
[44]  'NO, SOOT PARTICLE NO. DENSITY (S) FOR WAVELENGTHS '
      ,(⍕WL[1]),' AND ',(⍕WL[2]),' = ',(⍕(⍎('NOS',WW,'×10⋆
      12'))),' cm¯3'
[45]  PRINT 'NO, SOOT PARTICLE NO. DENSITY (S) FOR WAVELEN
      GTHS ',(⍕WL[1]),' AND ',(⍕WL[2]),' = ',(⍕(⍎('NOS',WW
      ,'×10⋆12'))),' cm¯3'
[46] ⍝ CALCULATE SOOT VOLUME FRACTION FOR FIRST RMAX AND T
      AU'
[47]  ⍎('FVS',WW,'←18.62×NOS',WW,'×RMAXS',WW,'⋆3')
[48]  'FV, SOOT VOLUME FRACTION (S) FOR WAVELENGTHS ',(⍕WL
      [1]),' AND ',(⍕WL[2]),' = ',(⍕(⍎('FVS',WW))),' '
[49]  PRINT 'FV, SOOT VOLUME FRACTION (S) FOR WAVELENGTHS
      ',(⍕WL[1]),' AND ',(⍕WL[2]),' = ',(⍕(⍎('FVS',WW))),'
       '
[50]  PRINT '   '
[51]  '  '
[52]  PRINT '  '
[53]  '  '
[54] RME:⍎('RMAXE',WW,'←RE')
[55]  →(RE<0)/END
```

```
[56]  TAUPRIMEE←TAUP1E
[57] ⍝ CALCULATE SOOT PARTICLE NO. DENSITY FOR SECOND RMAX
      AND TAU'
[58]  ⍎('NOE',WW,'←(TAU1÷(TAUPRIMEE×RMAXE',WW,'*2))') ⍝ NO
      E IN um
[59]  PRINT '   '
[60]  ⍎('RPRINT←1000×RMAXE',WW) ⍝ RMAXE IN um, RPRINT IN n
      m
[61]  '   '
[62]  'RMAX (E) FOR WAVELENGTHS ',(⍕WL[1]),' AND ',(⍕WL[2]
      ),' = ',(⍕RPRINT),' nm'
[63]  PRINT 'RMAX (E) FOR WAVELENGTHS ',(⍕WL[1]),' AND ',(
      ⍕WL[2]),' = ',(⍕RPRINT),' nm'
[64]  'NO, SOOT PARTICLE NO. DENSITY (E) FOR WAVELENGTHS '
      ,(⍕WL[1]),' AND ',(⍕WL[2]),' = ',(⍕(⍎('NOE',WW,'×10*
      12'))),' cm¯3'
[65]  PRINT 'NO, SOOT PARTICLE NO. (E) FOR WAVELENGTHS ',(
      ⍕WL[1]),' AND ',(⍕WL[2]),' = ',(⍕(⍎('NOE',WW,'×10*12
      '))),' cm¯3'
[66] ⍝ CALCULATE SOOT VOLUME FRACTION FOR SECOND RMAX AND
      TAU'
[67]  ⍎('FVE',WW,'←18.62×NOE',WW,'×RMAXE',WW,'*3')
[68]  'FV, SOOT VOLUME FRACTION (E) FOR WAVELENGTHS ',(⍕WL
      [1]),' AND ',(⍕WL[2]),' = ',(⍕(⍎('FVE',WW))),' '
[69]  PRINT 'FV, SOOT VOLUME FRACTION (E) FOR WAVELENGTHS
      ',(⍕WL[1]),' AND ',(⍕WL[2]),' = ',(⍕(⍎('FVE',WW))),'
       '
[70]  PRINT '   '
[71]  '   '
[72]  →(XIJ≤0)/END
[73] ⍝ INITIALIZE N FOR SAVER PROGRAM
[74]  H←⍎(INFO[2;]) ⍝ HEIGHT ABOVE BURNER
[75]  →(∧/((WL[1]),WL[2])=0.4579,0.6328)/N1
[76]  →(∧/((WL[1]),WL[2])=0.5145,0.6328)/N2
[77] N1:N←1
[78]  →SAVE
[79] N2:N←2
[80] SAVE:SAVER ⍝  RUN PROGRAM TO SAVE VALUES FOR ALL THE
      RUNS
[81]  PRINT '   '
[82] END:→0
[83]
[84]
    ∇
```

FUNCTION: SCATTER

```
    ∇ SCATTER
[1]  ⍝ COMPUTES THE ERROR IN THE Qvv/Kext RATIO FOR MIE SC
     ATTERING
[2]   ISS←SCAT ⍝          SCATTERED INTENSITY FROM SOOT
[3]   DELISS←SDSCAT ⍝     STD DEV OF ISS
[4]   I←GV ⍝              EXTINCTION MEASUREMENT THROUGH FLA
     ME
[5]   DELI←SDG ⍝          STD DEV OF I
[6]   I0←GV0 ⍝           EXTINCTION MEASUREMENT THROUGH N2
[7]   DELI0←SDGV0 ⍝       STD DEV OF I0
[8]   L←⌷INFO[4;] ⍝      PATHLENGTH THROUGH FLAME
[9]   DELL←0.05×L ⍝   ESTIMATE 5% VARIATION IN L (PATHLENGT
     H)
[10]
[11]  FACT←1+(1÷⍟(I÷I0))
[12]  XK←(⍟(I÷I0))÷(¯1×L) ⍝ MEAN EXTINCTION COEFFICIENT
[13]
[14] ⍝ CALCULATE Δ(Qvv/Kext)/(Qvv/Kext):
[15]  QKRATSQ←((DELISS÷ISS)*2)+((DELISN÷ISN)*2)+((FACT×DEL
     I0÷I0)*2)+((FACT×DELI÷I)*2)+(DELL÷L)*2
[16]  QKRAT←QKRATSQ*0.5
[17]
[18] ⍝ CALCULATE ΔQvv/Qvv:
[19]  DELQVV←((DELISS÷ISS)*2)+((DELISN÷ISN)*2)+((DELI0÷I0)
     *2)+((DELI÷I)*2)
[20]  DELQVV←DELQVV*0.5
[21]
[22]  CONST←1.73E¯8 ⍝  N2 SCATTERING CROSS SECT.× N2 NUMBE
     R DENSITY
[23] ⍝CALCULATE Qvv/Kext:
[24]  QK←¯1×CONST×ISS×I0×L÷(ISN×I×⍟(I÷I0))
[25]  'Δ(Qvv/Kext) ÷ Qvv/Kext = ',⍕QKRAT
[26]  '  '
[27]  'Qvv/Kext = ',⍕QK
[28]  '  '
[29]  'Δ(Qvv/Kext) = ',⍕(QK×QKRAT)
[30]  PRINT '  '
[31]  PRINT '*  *  *  *  *  *  *  *  *  *  *  *  *  *  *'
[32]  PRINT '  '
[33]  PRINT 'Δ(Qvv/Kext) ÷ Qvv/Kext = ',⍕QKRAT
[34]  PRINT '  '
[35]  PRINT 'Qvv/Kext = ',⍕QK
[36]  PRINT '  '
[37]  PRINT 'Δ(Qvv/Kext) = ',⍕(QK×QKRAT)
[38]  PRINT '  '
[39]  PRINT '*  *  *  *  *  *  *  *  *  *  *  *  *  *  *'
[40]  PRINT '  '
[41]  QVVMEAN←QK×XK
[42]  QVV←QVVMEAN
```

```
[43] ⍝ GET VALUES FROM Qvv/Kext TABLE
[44]  PAGNI(QK)
[45] ⍝ CHECK FOR OUT OF RANGE VALUES
[46]  →(QVV≤0)/END
[47]  →(XK≤0)/END
[48]  →((QVV÷XK)<0)/END
[49]
[50]  RNM←RmaxM×1000 ⍝ CONVERT TO RADIUS IN nm
[51]  'MOST PROBABLE RADIUS = ',(⍕RNM),' nm'
[52]  PRINT 'MOST PROBABLE RADIUS = ',(⍕RNM),' nm'
[53]  PRINT '  '
[54]  '  '
[55]  RMEAN←RNM
[56] ⍝ FIND NoM FROM SCATTERING MEASUREMENT, Qvv
[57]  NoM←(2÷27)×QVV÷(QFACM×10*¯8) ⍝ QFACM COMES FROM PAGN
      I FUNCTION
[58]  'NUMBER DENSITY  NoM = ',(⍕(NoM)),' CM¯3 '
[59]  PRINT 'NUMBER DENSITY  NoM = ',(⍕(NoM)),' CM¯3 '
[60]  NMEAN←NoM
[61] ⍝ FIND Fv
[62]  FvM←18.62×NoM×(RmaxM×10*¯4)*3 ⍝ RmaxM WAS IN uM, NOW
       IN CM
[63]  FVMEAN←FvM
[64]  PRINT '   '
[65]  '  '
[66]  'VOLUME FRACTION  FvM = ',⍕(FvM)
[67]  PRINT 'VOLUME FRACTION  FvM = ',⍕(FvM)
[68]  MSCAVE ⍝ SAVE MEAN VALUES
[69]  '  '
[70] ⍝ GET VALUES FROM Qvv/Kext TABLE FOR LOWEST RATIO VAL
      UE:
[71]
[72]  'LOWEST Q/K:'
[73]  QKLOW←QK-(QK×QKRAT)
[74] ⍝ 'LOWEST QVV: '
[75] ⍝ QVV←QVVMEAN-(DELQVV×QVVMEAN)
[76]  'MAX QVV :' ⍝  GIVES MOST EXTREME VALUES FOR LOWEST
      Q/K RESULTS
[77]  QVV←QVVMEAN+(DELQVV×QVVMEAN)
[78]  PRINT 'LOWEST Qvv/Kext VALUES: '
[79]  PAGNI(QKLOW)
[80] ⍝ CHECK FOR OUT OF RANGE VALUES
[81]  →(QVV≤0)/END
[82]  RNM←RmaxM×1000 ⍝ CONVERT TO RADIUS IN nm
[83]  'MOST PROBABLE RADIUS = ',(⍕RNM),' nm'
[84]  PRINT 'MOST PROBABLE RADIUS = ',(⍕RNM),' nm'
[85]  PRINT '  '
[86]  RMIN←RNM
[87] ⍝ FIND NoM FROM SCATTERING MEASUREMENT, Qvv
[88]  NoM←(2÷27)×QVV÷(QFACM×10*¯8)
[89]  'NUMBER DENSITY  NoM = ',(⍕(NoM)),' CM¯3 '
```

```
[90]  PRINT 'NUMBER DENSITY  NoM = ',(⍕(NoM)),' CM¯3 '
[91]  NMIN←NoM
[92] ⍝ FIND Fv
[93]  FvM←18.62×NoM×(RmaxM×10*¯4)*3 ⍝ RmaxM WAS IN uM, NOW
       IN CM
[94]  FVMIN←FvM
[95]  PRINT '    '
[96]  '  '
[97]  'VOLUME FRACTION  FvM = ',⍕(FvM)
[98]  PRINT 'VOLUME FRACTION  FvM = ',⍕(FvM)
[99]  '  '
[100]  PRINT '  '
[101]  MSCAVE ⍝ SAVE MINIMUM VALUES
[102]
[103] ⍝ GET VALUES FROM Qvv/Kext TABLE FOR HIGHEST Q/K VAL
      UE:
[104]  'MAXIMUM Q/K RATIO RESULTS:'
[105]  QKHI←QK+(QK×QKRAT)
[106] ⍝ 'MAX QVV :'
[107] ⍝ QVV←QVVMEAN+(DELQVV×QVVMEAN)
[108]
[109]  'LOWEST QVV: ' ⍝ GIVES MOST EXTREME VALUES FOR MAX
      Q/K RESULTS
[110]  QVV←QVVMEAN-(DELQVV×QVVMEAN)
[111]
[112]  PAGNI(QKHI)
[113]  PRINT 'RESULTS FOR MAXIMUM Qvv/Kext: '
[114] ⍝ CHECK FOR OUT OF RANGE VALUES
[115]  →(QVV≤0)/END
[116]  →(XK≤0)/END
[117]  →((QVV÷XK)<0)/END
[118]  RNM←RmaxM×1000 ⍝ CONVERT TO RADIUS IN nm
[119]  'MOST PROBABLE RADIUS = ',(⍕RNM),' nm'
[120]  PRINT 'MOST PROBABLE RADIUS = ',(⍕RNM),' nm'
[121]  PRINT '  '
[122]  RMAX←RNM
[123]  '  '
[124] ⍝ FIND NoM FROM SCATTERING MEASUREMENT, Qvv
[125]  NoM←(2÷27)×QVV÷(QFACM×10*¯8)
[126]  'NUMBER DENSITY  NoM = ',(⍕(NoM)),' CM¯3 '
[127]  PRINT 'NUMBER DENSITY  NoM = ',(⍕(NoM)),' CM¯3 '
[128]  NMAX←NoM
[129] ⍝ FIND Fv
[130]  FvM←18.62×NoM×(RmaxM×10*¯4)*3 ⍝ RmaxM WAS IN uM, NO
      W IN CM
[131]  FVMAX←FvM
[132]  PRINT '    '
[133]  '  '
[134]  'VOLUME FRACTION  FvM = ',⍕(FvM)
[135]  PRINT 'VOLUME FRACTION  FvM = ',⍕(FvM)
[136]  MSCAVE ⍝ SAVE MAXIMUM VALUES
```

```
[137]  RPERCENT←100×|((RMAX-RMIN)÷RMEAN)
[138]  NPERCENT←100×|((NMAX-NMIN)÷NMEAN)
[139]  FVPERCENT←100×|((FVMAX-FVMIN)÷FVMEAN)
[140]  '★=========================================★'
[141]  '             SCATTERING TECHNIQUE'
[142]  ' PERCENT VARIATION IN: '
[143]  '  '
[144]  ' Rmax : ',⍕RPERCENT
[145]  ' No   : ',⍕NPERCENT
[146]  ' Fv   : ',⍕FVPERCENT
[147]  '   '
[148]  '★=========================================★'
[149]  PRINT '★=========================================★'
[150]  PRINT '             SCATTERING TECHNIQUE'
[151]  PRINT ' PERCENT VARIATION IN: '
[152]  PRINT '  '
[153]  PRINT ' Rmax : ',⍕RPERCENT
[154]  PRINT ' No   : ',⍕NPERCENT
[155]  PRINT ' Fv   : ',⍕FVPERCENT
[156]  PRINT '   '
[157]  PRINT '★=========================================
      ★'
[158] END:
    ∇
```

APPENDIX B- PART III: COMPUTER PROGRAMS FOR THERMOCOUPLE CORRECTIONS

FUNCTION: CORRECT

```
    ∇ R←CORRECT Tb;I;THETA;k;h;Eb;Tg;TgOLD;Tp;TB;To;T1;T2;
      T3;T4;T5
[1]   ⍝ CORRECTS 3-MIL, PT/PT-RH T/C BEAD TEMPERATURE TO FI
      ND
[2]   ⍝ GAS TEMPERATURE IN A FLAME, USING ANG/PAGNI METHOD
[3]    Tg←1.05×Tb ⍝ PICK A STARTING GUESS FOR THE GAS TEMP.
[4]    Tp←1000 ⍝ DEG K, GUESS AT UPPER PLATE TEMPERATURE
[5]    TB←800 ⍝ DEG K, APPROXIMATE BURNER SURFACE TEMPERATU
       RE
[6]    To←298 ⍝ DEG K, AMBIENT TEMPERATURE
[7]    I←0
[8]   AGAIN:THETA←Tg÷2200
[9]    I←I+1
[10]   'I =',⍕I
[11]   TgOLD←Tg
[12]  ⍝ CALCULATE k FOR CO2 AND H20 (FLAME PRODUCTS)
[13]  ⍝ VALUES ARE A CURVEFIT OF A TABLE FROM KREITH'S BOOK
[14]   kCO2←(Tg∘.* 0 1 2)+.× 0.0130881 8.80907E¯5 ¯1.94089E
       ¯8
[15]   kH20←(Tg∘.* 0 1 2)+.× ¯9.17447E¯3 1.341E¯4 ¯6.03739E
       ¯9
[16]   k←((4÷7)×kH20)+((3÷7)×kCO2) ⍝ APPROXIMATE USING STOI
       CHIOMETRIC FLOW
[17]   h←k÷8E¯5 ⍝ SIZE OF THERMOCOUPLE LEADS=80 MICRONS, FO
       R WHICH Nu=1
[18]   Eb←(1.507E¯4×Tb)-1.596E¯8×Tb*2
[19]   T1←Tb*4
[20]   T2←0.276×0.3×Tp*4
[21]   T3←0.276×0.1×TB*4
[22]   T5←0.448×To*4
[23]  REDO:TgTRY←Tg
[24]   T4←0.0345×Tg*4
[25]   Tg←Tb+(Eb×5.67E¯8÷h)×(T1-T2-T3-T4-T5)
[26]   →(|(TgTRY-Tg)>1)/REDO
[27]   →(|(Tg-TgOLD)>1)/AGAIN
[28]   R←Tg
    ∇
```

NASA
National Aeronautics and Space Administration

Report Documentation Page

1. Report No.	2. Government Accession No.	3. Recipient's Catalog No.
NASA TM-101305		

4. Title and Subtitle	5. Report Date
Optical Measurements of Soot in Premixed Flames	August 1988
	6. Performing Organization Code

7. Author(s)	8. Performing Organization Report No.
Valerie J. Lyons	E-4295
	10. Work Unit No.
	505-62-21

9. Performing Organization Name and Address	11. Contract or Grant No.
National Aeronautics and Space Administration Lewis Research Center Cleveland, Ohio 44135-3191	
	13. Type of Report and Period Covered
	Technical Memorandum

12. Sponsoring Agency Name and Address	14. Sponsoring Agency Code
National Aeronautics and Space Administration Washington, D.C. 20546-0001	

15. Supplementary Notes

This report was a dissertation submitted in partial satisfaction of the requirements for the degree of Doctor of Philosophy in Mechanical Engineering in the Graduate Division of the University of California, Berkeley, California.

16. Abstract

Two laser diagnostic techniques were used to measure soot volume fractions, number densities and soot particle radii in premixed propane/oxygen flat flames. The two techniques used were two-wavelength extinction, using 514.5 nm–632.8 nm and 457.9 nm–632.8 nm wavelength combinations, and extinction/scattering using 514.5 nm light. The flames were fuel-rich (equivalence ratios from 1.8 to 2.8) and had cold gas velocities varying from 3.4 to 5.5 cm/s. Measurements were made at various heights above the sintered-bronze, water-cooled flat flame burner with the equivalence ratio and cold gas velocity fixed. Also, measurements were made at a fixed height above the burner and fixed cold gas velocity while varying the equivalence ratio. Both laser techniques are based on the on the same underlying assumptions of particle size distribution and soot optical properties. Full Mie theory was used to determine the extinction coefficients, K_{ext}, and the scattering efficiencies, Q_{vv}. Temperature measurements in the flames were made using infra-red radiometry and fine-wire thermocouples. Good agreement between the two techniques in terms of soot particle radii, number density and volume fraction was found for intensity ratios (I/I_0) between 0.1 and 0.8. For intensity ratios higher, or lower than this range, the differences in extinction coefficients at the wavelengths chosen for the two-wavelength method are too small to give accurate results for comparing particle radii and number densities. However, when comparing only soot volume fractions, the agreement between the two techniques continued to be good for intensity ratios up to 0.95.

17. Key Words (Suggested by Author(s))	18. Distribution Statement
Laser diagnostics; Soot; Premixed flames; Combustion; Optics	Unclassified - Unlimited Subject Category 34

19. Security Classif. (of this report)	20. Security Classif. (of this page)	21. No of pages	22. Price*
Unclassified	Unclassified	179	A09

NASA FORM 1626 OCT 86

*For sale by the National Technical Information Service, Springfield, Virginia 22161